Wind Uplift Resistance of Roof Edge Components

By
Wassim Alassafin

A thesis presented to the University of Ottawa
in partial fulfilment of
the requirements for the degree of

Master of Applied Science in Civil Engineering

Department of Civil Engineering
University of Ottawa
Ottawa, Ontario, Canada
March 2013

M.A.Sc in Civil Engineering is a joint program
with Carleton University administrated by the
Ottawa-Carleton Institute for Civil Engineering (OCICE)

Abstract

A roof is a critical envelope of a building. It provides protection for the building interior against various weather elements, such as snow, rain and wind. Roofs are normally composed of several components such as insulation, barriers and water proofing membrane. A roof edge is the perimetric part of a roof that serves as termination for roof components. In generic terms, a roof edge system is composed of a parapet with metal components, such as coping and cleat/clip. The edge system is typically subjected to negative pressure (suction) due to wind flow over the roof. Therefore, a roof edge is the front-line of defence against wind action. To develop testing standards and design guidelines for roof edges, a project referred as REST (Roof Edge Systems and Technologies) has been initiated in cooperation with the NSERC (Natural Sciences and Engineering Research Council). For the REST project, this thesis contributes in two folds: wind design procedure and the development of an experimental method for testing roof edge components.

The present thesis analyzes the wind load calculation procedures as per the National Building Code of Canada (NBCC) and American Society of Civil Engineers (ASCE). This has been achieved by taking side-by-side cities along Canada-USA border; wind load calculations were performed to demonstrate the differences and similarities between the NBCC and ASCE. As a part of the current contribution, the existing version of the online Wind-RCI Calculator was updated from NBCC2005 to NBCC2010 provisions.

Towards the experimental contribution, the current study presents a new experimental method for testing and evaluating wind uplift resistance of roof edge systems by simulating wind loads in a lab environment on full-scale mock-ups. The test apparatus had a gust

simulator device to mimic wind gusting (dynamic loading). This research investigates three widely used edge systems in North America: Continuous Cleat Configuration (CCC), Discontinuous Cleat Configuration (DCC) and Anchor Clip Configuration (ACC). Preliminary data show that CCC edge system has higher resistance in comparison to DCC and ACC edge systems. The experiments also revealed the need for experimental setup enhancement. Additional investigations by using the enhanced experimental setup were performed on both CCC and DCC edge systems.

Acknowledgments

It is impossible to walk alone on the journey of life, and no one can succeed without the support of those surrounding us. I would to take this opportunity to express my gratitude to all the people who have given their support toward the completion of this thesis.

I would like to express my deep appreciation to *Dr. Appupillai Baskaran*, my supervisor, who has provided me with tremendous guidance during this work. Needless to say that *Dr. Baskaran* has been a source of boundless inspiration and invaluable experience that led this work to succeed. Without his vital encouragement and persistent help this dissertation would not have been possible.

I also would like to express my deep sense of gratitude to *Dr. Beatriz Martin-Perez*, my co-supervisor, for her great support and assistance during the course of this work. Her recommendations and advices significantly contributed to the success of this work.

My warmest thanks go to the great staff of the NRC including Amor, David, Pascal, Suda, Steven and others who helped in operating the facilities and offered a wide range of technical support and academic assistance.

In addition, a big thank-you to the sponsoring companies and organizations who funded this project and provided us with the technical assistance as well as the material necessary for the experimental work.

Besides, I would like to sincerely thank the University of Ottawa, especially my committee members *Dr. Elena Dragomirescu* and *Dr. David Lau* (Carleton University), whose comments and recommendations have been very constructive and helpful.

I owe my heartfelt gratitude to my beloved wife, *Lama*, and my son, *Pierre Karam* for their and endless love and patience. Also, my sincere thanks go to my parents and my brothers for their emotional support and love.

Ottawa, March 2013

Wassim Alassafin

Contents

List of Figures

List of Tables

Glossary

Symbols

P, p	Pressure, external pressure
p_i	Internal pressure
q_{fz}	Field of roof pressure at a height of z
GC_p	External pressure coefficient
GC_{pi}	Internal pressure coefficient
I_w	Importance factor
S	Rating of edge system by RE-1
SF	Safety factor
r	Horizontal distance to first row of fasteners from the edge of the system
F	Applied force
l	Flashing/Coping length
b	Flashing/Coping width
F_h	Horizontal load
F_v	Vertical load
h	Flashing/Coping height
OC	On centre
q	Reference velocity pressure
q_i	Velocity pressure evaluated at the roof's height (or at the highest opening for positive internal pressure)
C_e	External pressure coefficient
C_g	Gust factor
C_{gi}	Internal gust factor
C_p	External pressure coefficient
C_{pi}	External pressure coefficient

C_pC_g	External peak composite pressure-gust coefficient
q_z, q_h	Velocity pressure at height of z or h
K_d	Wind directionality factor
K_z	Velocity pressure exposure coefficient
K_{zt}	Topographic factor
V	Wind speed
V_R	Wind speed corresponding to return period of R
λ	Adjustment factor for height and exposure (ASCE)
p_{net30}	Net design wind pressure for exposure "B" at a height of 9.1 m (30 ft)
RF	Effective area reduction factor
EAF	Exposure adjustment factor
G	Gust-effect factor
C_N	Net pressure coefficient
λ	Exceedance rate (experimental approach)
u	Wind speed threshold
k	number of data points exceeding the threshold u
n_{yr}	length of wind speed record in years
R	Return period
L	Length of test segment of coping
L_d	Length of dummy segment of coping
PT	Test pressure

Abbreviations

AC	Alternating Current
ACC	Anchor Clip Configuration
ANSI	American National Standards Institute
ASCE	American Society of Civil Engineers
CSA	Canadian Standards Association
CCC	Continuous Cleat Configuration
DAQ	Data Acquisition System
DCC	Discontinuous Cleat Configuration
DRF	Dynamic Roofing Facility
Ga	Gauge (Sheet metal thickness)
GPD	General Pareto Distribution
MRI	Mean Recurrence Interval (return period)
NBCC	National Building Code of Canada
NIST	National Institute of Standards and Technologies
NRCC	National Research Council of Canada
NRCA	National Roofing Contractors Association
RCABC	Roofing Contractors Association of British Columbia
REST	Roof Edge Systems and Technologies
RICOWI	Roofing Industry Committee on Weather Issues
RMS	Root Mean Square
SPRI	Single Ply Roofing Industry

Chapter 1. Introduction

1.1 Roofs

A roof is a critical envelope of a building. It provides protection for the building interior against various weather elements, such as snow, rain and wind. Roofs are normally composed of several components such as insulation, barriers and water proofing membrane.

Roofs are divided into two groups: residential and commercial. A residential roof is normally a steep-slope, i.e. the slope is greater than 7˚. On the contrary, commercial buildings employ low-slope roofs where the slope typically ranges from 0˚ to 7˚. Figure 1.1 shows an example of commercial and residential roofs.

(a) Commercial

(b) Residential

Figure 1.1: Commercial and residential roofs

1.2 Roof Edge Systems

A roof edge is perimetric part of a roof that serves as termination for roof components. Generally speaking, a roof edge system is composed of a parapet with metal components, such as coping and cleat/clip. It is the front-line of defence against wind actions, consequently it shares hazard as does the roofing system. Parapets can have various substrates, such as wood, metal, concrete and others. A load transferring metal component, commercially known as "cleat" or "clip" is installed on the parapet's substrate and secured by fasteners or nails. The substrate is then covered by a metal cap along its length; the cap is called coping. The coping is typically secured by using metal clips/cleats through various arrangements such as clamping or snap-on. Various roof edge system types are available, and most of them share similar structural components. Figure 1.2 shows typical roof edge systems installed on commercial roofs.

Roof edge systems offer three major benefits: aesthetic, protective, and aerodynamic benefits. All three combine to produce a substantial justification behind using roof edge systems:

Aerodynamic Role of the Roof Edge System

In reality, the passage of wind over a roof typically produces negative pressure (suction) across the surface, i.e. uplift forces. The presence of an edge system all around the perimeter of a roof would influence the resulted uplift forces by breaking vortices or eddies of the wind flow. Kopp et al. (2005) found that a roof edge modifies the flow in such a way that the corner vortices of the flow are raised above the roof surface, resulting in lower suction over the roof's surface.

Protective Role of the Roof Edge System

By providing a proper termination for its components, a roofing system is guaranteed a minimum level of protection against most common wind-triggered problems, including wind uplifts. The resulted wind uplift forces affect the coverings of the roof system such that a poorly finished or unfinished roof edge would lead to a weaker roofing system. In additions, the threat of water intrusion becomes greater in the absence of a properly designed and constructed roof edge system which blocks any water intrusion path through the roof components.

Aesthetic Role of Roof the Edge System

The presence of finished edges all around the roof of a building contributes to an attractive appearance. An edge system should properly cover the transitional zone between the roof and the wall such that none of the roof layers is visible.

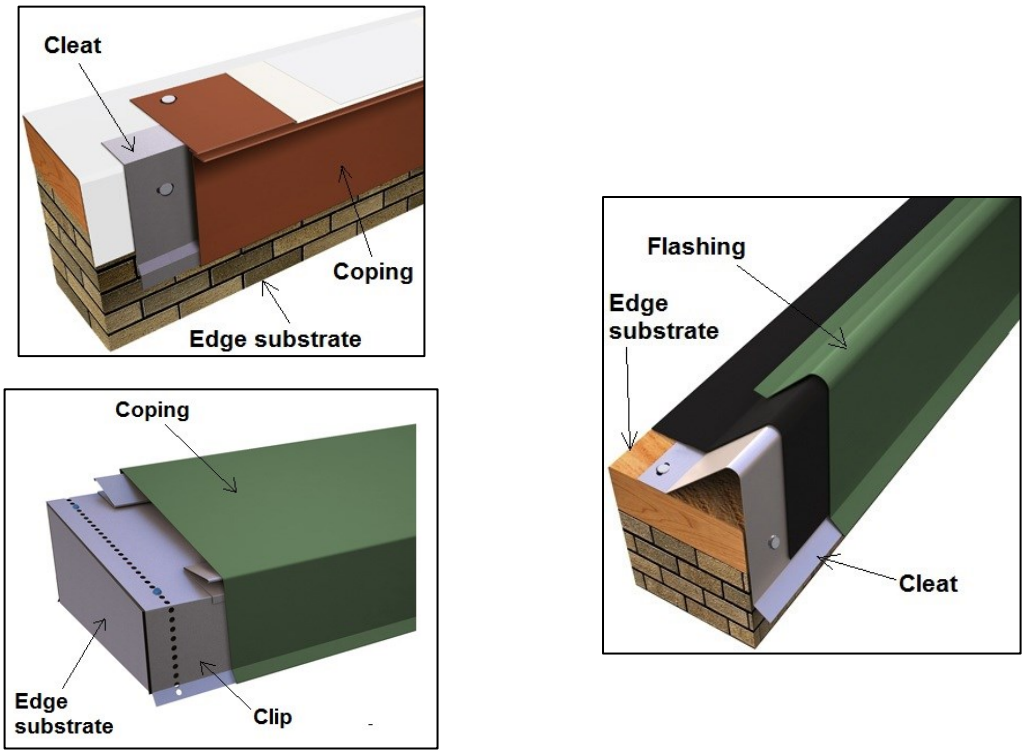

Figure 1.2: Typical roof edge systems installed on commercial roofs

1.3 Wind Performance of Roof Edge Systems

As a consequence of wind flow over the roof of a building, the roof edge system is subjected to negative pressure (suction) which acts on the surface of the edge's coping. Thus, the roof edge components should be designed such that they withstand the resulted loads. Due to the complex wind integration between its components, a roof edge system may be difficult to be designed analytically. Rather, it can be evaluated by testing full scale mock-ups representing the actual roof edge system. The observed strength of a roof edge system must be equal to or greater than the design wind loads to ensure a satisfactory performance and long term reliability.

1.4 Roof Edge Systems and Technologies Project (REST) - Overview

Roof edge systems include their components and interface with the whole roof assembly as well as the technologies related to the design tools and test procedures. Investigations of recent hurricane effects (Charley, Katrina and Ike) identified major failures of roof edge systems (Baskaran et al., 2007). In fact, evidence observed during and after strong wind events suggests that actual wind loads on roof edges are not properly accounted for by current standards. To develop a testing and design guidelines for roof edges, a project referred as REST (Roof Edge Technologies and Systems) has been initiated in cooperation with NSERC (Natural Sciences and Engineering Research Council). Project partners are the Department of Civil Engineering of the University of Ottawa, the National Research Council of Canada (NRCC) and members of the Canadian Roofing Industry (Firestone Building Products, Menzies Metal Products, Soprema Inc. and RCABC together

with in-kind contributors JRS Engineering Group and Metal-Era). The REST project includes the following tasks:

TASK 1: Experimental Investigation of:

1.1 Components of Roof Edge Systems

1.2 Roof Edge Systems (Interaction with roofing systems)

1.3 In-Situ Roof Edge Systems

TASK 2: Formulation of a numerical model by using finite element analysis.

TASK 3: Development of wind design guide and standards.

The present thesis includes the achievements under Task 1.1.

1.5 Research Objectives of the Present Study

The main objectives of the research include:

1. Presenting a detailed review of the major wind load provisions in North America, namely the National Building Code of Canada (NBCC) and American Society of Civil Engineers Code (ASCE).
2. Updating the existing online Wind-RCI Calculator with the latest version of NBCC (2010). Wind-RCI Calculator is a web-based tool for calculating wind design loads on roof components and claddings in accordance with the NBCC provision.
3. Under Task 1, this study was intended for developing an experimental method to evaluate wind resistance of roof edge components. The evaluation is based on subjecting full scale edge systems to dynamic loading in a lab environment. Roof edge

configurations that are most commercially used in the roofing industry were investigated by this research.

1.6 Dissertation Outlines

Including this chapter, this section draws a summary of the rest of the thesis chapters, as follows:

Chapter 2 contains a literature review of most recent studies and reports in the field of wind performance of roof edge systems.

Chapter 3 includes a critical review of the NBCC and ASCE codes in terms of wind load calculation procedures for roof claddings and components. In addition, this chapter shows the process of updating the existing version of the online Wind-RCI Calculator with the latest version of the NBCC.

Chapter 4 discusses the experimental methodology and setup of the developed experimental method, including the installation process of the tested edge systems, instrumentation setup as well as simulated test protocols for wind loading.

Chapter 5 presents and discusses the experimental results of the tested edge systems subjected to static and dynamic wind load in a lab environment. Further, side-by-side performance comparisons of the three most commercially used roof edge systems (CCC, DCC and ACC) were completed to understand the pros and cons of each one of them. In addition, the term "Rigidity Index" was also proposed and analysed as an indication of the edge system reliability.

Chapter 6 presents the lessons learnt in the development of the experimental setup. It offers enhancement to the developed experimental setup to identify the weakest link in the system. In addition, limited edge systems were also investigated by using the enhanced experimental setup.

Chapter 7 concludes and summarizes the research achievements as well as the suggested recommendations for future research.

Chapter 2. Literature Review

Introduction

High wind activities have dramatically increased due to enormous climate and environmental changes the earth has been undergoing. Consequently, in the last few decades, several hurricanes and tornadoes caused extensive destruction and damage.

During wind action, a roof system is exposed to negative pressure which varies in magnitude depending on the intensity of the storm. As a result, the roofing system can fail if the load exceeds the design resistance of the roof. Related reports show that 60% of the building losses were caused by failure due to roof damage (ANSI/SPRI/FM, 2011). Wind-induce damage can be triggered if significant damage occurs to the roof edge system which surrounds a building's roof and protects its components. In other words, when a roof edge fails, the roofing system becomes more susceptible to vital damage. Hence, that may lead to component failure resulting in structural failure of the roof or even the building as whole. Furthermore, a roof edge will effectively contribute to a strong roofing system only by withstanding the wind loads acting on it.

This chapter reviews wind performance of roof edge systems under wind action and the distribution of wind pressure on an edge's surface. Also, the chapter includes a review of the existing method for designing and evaluating roof edge systems against wind loads. The discussion is supported by reviewing a case study about wind-induced damage to roof edge systems and possible enhancements for a better performance.

2.1 Wind Pressure Distribution on Edge Flashings

An edge as a structure is the first line of defence against wind action. In order for an edge to be able to resist wind loads during its service life, it should be structurally stable. That is to say, edge components shall be properly designed and installed. As for the roof edge design, the nature of wind loads acting on roof edge components needs to be identified as a part of the design process.

McDonald et al. (1997) conducted a set of wind tunnel tests at the Texas Tech Wind Engineering Research Field Laboratory (WERFL). They presented a study on a typical full-scale roof edge flashing to determine how wind pressure distributes over the flashing's surface under a direct attack of wind at different angles. The flashing was installed on the edge of a test building that is shown in Figure 2.1 (a). The roof edge flashing geometry is illustrated in Figure 2.1 (b). Metal thickness and component attachment were of no interest since the study was intended for pressure measurements. Five pressure taps were installed over the height of the flashing, in addition to one at its top (Figure 2.1 (c)). Pressure data were collected in form of 15-min data runs at a sampling rate of 30 samples per second.

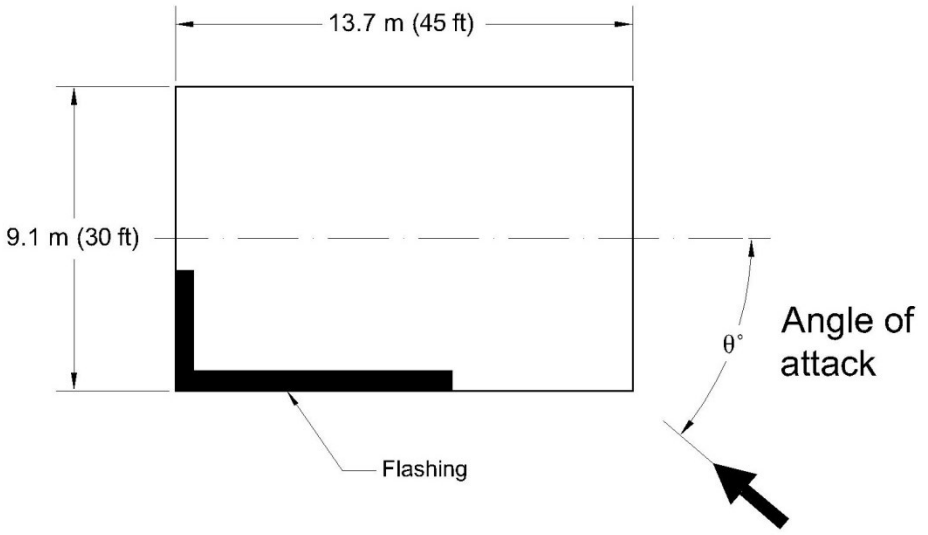

(a) Building plan and location of roof edge flashing

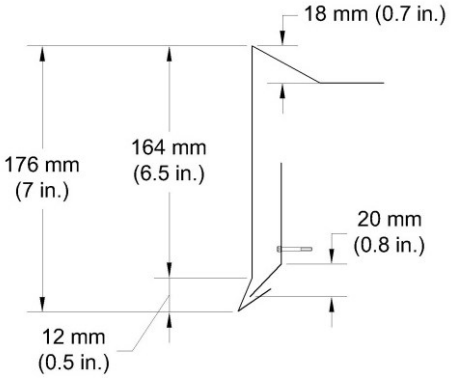

(b) Roof edge flashing geometry

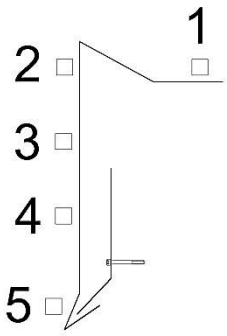

(c) Pressure tap locations

Figure 2.1: Roof edge flashings for field investigation (McDonald et al., 1997)

They found that the worst wind load combination occurred in the windward direction, where the airflow perpendicularly hit the flashing. The pressure readings were converted

to pressure coefficients. Table 2.1 shows the mean, maximum, minimum and root mean square (RMS) of the pressure coefficients collected at the five pressure taps.

Table 2.1: Pressure coefficients at installed pressure taps (McDonald et al., 1997)

Tap	Mean	Maximum	Minimum	RMS
1	-0.92	0.04	-3.67	0.339
2	-0.32	0.55	-1.71	0.178
3	-0.06	1.07	-1.47	0.215
4	-0.14	1.15	-1.70	0.255
5	-0.27	0.85	-1.88	0.224

Apart from the positive values, the negative pressure coefficients indicated that the flashing was mainly exposed to negative pressure (suction). The pressure reached its maximum absolute value on the top of the flashing. It was also noted that minimum and RMS values of pressure were fairly constant along the flashing's height.

Jiang (1995) used the same building for investigating different flashing configurations (Figure 2.2). The plan of the test building and the flashing locations are shown in Figure 2.3. He mainly used cleated and un-cleated flashings located at different roof edge zones (i.e. perimeter and corner). The aim was to draw a profile of the pressure distribution over the flashings' surface. For this purpose, each flashing configuration was investigated at three different angles of attack: windward, leeward and parallel. Quartering winds were also considered for the corner flashing. Several pressure taps were installed on each flashing's surface in order to calculate the external pressure coefficients. In addition, some pressure taps were installed underneath the flashing to measure the internal

pressure coefficients. The pressure coefficients were calculated by using several data runs from the pressure taps. Only the mean pressure coefficients were of interest since they tended to be more stable about which fluctuations normally occur.

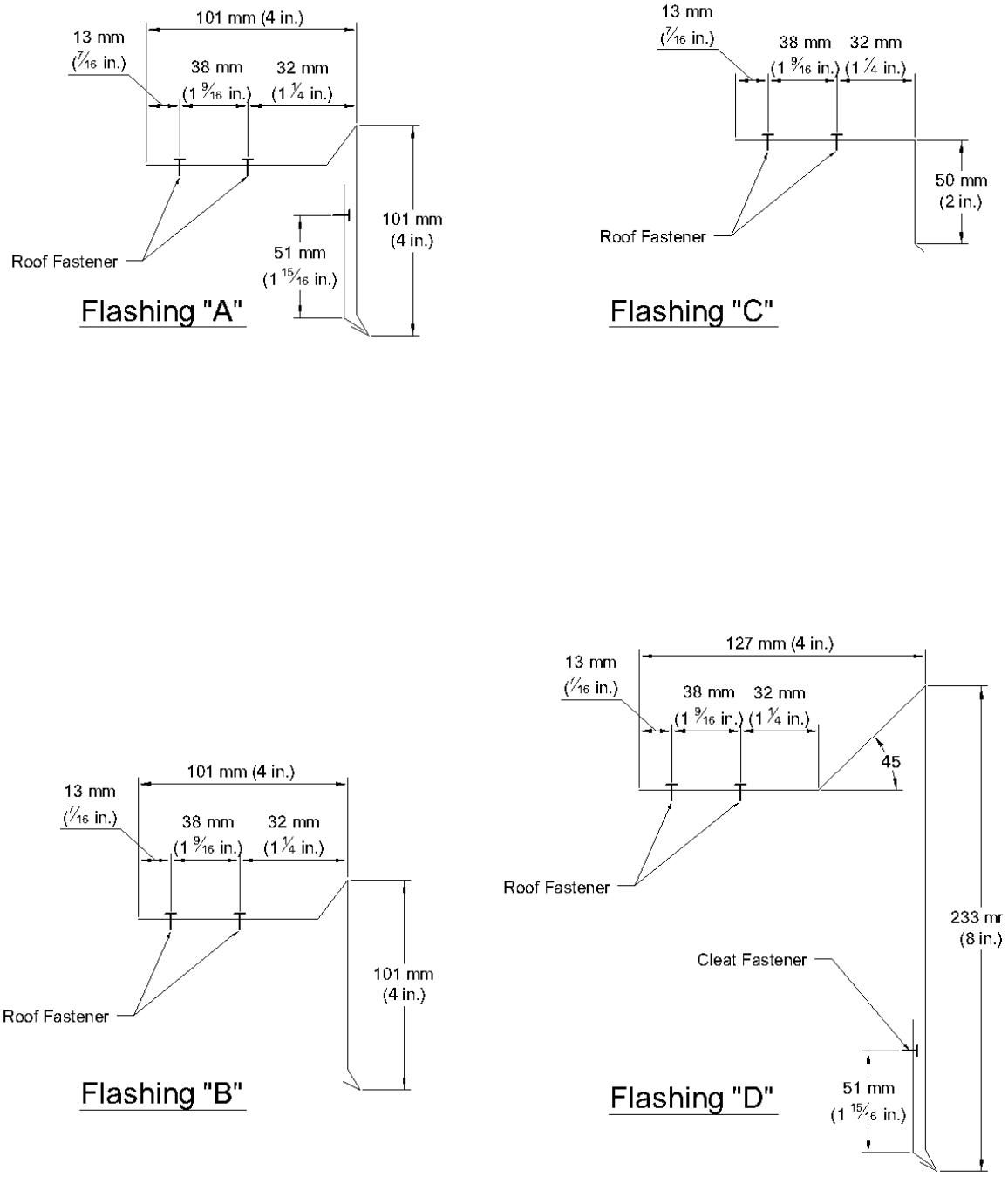

Figure 2.2: Roof edge flashing geometry (Jiang, 1995)

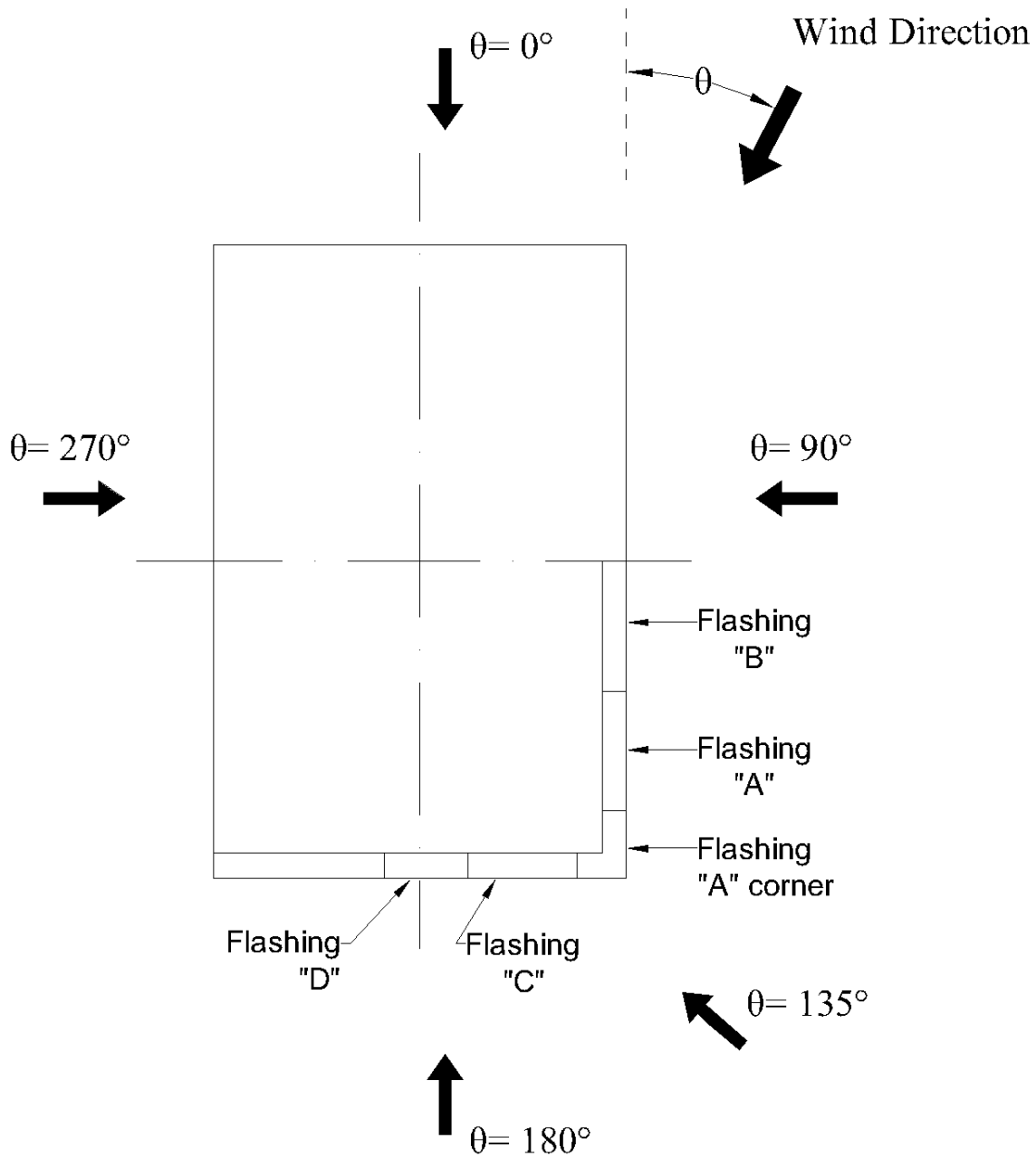

Figure 2.3: Test building plan and flashing locations (Jiang, 1995)

Eventually, Jiang could produce several plots showing the pressure distribution profile of each of the installed flashings. Figure 2.4 illustrates an example of the pressure distribution plots obtained.

Based on the presented papers, two factors were observed to affect the results:

1. **Wind direction.** Windward wind and quartering wind generally produced the highest negative pressure on all flashing configurations.
2. **Flashing's geometry.** The flashing with the least face height was exposed to the highest negative pressure from the windward direction.

Pressure measurements also showed that internal positive pressure was present underneath the flashing. Internal pressure, in this case, indicated that the flashings were subjected to forces acting on their inner surface (pushing), resulting in even higher outward forces.

The foregoing findings reveal that an edge generally experiences negative pressure (suction) when exposed to wind flow. Furthermore, the highest pressure would be caused by windward and quartering winds. The shape of the flashing was observed to have an effect on the pressure magnitude, where the pressure was found to be higher for smaller flashings.

The available literature offers pressure coefficient analysis for the tested roof edges, which is not sufficient to identify neither the ultimate resistance nor the performance at failure. Such information can be obtained only through experimental testing for roof edge components by simulating wind loads. The next section discusses the ANSI/SPRI/FM/ES-1 Standard which offers an experimental procedure to rate edge systems.

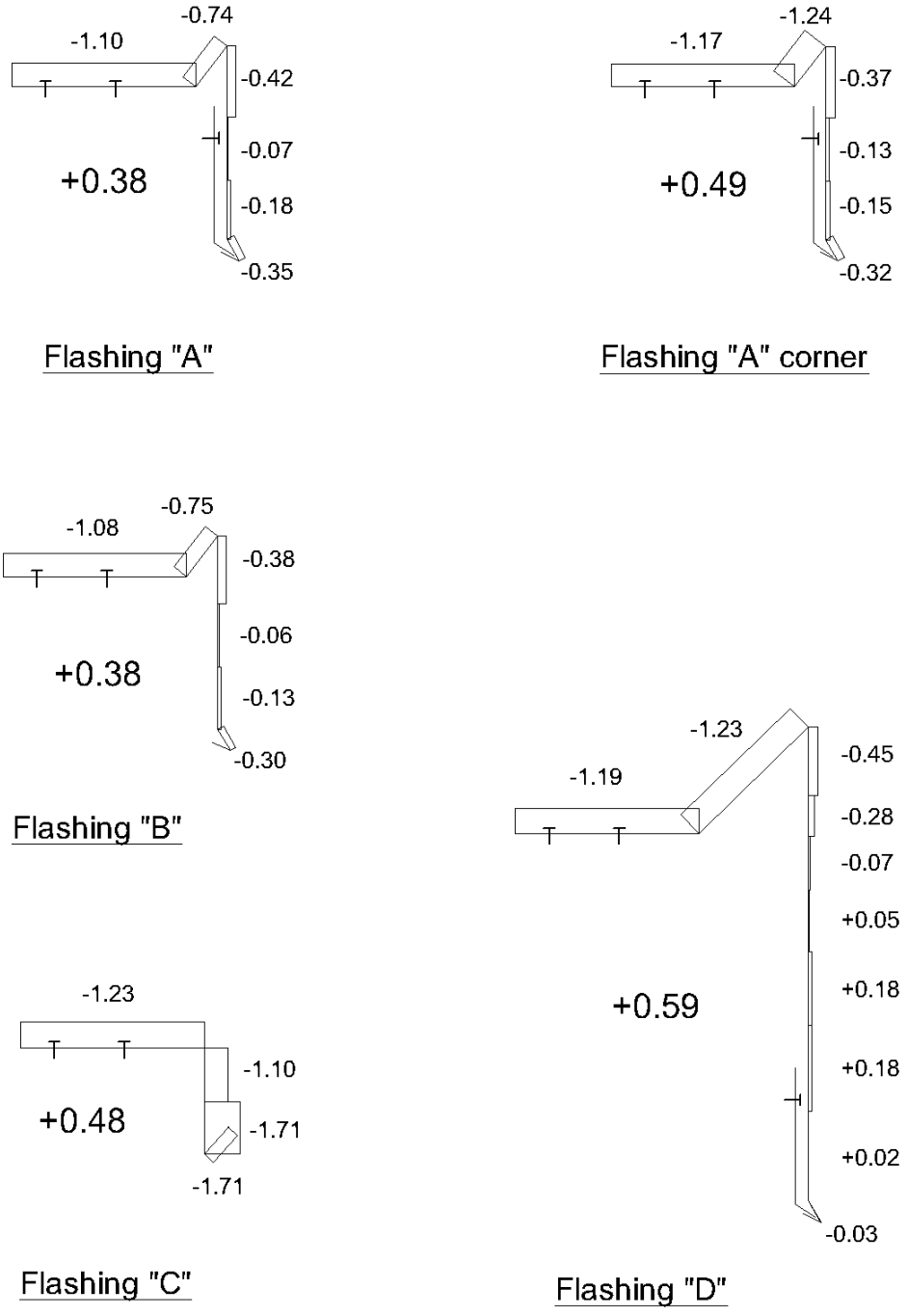

Figure 2.4: Internal/external mean pressure coefficients at windward direction (Jiang, 1995)

2.2 Roof Edge Resistance Evaluation as per ANSI/SPRI/FM/ES-1

Building codes do not deal with wind design for roof edge systems; however, a code-based method for designing and testing roof edge component is available. ANSI/SPRI/FM4435/ES-1 is the only standard available for this purpose. It is composed of two parts: Wind Design of Edge Systems and Edge System Testing. The first part is a guide for calculating design wind loads on roof edges of low-slope roofs, whereas the second part specifies the minimum requirements for roof edge systems based on a test approach. Nevertheless, in Canada, there is no design guide for roof edge systems.

As per ANSI/SPRI/FM 4435/ES-1, the wind load acting vertically/horizontally on a roof edge is calculated by using the following equation:

$$P = 2.0 \times q_{fz} \times GC_p \times I \quad (2.1)$$

where: 2.0 = Design factor

q_{fz}= Field of roof pressure at height z

GC_p= External pressure coefficient

I = Importance factor

The equation parameters are explained and discussed in the ANSI/SPRI/FM4435/ES-1 standard.

2.2.1 Roof Edge Component Testing

The wind loads calculated during the design stage are verified by testing the edge system being considered, using a set of tests presented in ANSI/SPRI/FM4435/ES-1. A full scale specimen should be tested by the three tests: RE-1, RE-2 and RE-3. Each part is discussed and described below:

2.2.1.1 RE-1

Blowing winds over the surface of a roof produces negative pressure across the roof's surface, causing the covering membrane to balloon (deform). Consequently, the resulted tension in the membrane tends to take the flashing/coping off the edge substrate. RE-1 test is intended for simulating this effect to ensure that the edge is capable of resisting the respected tension. This test applies only to mechanically attached systems or ballasted systems with no peel stop within a distance of 305 mm (12 in.) of the roof edge.

Specimen Preparation and Test Performance

The specimen (membrane and edge) should contain at least three attachment fasteners at the design spacing or is 915 mm (3 ft) in length, whichever is greater. As for the test performance, the membrane is pulled at an angle of 25˚ at a constant rate of 50 mm/min (2 in./min). The test is stopped when the membrane or any other components of the edge come off (structural failure). Figure 2.5 shows a schematic drawing of the RE-1 test.

Test Results

The rating of the tested system equals the load recorded at failure for a 305 mm (12 in.) wide sample. The system's rating shall be equal to or less than the calculated design load which is given by the following formula:

$$S = SF \times 2.37 \times q_{fz} GC_p \frac{r}{2}$$

where: SF = Safety factor (the default value is 2.00)

r = Horizontal distance to first row of fasteners from the edge of the system

q_z = Field of roof pressure at height z

GC_p = External pressure coefficient

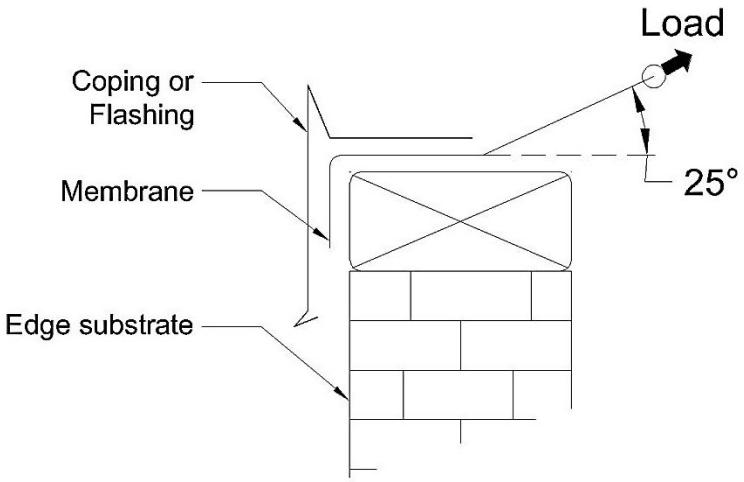

Figure 2.5: Schematic drawing of ES-1/RE-1 test

2.2.1.2 RE-2

As indicated in Section 2.1, the surface of a roof edge flashing/coping normally experiences negative pressure (suction) regardless of the wind direction. The RE-2 test is designed for simulating the wind-induced suction on the face of roof edge systems to ensure a proper resistance. This test is applicable if the width of the exposed horizontal flashing/coping's face equals 4 in. (100 mm) or less.

Specimen Preparation and Test Performance

The test requires the edge being tested to be at least 2.4 m (8 ft) long. Technically, the load is applied by using a set of pistons and chains mounted against the edge such that the pistons uniformly pull on the vertical face of the coping/flashing within 300 mm (12 in.) of its centerline. The loading is applied incrementally such that it is completely released in between the incremental loads until the sample comes to a complete rest. Up to half of the expected failure, the load should be applied at a fixed increment of 120 kg/m^2 (25 psf). However, past half of the expected failure, the incremental load must not exceed

50 kg/m^2 (10 psf). The load should be reached in a maximum of 60 seconds up to 7.2 kPa (150 psf) and in a maximum of 120 seconds beyond that. Figure 2.6 and Figure 2.7 show a schematic drawing of RE-2 test and the ES-1 test protocol, respectively.

Test Results

Similar to RE-1, the rating of the edge system is equal to the maximum incremental load recorded prior to failure. Failure can be identified by any type of edge component failure, such as disengagement of a component, loss of securement, significant deformations leading to poor weather protection, or any combination of them.

The applied load is calculated using the following equation:

$$P = \frac{Outward\ Force}{Face\ Height \times Face\ Length}$$

The obtained rating must be equal to or greater than the design load calculated by (2.1).

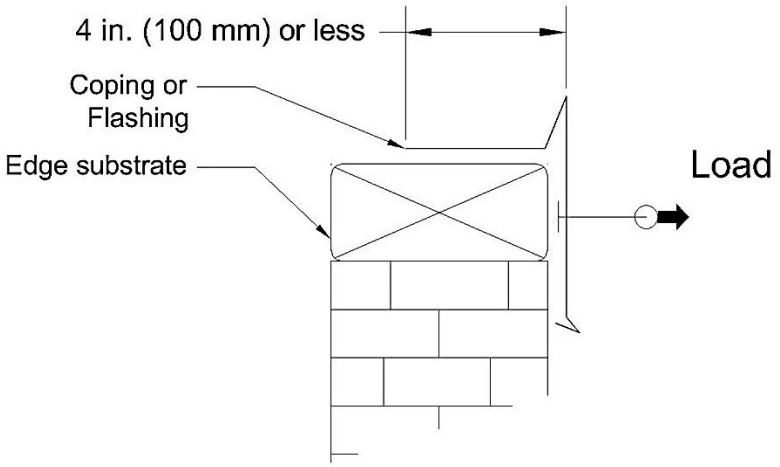

Figure 2.6: Schematic drawing of ES-1/RE-2 test

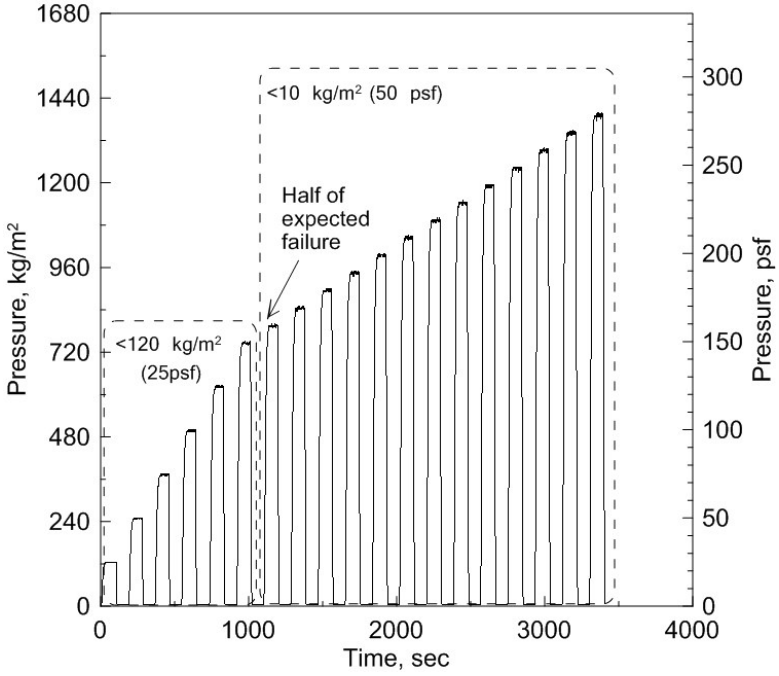

Figure 2.7: ES-1 test protocol

2.2.1.3 RE-3

Unlike RE-2, RE-3 test is intended for simulating wind loads acting on both horizontal and vertical face of a roof edge simultaneously. The loading is also applied by using pistons and chains such that they pull on the edge vertically and horizontally at the same time.

Specimen Preparation and Test Performance

The edge is prepared similar to what is followed in RE-2. However, the horizontal and vertical load components shall be applied simultaneously. The test requires both load components to maintain a ratio of $\frac{F_h}{F_v} = \frac{h \times GC_{p,h}}{b \times GC_{p,v}}$ throughout the test process, where F_h= Horizontal load; F_v= Vertical load; $GC_{p,h}$=Horizontal external pressure coefficient; and

$GC_{p,v}$= Vertical external pressure coefficient. Same loading protocol is followed as shown in Figure 2.7. A schematic drawing of RE-3 test is shown in Figure 2.8.

Test Results

The same failure criteria of RE-2 test apply to RE-3 test. The system is given a rating based on both directions that is the maximum incremental load recorded prior to failure. The rating of the system must be equal to or greater than both the horizontal and vertical design loads.

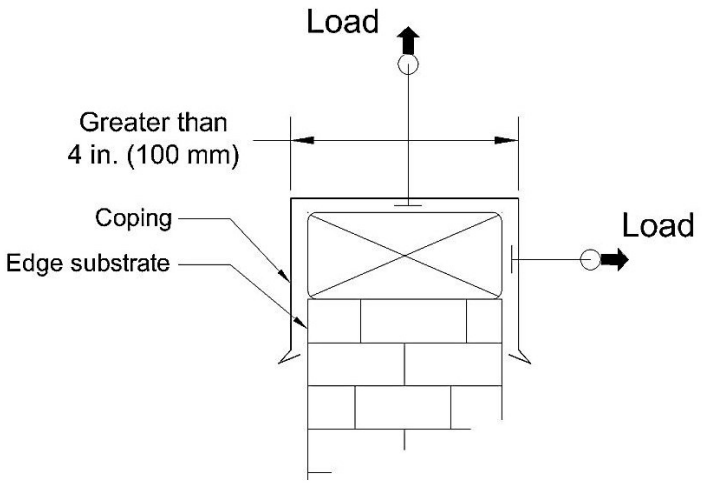

Figure 2.8: Schematic drawing of ES-1/RE-3 test

Example: *A partially enclosed 18.3 m (60 ft) high building, with low-slope roof and edged perimeter, is located in a suburban area in Seattle, USA. The building is categorized under Risk Category II. The expected wind loads on the edge metal flashing/coping are calculated as follows:*

Category II $\rightarrow I = 1.00$ *(Table A1, Appendix A of ANSI/SPRI/FM4435/ES-1)*

Suburban Area $\rightarrow$ *Exposure Category "B"(Table 1 of ANSI/SPRI/FM4435/ES-1)*

Seattle $\rightarrow V = 38.25$ *m/sec (85 mph) (Wind Speed Map of ASCE 7-05)*

Table A2 and partially enclosed $\rightarrow q_{fz} = 1.3 \times 0.89 = 1.16\ kPa\ (24.18\ psf)$

$GC_p \rightarrow$

	Corner	Perimeter
Horizontal	-1.13	-0.95
Vertical	-2.16	-1.52

By applying Equation 2.1, the estimated wind loads will be as follows:

Table 2.2: Example of calculating design wind loads by ANSI/SPRI/FM4435/ES-1

	Corner *kPa (psf)*	Perimeter *kPa (psf)*
Horizontal (Acting outward)	2.62 (55)	2.20 (46)
Vertical (Acting upward)	5.00 (105)	3.52 (74)

In this example, the installed edge systems should have a resistance (rating) equal to or greater than design loads shown in Table 2.2 in order to ensure satisfactory performance.

2.2.2 Observations of ES-1 Test Method

Based on the foregoing review of the ES-1 test method, a number of observations, that represent the main criticism about this test method, are presented as follows:

1. The ES-1 test simulates wind loads by using **mechanical, concentrated forces** produced by pistons and chains. On the contrary, wind flow produces **pressure** which distributes across the surface of a roof edge.

2. The ES-1 uses a test protocol that lacks the simulation of the **dynamic nature** of wind, where wind typically acts in form of loading/unloading cycles at various magnitudes.
3. Since ES-1 test does not simulate cyclic loading, it cannot measure **fatigue**. The presence of dynamic loading is necessary to include the fatigue factor in the evaluation process.

Further discussion will be found in Table 2.3.

2.3 Field Case Study

As a part of a report submitted to the Roofing Industry Committee on Weather Issues (RICOWI), LeClare (2010) presented a case study on roof edge damage caused by Hurricane Ike. The study included a detailed review of typical roof edge systems and their performance on wind loads. Additionally, the study suggested improvements to the installed roof edges, where the proposed improvements were further verified by ES-1 test results.

2.3.1 Effect of Cleat (Case 1)

LeClare conducted a field investigation for roof edge flashings installed on a 6 m (20 ft) high building. At the location of the building, the maximum wind speed recorded was 45 m/s (100 mph) which was below the design wind speed specified by the ASCE7-05. Figure 2.9 (a) illustrates the installed roof edge flashing. Further, as Figure 2.9 (b) depicts, the installed flashing was tested as per ES-1/ RE-2 test, which yielded unsatisfactory results as the flashing failed at very low load.

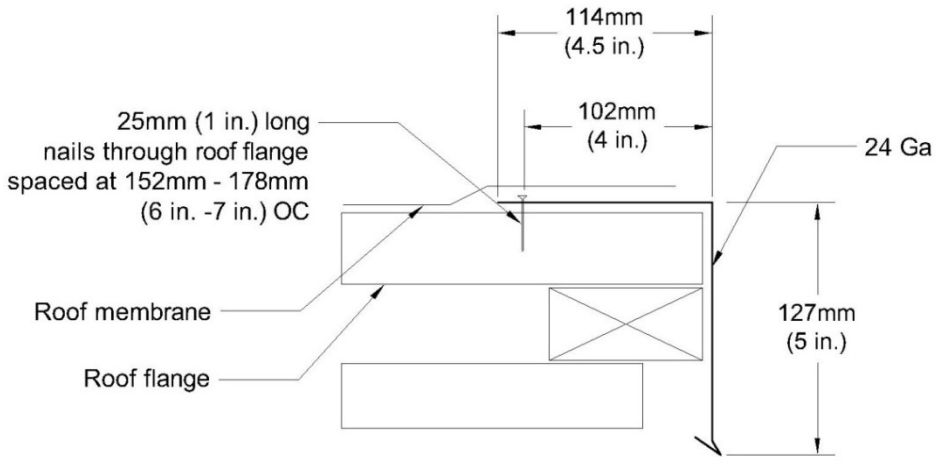

(a) Geometry of installed roof edge flashing (Ga. is a unit for sheet metal thickness)

(b) ES-1 test for the installed roof edge flashing

Figure 2.9: Installed roof edge flashing- Case 1 (LeClare, 2010)

As shown in Figure 2.10 (a) and (b), the installed edge eventually failed, where the metal flashing fully disengaged from the edge substrate. That is attributed to the absence of a cleat for securing the flashing. Moreover, the edge substrate itself partially collapsed due

to poor construction and securement, where the top plywood board was fastened by six fasteners per 20 mm (8 in.).

(a) Un-cleated edge flashing peeled off the edge

(b) Failure of edge flashing

Figure 2.10: Damage to installed roof edge flashing- Case 1 (LeClare, 2010)

Suggested Improvements to the Installed Roof Edge Flashing

As shown in Figure 2.11 (a), the report suggested the installation of a 22 Ga continuous cleat secured by 38 mm (1.5 in.) long fasteners with a spacing of 305 mm (12 in.). The top wood nailer was secured by 72 mm (3 in.) long fasteners spaced at 406 mm (16 in.). The improved flashing was further tested by ES-1/RE-2, and its rating was 20.6 kPa (430 psf); see Figure 2.11 (b).

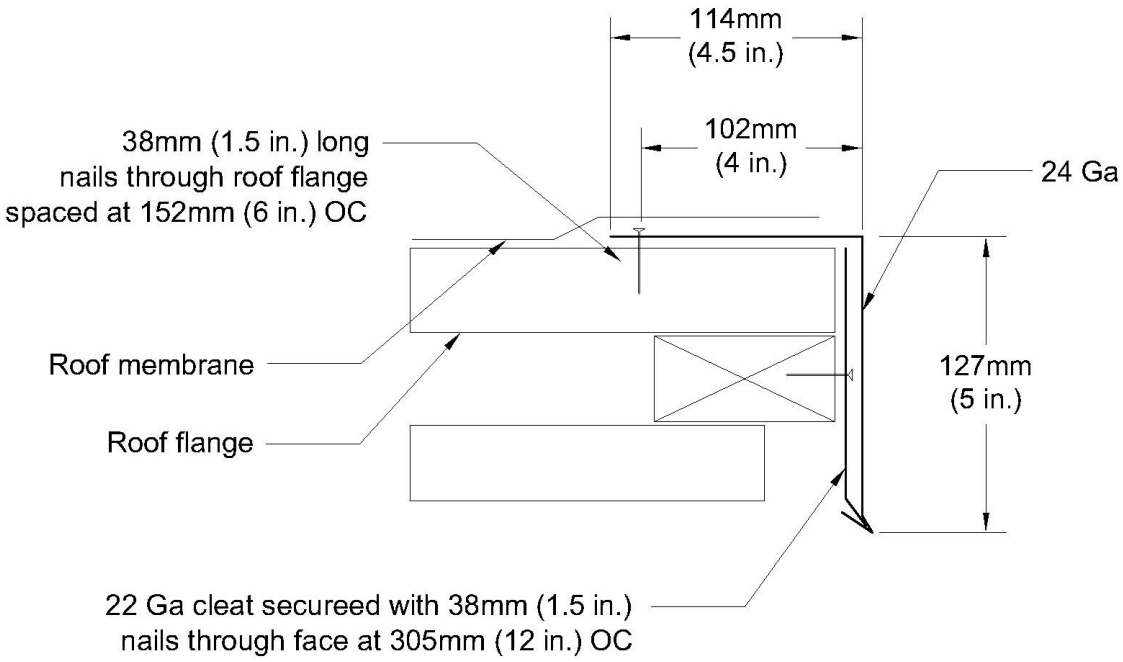

(a) Geometry of improved roof edge flashing

(b) ES-1 test for improved roof edge flashing: failed at 20.6 kPa (430 psf)

Figure 2.11: Improved roof edge flashing- Case 1 (LeClare, 2010)

This case demonstrated that the installed flashing performed unsatisfactorily when subjected to wind loads lower than those specified by the code. This observation was further supported by the ES-1 test results. The inclusion of the continuous cleat considerably showed better resistance. Thus, the presence of a cleat was found to be essential in order to reach the required resistance against the design wind loads.

2.3.2 Effect of Cleat Securement and Metal Thickness (Case 2)

The report also investigated roof edge flashings installed on an 8.25 m (27 ft.) high building located in an area where the maximum wind speed recorded was 40 m/sec (90 mph). The design wind speed was 49 m/sec (110 mph) as specified by the ASCE7-05. The geometry of the installed roof edge flashing is shown in Figure 2.12 (a). The installed edge was tested by ES-1/RE-2, and the rating was 1.87 kPa (39 psf).

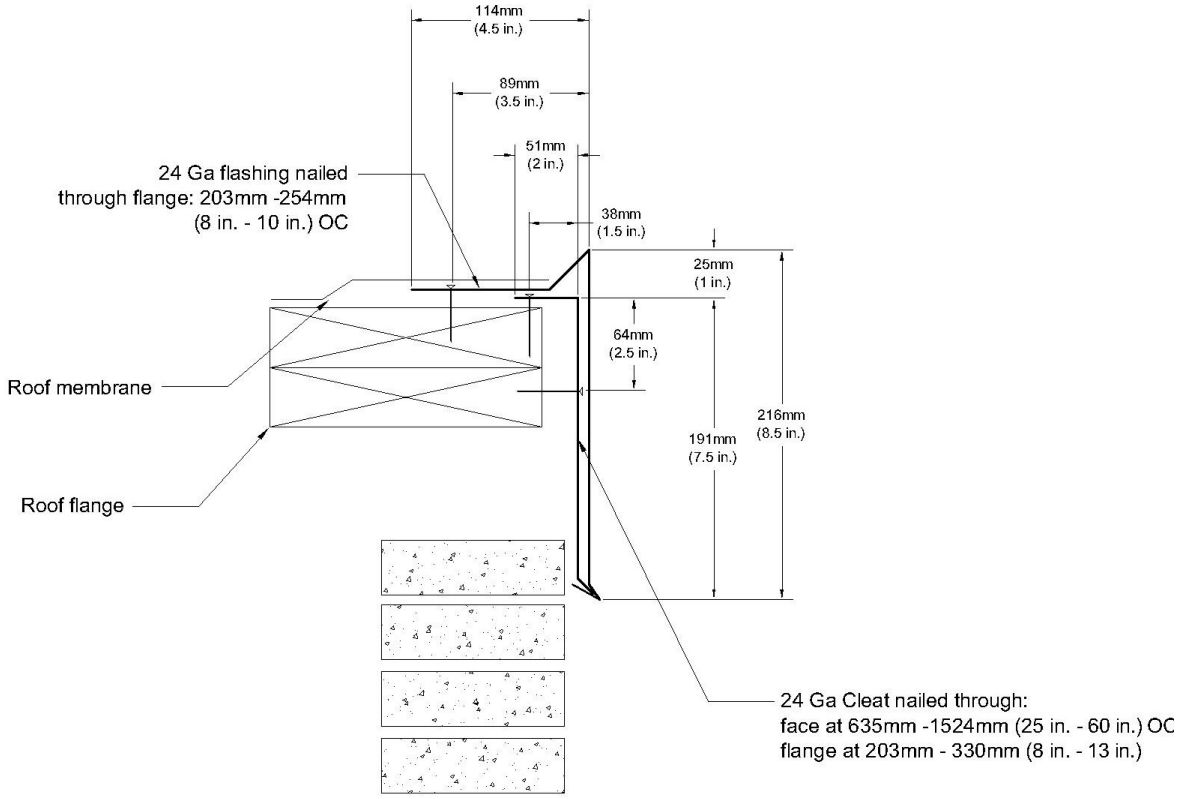

(a) Geometry of installed roof edge flashing

(b) ES-1 test for installed roof edge flashing: failed at 1.87 kPa (39 psf)

Figure 2.12: Installed roof edge flashing- Case 2 (LeClare, 2010)

As shown in Figure 2.13 (a) and (b), edge failure occurred as the flashing disengaged from the cleat as a consequence of severe cleat rotations due to the use of a light gauge (24 Ga) and poor securement. At other locations of the roof edge, a complete separation of the cleat from the wood nailer was observed. In addition, the wood nailer was not flush with the cleat, contributing to even poorer securement and weaker system.

(a) Flashing disengaged from cleat

(b) Cleat came off the edge substrate

Figure 2.13: Damage to installed roof edge flashing- Case 2 (LeClare, 2010)

Suggested Improvements to the Installed Roof Edge Flashing

As Figure 2.14 (a) shows, the edge system was improved by increasing the gauge of both the flashing and cleat from 24 Ga to 22 Ga. Moreover, the cleat was further secured with additional nails at the top and bottom. The wood nailer was also made flush with the edge by filling the installed gap. The improved flashing was rated at 5.50 kPa (115 psf) as per ES-1 test; see Figure 2.14 (b).

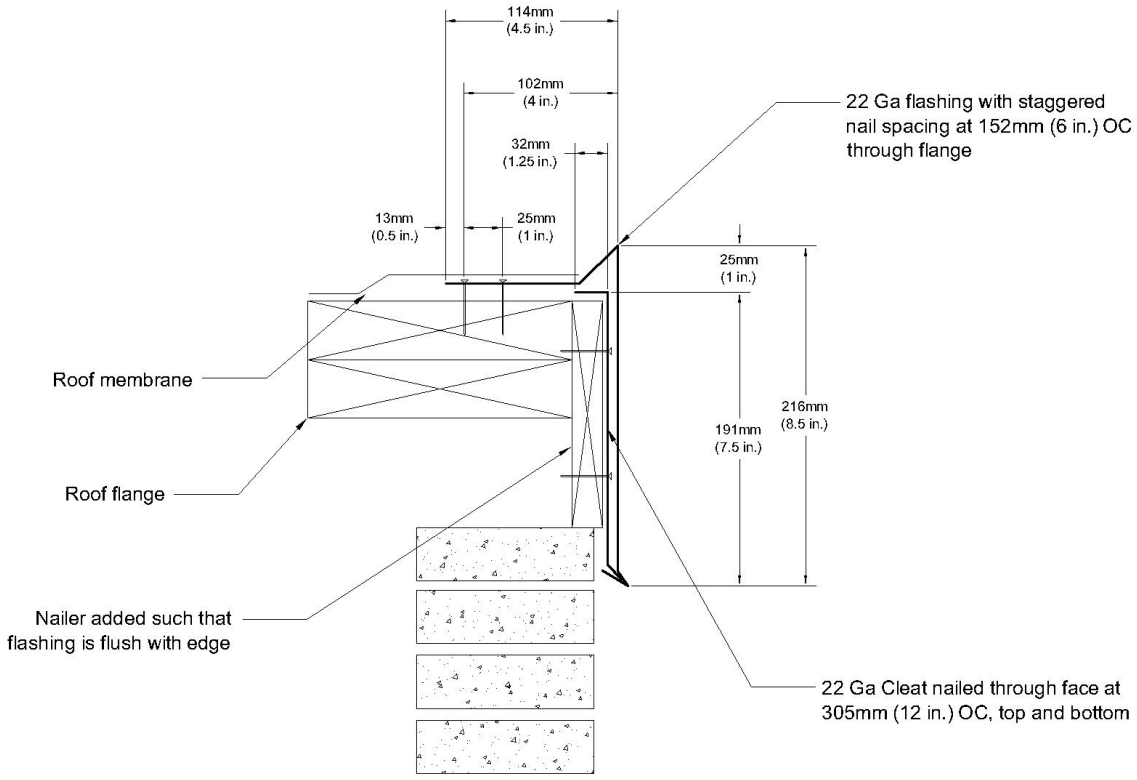

(a) Geometry of improved roof edge flashing

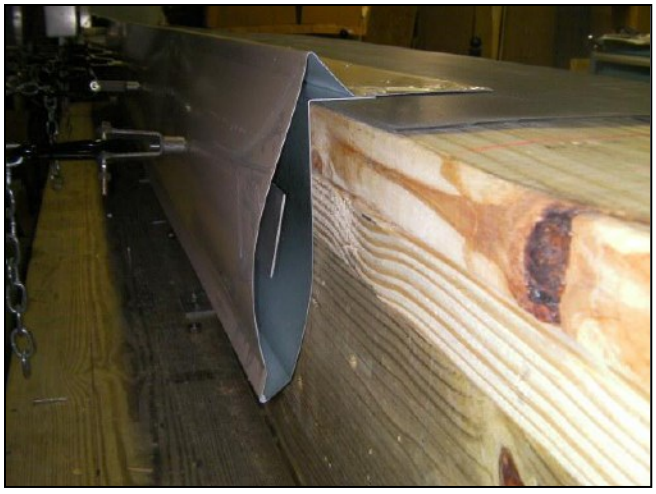

(b) ES-1 test for improved roof edge flashing: failed at 5.50 kPa (115 psf)

Figure 2.14: Improved roof edge flashing- Case 2 (LeClare, 2010)

This case showed that light gauge metal greatly contributed to the weakness of the edge system, where severe deformations and rotations were observed for both the flashing and cleat. Furthermore, the poorly secured cleat was found to be a primary cause of premature failure. The poor construction was improved by using a heavier gauge and better cleat securement. The improvement showed a greater ES-1 rating compared to that of the installed one. That is to say it is critical to use an appropriate metal gauge and proper securement of the components in order to avoid premature wind-induced failure and to maintain satisfactory performance.

Any attempt for developing a method for testing roof edge components should take into consideration the observations discussed in Sections 2.1, 2.2 and 2.3. Table 2.3 illustrates these observations and the suggested requirements for such a test method.

Table 2.3: Observations from the existing literature and test requirements

Observation	Test Requirement
Wind has a dynamic nature.	A realistic test shall be able to simulate dynamic/cyclic loading.
Wind loads act in form of pressure that distributes across an edge's surface.	Loading should be applied in form of pressure.
Roof edges are subjected to negative pressure acting on its surface.	Simulating negative pressure on the outer surface.
Positive internal pressure exists underneath flashing	Internal pressure shall be accounted for by including it in the load simulation process.
Roof edge failure can occur as a result of failure of any edge component.	All roof edge components and their attachment should be evaluated.
The shape of the flashing noticeably impacts the pressure magnitude and distribution.	A wide range of roof edge configurations and geometries should be tested, i.e. different heights and shapes, such as gravel stop and cap coping shall be considered in order to acquire trusted results.

2.4 Conclusion

Wind tunnel tests revealed valuable information regarding the nature and distribution of wind loads on roof edge systems. The experimental data indicated that a roof edge typically experiences negative pressure (suction) over its surface regardless of the direction of wind. Furthermore, the ANSI/SPRI/ES-1 was reviewed as a standard for designing and evaluating wind resistance of roof edge systems. The ES-1 test method is criticized for its wind simulation method and the absence of fatigue-based evaluation. The chapter also presented a field case study that demonstrated some field observations for roof edge failures. The study proved the significance of the presence of cleats and proper component

securement. It was also showed that the metal gauge plays a key role in the structural stability and appropriate resistance. In addition, the study suggested possible improvements for the roof edge systems based on ES-1 results in order to enhance their wind performance. Based on the existing literature, a number of suggestions were presented as requirements for an efficient method for testing roof edge systems.

Chapter 3. Wind Load Design for Roof Claddings

Introduction

A proper design for a roof system ensures long-term reliability and minimal repair costs. Thus, an easy-to-use, reliable calculation method will help in facilitating the design process. Roofers and designers use local codes and design manuals to calculate design wind loads. Systematic procedures for calculating wind loads are specified by building codes. In North America, the National Building Code of Canada (NBCC) and American Society of Civil Engineers code (ASCE) are widely used. The discussion is exclusively limited to the code procedures of wind design for roof claddings in NBCC and ASCE. To simplify the NBCC design procedure, an online tool, the Wind-RCI Calculator, is reviewed. In addition, the latest updates for the calculator are discussed. Sample calculations and a parameter discussion of NBCC2010 and ASCE7-10 are included. Further, the chapter presents one of the most common methods for calculating design wind loads based on field data.

3.1 The National Building Code of Canada (NBCC)

The NBCC is the model code in Canada issued by the National Research Council of Canada (NRCC), and it has been adopted by all Canadian provinces with modifications to satisfy local needs.

The first NBCC edition was issued by the federal government of Canada in 1941. Since then, the revisions have been published approximately every five years. The most recent version is NBCC2010; the last four digits stand for the edition year. The NBCC2010 is composed of two volumes:

1. **Volume (1),** including Division A and Division C
2. **Volume (2),** including Division B and the Structural Commentary

3.1.1 Design Wind Load Calculations as per NBCC2010

The NBCC2010 utilizes a straightforward approach for calculating wind loads on roof claddings. It is called the "static approach". The procedure starts with the determination of a number of parameters, some of which are directly affected by the aerodynamics of the considered building, whereas the others depend upon the location of the building.

The calculated parameters are substituted into a design equation to produce the expected value of the external and internal wind pressure. In turn, the design load (pressure) is given by the algebraic sum of the calculated external and internal pressure. The NBCC2010 also provides figures and charts for determining the distribution of the computed loads based on the type of roof. Furthermore, another approach called the "dynamic procedure" is included in the code but not applicable to cladding design. The following is a detailed review of the NBCC2010 design procedure of roof claddings.

External/Internal Pressure Calculations

Roofing systems typically experience two types of pressure: external and internal. The NBCC2010 proposes a simple formula to estimate the design value of the external pressure, as follows:

$$p = I_w . q . C_e . C_g . C_p$$

Similarly, the internal pressure can be computed as follows:

$$p_i = I_w . q . C_e . C_{gi} . C_{pi}$$

The following is a brief description of each parameter:

- **Importance factor I_w** *(Table 4.1.1.1)* is an indicator for the importance level of the building based on factors such as occupancy level and the presence of hazardous materials.
- **Reference velocity pressure q** *(Table C-1)* is a distinct value for various Canadian cities based on 50-year return period.
- **Exposure factor C_e** *(Sentence "5" in 4.1.7.1)* adjusts the reference velocity pressure based on the building's height and terrain roughness.
- **External gust factor C_g** *(Sentence "6" in 4.1.7.1)* accounts for phenomena such as turbulence acting for short durations caused by approaching winds.
- **Internal gust factor C_{gi}** *(Sentence "6" in 4.1.7.1)*
- **External pressure coefficient C_p** is a dimensionless number reflecting the aerodynamic characteristics of the building. The NBCC2010 specifies $C_p$values as combination with C_g values that is called the external peak composite pressure-gust coefficient. The value of this parameter varies depending on the location at which the pressure is calculated (corner, edge or field).
- **Internal pressure coefficient C_{pi}** *(Structural Commentary I – Clause 30).*

External Peak Composite Pressure-Gust Coefficient

The NBCC2010 introduces the external peak composite pressure-gust coefficient (C_pC_g) as a product of the external pressure coefficient and the external gust factor. This product can be extracted from the provided figures that are categorized in accordance with the building's height and roof type:

1. High-rise buildings where the roof's height is 20 m (65 ft) or greater
2. Low-rise buildings where the roof's height is less than 20 m (65 ft). Also low-rise building should satisfy:

$$\frac{h}{w} < 0.5 \; or \; 1.0$$

where h: Height of building's roof

w: Least horizontal dimension of building

The external peak composite pressure-gust coefficient can be found in the structural commentary of the NBCC2010 *(Structural Commentary I: Table 1-2)*.

Net Design Load (Net Pressure)

The net pressure acting on the considered cladding element is computed by algebraically summing the external and internal pressures. As a roof is divided into three zones, corner, edge and field, the net pressure varies for each roof zone ($C_p C_g$ is dependent on the roof zone). In fact, the external pressure has a negative sign (suction), whereas the internal pressure may be positive or negative. Thus, both signs should be considered such that the design load is maximized (worst load combination).

3.1.2 NBCC2010 vs. NBCC2005

As for the wind design procedures for claddings, the NBCC2010 has very few changes over NBCC2005, and those do not affect the algorithm of calculating design wind loads on claddings. A quick overview of these changes is presented as follows:

1. The NBCC2010 requires buildings with height of 60 m (197 ft) or above to be designed by using the dynamic approach. On the other hand, buildings with height of

120 m (394 ft) or above should be design by the dynamic approach based on the NBCC2005

2. The NBCC2010 requires buildings with a natural frequency of 1 Hz or below to be designed by using the dynamic approach. However, the NBCC2005 does not include this requirement.
3. The NBCC2010 requires an experimental design approach for buildings with natural frequency of 0.25 Hz or below, whereas this condition does not exist in the NBCC2005.

Even though the cladding design procedure remains unchanged between the 2005 and 2010 versions, some modifications affect the calculation of design loads due the change in the reference velocity pressure (q). For several cities, the reference velocity pressure was modified, and some new cities were added in the 2010 version. The present study accounted for these changes.

3.1.3 Wind-RCI Calculator on the Internet

3.1.3.1 Software

Baskaran and Smith (2005) published a six-step procedure for calculating wind uplift (load) on claddings and roof coverings based on the NBCC2005. The design procedure was reproduced in form of an online tool called Wind-RCI Calculator (Baskaran et al., 2008). As for the user's interface of the program, the calculator is provided with information about the location, building geometry, exposure category as well as the roof type. Figure 3.1 demonstrates the snapshots of Wind-RCI:

1. **Screen (1): Building Location.** It prompts the user to enter information about the location of the building, i.e. province and city.
2. **Screen (2): Building Geometry.** The user should enter the building's dimensions, including whether the building is high-rise or low-rise.
3. **Screen (3): Roof Type.** Six options are available such as low-slope and gable.
4. **Screen (4): Building Exposure.** The type of terrain of the location is selected, i.e. open or rough terrain.
5. **Screen (5): Building Opening.** One of the three categories must be selected depending on the percentage of the openings on the building.
6. **Screen (6): Importance Category.** The user picks one of the three categories based on the level of importance of the building.

When "Calculate Wind Loads" button is selected, the Wind-RCI produces a report including a summary of the input data and a diagram of the roof zones with the wind uplift (pressure) values, i.e. edge, corner, and field. (Figure 3.2).

(a) Building location

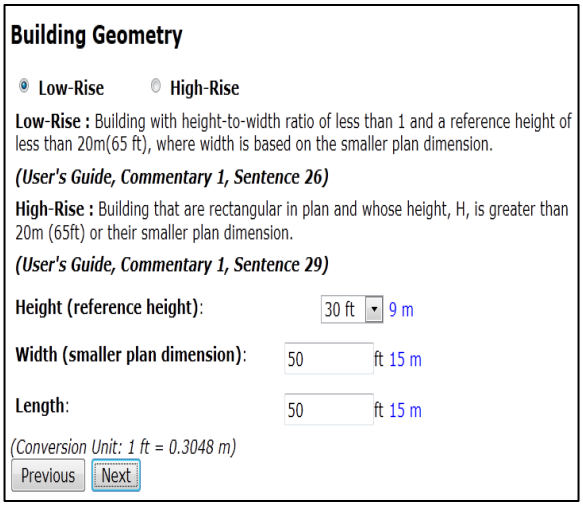

(b) Building geometry

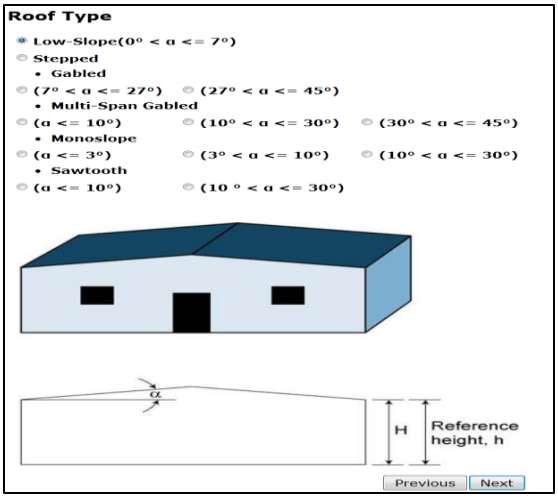

(c) Roof type

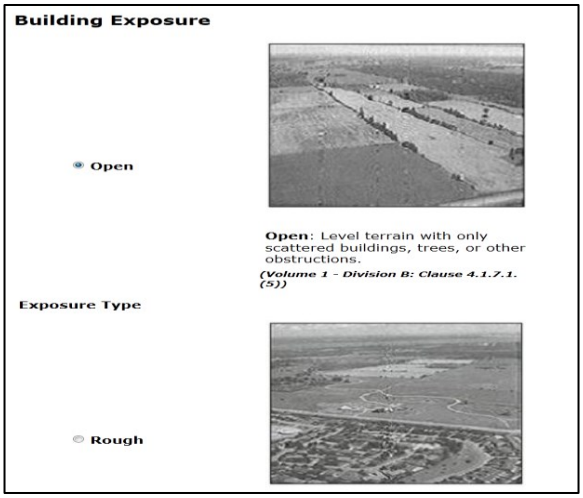

(d) Building exposure

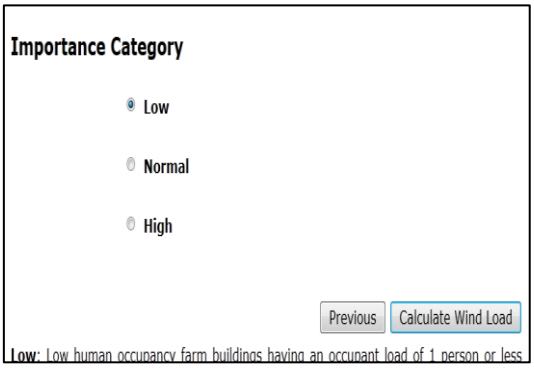

(e) Importance category

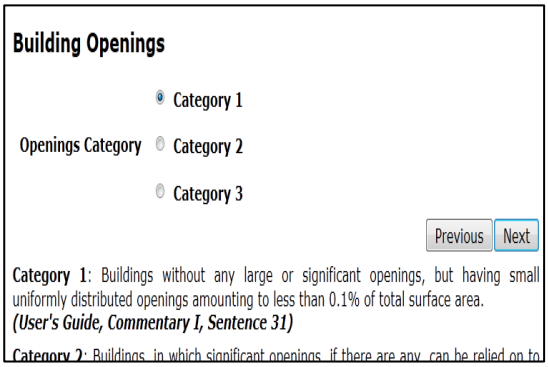

(f) Building opening

Figure 3.1: Snapshots of Wind-RCI Calculator

Wind Load Calculation for Roof Covering

Wind-RCI
Roof Calculator on Internet

Roof Cladding Wind Design Loads

Building Location

Split Lake, Manitoba

Building Geometry:

Low Rise: Low sloped Roof 0° < α <= 7°
Height: 30 ft (9 m)
Width: 50 ft (15 m)
Length: 50 ft (15 m)

Building Exposure:

Open

Building Openings:

Category 1

Building Importance Category:

Normal

Roof Wind Loads:

End Zone Width, z: 5 ft (2 m)
Corner, (C) : -54 psf (-2.6 kPa)
Edge, (S) : -25 psf (-1.2 kPa)
Field, (r) : -18 psf (-0.9 kPa)

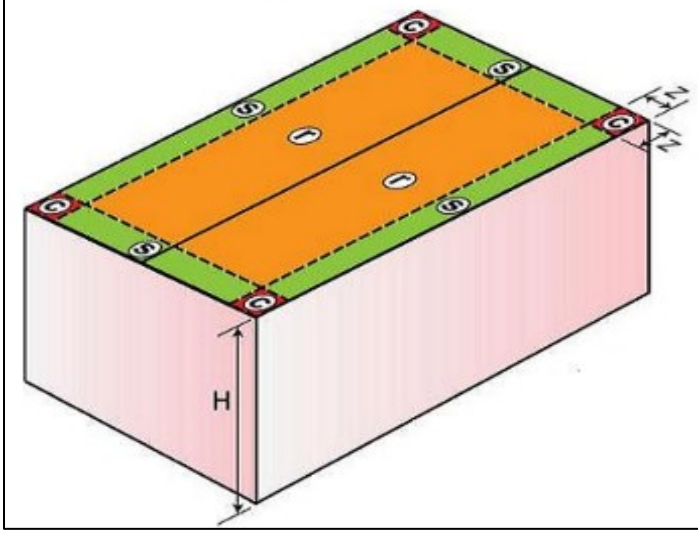

Figure 3.2: Report produced by Wind-RCI Calculator

3.1.3.2 Updating Wind-RCI Calculator with NBCC2010

As a part of this research, the Wind-RCI Calculator was updated to comply with the NBCC2010. In fact, the contribution includes three components:

1. *Updating the reference velocity pressure values:*

   Wind-RCI database was updated to account for the change in reference velocity pressure of each city.

2. *Inclusion of the additional cities:*

   The additional cities were included in the updated version of the calculator.

3. *Inclusion of a new feature:*

   The updated version of the calculator allows for wind load reduction in buildings with parapets higher than 1 m (3.28 ft); see Figure 3.3.

The most up-to-date version of Wind-RCI Calculator was launched in cooperation with the NRCC in April 2012. A free version of the calculator is accessible through SIGDERS' website at www.sigders.com.

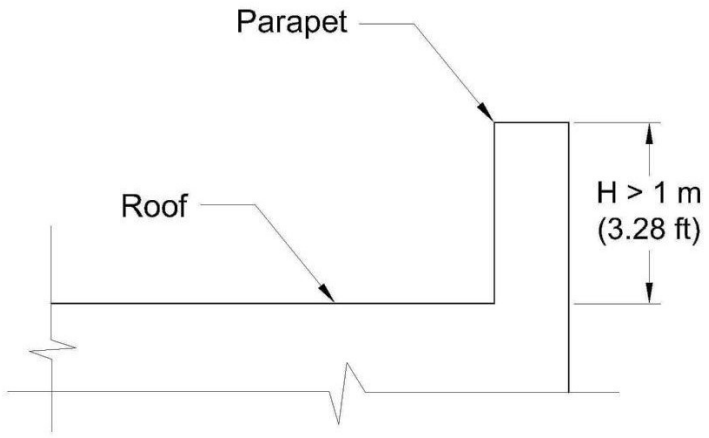

Figure 3.3: Roof with parapet higher than 1 m (3.28 ft)

3.2 The American Society of Civil Engineers Wind Guide (ASCE)

The ASCE wind document was referenced by several building codes in the United States. It has been published in a number of versions since the first edition originally published in 1988. Later, revisions came out in years 1998, 2002, 2005 and recently in 2010 (ASCE7-10)

The ASCE7-10 specifies minimum load requirements for various climate loads including wind load design. This section is focused on the ASCE7-10 methods for calculating design wind loads on roof claddings.

Chapter 30 of the ASCE7-10 is dedicated to calculating wind loads on claddings. As shown in Figure 3.4, five methods are available based on the building's height and enclosure category as defined in the ASCE7-10.

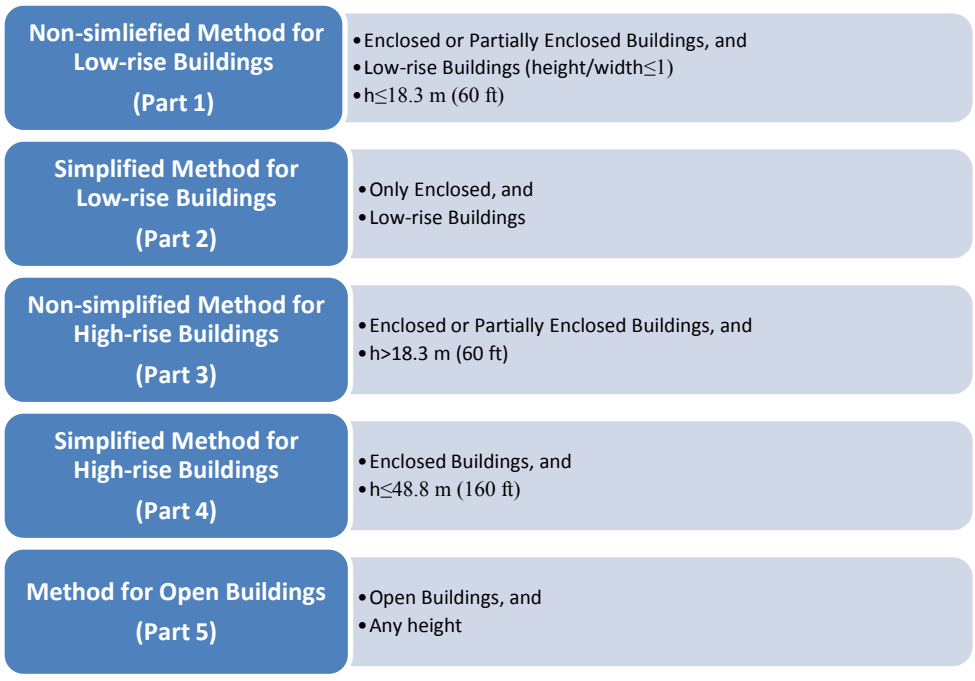

Figure 3.4: ASCE7-10 methods for calculating design wind loads on claddings

The ASCE7-10 specifies a set of conditions for the use of these methods, as follows:

- Building should be regularly shaped with no geometrical irregularity.
- Building should be rigid, i.e. natural frequency is greater than or equal to 1 Hz.
- Building should not have response characteristics such that it is subjected to cross wind-loading, vortex shedding, galloping or flutter induced instability.
- Building's location should be away from channelling effects.

3.2.1 Non-simplified Method for Low-rise Buildings (ASCE7-10/ Part 1)

For enclosed or partially enclosed buildings with mean roof's height less than 18.3 m (60 ft), the design wind load on claddings can be calculated by the below equation:

$$p = q_h.\left[\left(GC_p\right) - \left(GC_{pi}\right)\right]$$

Where q_h= Velocity pressure at mean roof's height (ASCE7-10/Section 30.3)

GC_p= External pressure coefficient based roof type (ASCE7-10/Figs. 30.4-1, 30.4-2A to 30.4-2C, 30.4-3, 30.4-4, 30.4-5A, 30.4-5B, 30.4-6, 30.4-7, 27.4-3

GC_{pi}= Internal pressure coefficient (ASCE7-10/Table 26.11-1)

The "velocity pressure" at height "z" may be calculated from the formula below:

$q_z = 0.00256 \times K_z K_{zt} K_d V^2$ (psf); where V in mph

$q_z = 0.613 \times K_z K_{zt} K_d V^2$ (Pa); where V in m/s

K_d= Wind directionality factor (ASCE7-10/Section 26.6)

K_z= Velocity pressure exposure coefficient (ASCE7-10/Section 30.3-1)

K_{zt}= Topographic factor (ASCE7-10/Section 26.8)

V = Basic Wind Speed (ASCE7-10/Section 26.5)

3.2.2 Simplified Method for Low-rise Buildings (Enclosed) (ASCE7-10/ Part 2)

This method can be used for enclosed buildings with h ≤ 18.3 m (60 ft) if the following is true:

1. Enclosure should be defined according to Section 26.2 of the ASCE7-10. The building also should obey debris provisions in Section 26.10.3 of the ASCE7-10
2. The roof cannot be other than flat, gable with θ ≤ 45˚, or hip with θ ≤ 27˚

The design wind load acting on claddings can be calculated by:

$$P_{net} = \lambda K_{zt} p_{net30}$$

where λ= Adjustment factor for height and exposure (ASCE7-10/Fig. 30.5-1)

K_{zt}= Topographic factor at third the mean roof's height (ASCE7-10/Section 26.8)

p_{net30}= Net design wind pressure for exposure "B" at height of 9.1 m (30 ft) (ASCE7-10/Section 30.5-1)

3.2.3 Non-simplified Method for High-rise Buildings (ASCE7-10/ Part 3)

If the building is enclosed or partially enclosed and taller than 18.3 m (60 ft), the design wind load can be calculated as follows:

$$p = q(GC_p) - q_i(GC_{pi})$$

;where

GC_p= External Pressure Coefficient

(ASCE7-10/Fig. 30.6-1, 27.4-3, 30.4-7, Note 6 of Fig. 30.6-1 for other roof types)

GC_{pi}= Internal Pressure Coefficient (ASCE7-10/Table 26.11-1)

q= Velocity Pressure evaluated at the roof's height

q_i= Velocity pressure evaluated at the roof's height (or at the highest opening for positive internal pressure)

Both q and q_i should be calculated based on exposure definition in ASCE7-10 (Section 26.7.3)

3.2.4 Simplified Method for High-rise Buildings (ASCE7-10/ Part 4)

This method is applicable to buildings with height below or equal to 48.8 m (160 ft). Design wind load is given by the following expression:

$$p = p_{table}(EAF)(RF)K_{zt}$$

where RF = Effective area reduction factor (ASCE7-10/Table 30.7-2)

EAF = Exposure adjustment factor (ASCE7-10/Table 30.7-2)

K_{zt}= Topographic Factor (ASCE7-10/Section 26.8)

3.2.5 Method for Open Buildings (ASCE7-10/ Part 5)

This procedure applies to buildings with monoslope, pitched, or troughed roof. The design wind load is given by the following expression:

$$p = q_h G C_N$$

where q_h= Velocity pressure at the roof's height based on the highest exposure

G= Gust-effect factor (ASCE7-10/Section 26.9)

C_N= Net pressure coefficient; it can be found in:

ASCE7-10/Fig. 30.8-1 for monoslope roofs

ASCE7-10/Fig. 30.8-2 for pitched roofs

ASCE7-10/Fig. 30.8-3 for troughed roofs

3.3 NBCC2010 vs. ASCE7-10

3.3.1 Sample Calculations

Several cases were selected as examples to demonstrate the process of designing roof claddings as per the NBCC2010 and the ASCE7-10. The examples were intended for spotting the differences between the NBCC2010 and ASCE7-10. In fact, each of the codes is designed for a different environment; consequently, attempts to compare between the two codes may be a problematic task. To address this issue, the calculations were done for hypothetical buildings located in border cities between Canada and the United states. For instance, Victoria (Canada) and Seattle (USA) are fairly affected by the same meteorological conditions. Accordingly, design wind loads should theoretically be similar for the same building under same conditions.

Three cases were presented, where each one represents the design process for roof claddings of a hypothetical **low-rise** building located in a pair of border cities as follows (Figure 3.5):

Case (1). Victoria (Canada) vs. Seattle (USA)

Case (2). Windsor (Canada) vs. Detroit (USA)

Case (3). Niagara Falls (Canada) vs. Niagara Falls (USA)

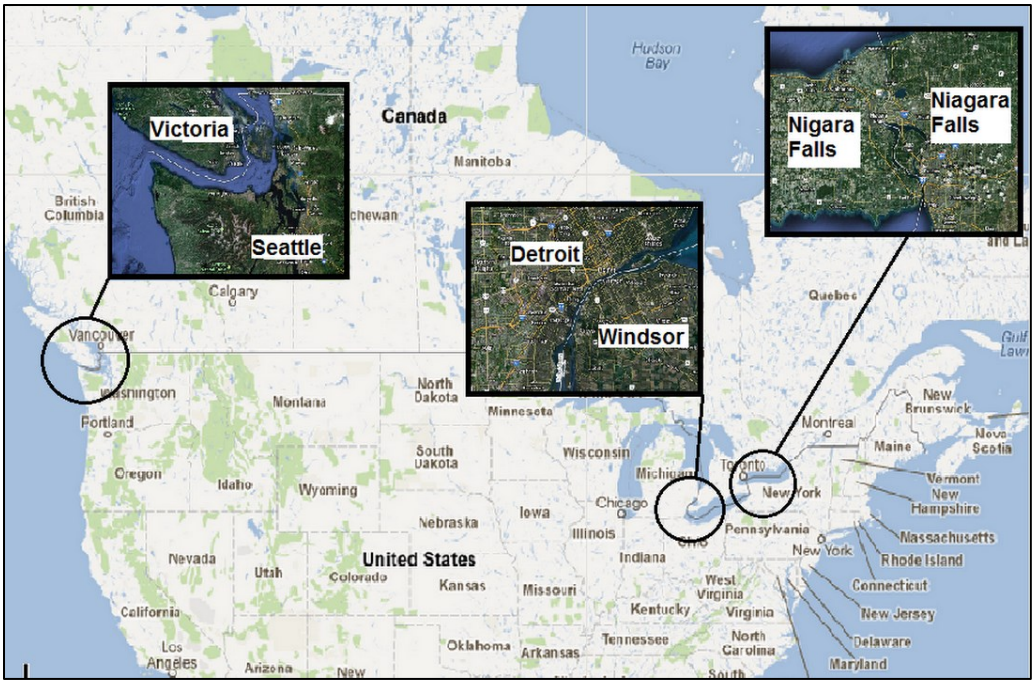

Figure 3.5: Canada-USA border cities for the case study

Calculations for Case (1) (Table 3.1) are shown in Table 3.2and Table 3.3 below.

Table 3.1: Properties of hypothetical low-rise building for Case (1), Case (2) and Case (3)

Location	**Victoria- Mt Tolmie (Canada)**	**Seattle (United States)**
Geometry	Length: 51.8 m (170 ft); Width: 30.5 m (100 ft); Height: 18.3 m (60 ft) Low-rise building	
Roof type	Low slope	
Importance	High	Risk Category II
Terrain	Suburban	Suburban

Table 3.2: Calculation of design wind loads based on NBCC2010 (Case 1)

NBCC2010 (Victoria-Mt Tolmie, Canada)- Low-rise Building		
Importance factor (I_w)	1.15	*High Importance Division B: Table 4.1.7.1*
Wind Velocity Pressure (q)	0.63 kPa (13.17 psf)	*Division B: Table C-2 (Victoria- Mt Tolmie)*
Reference height (h)	18.3 m (60 ft)	*Structural Commentary I: Reference Height, page I-4*
Exposure factor (C_e)	For external pressure: $C_e = 0.7 \times \left(\frac{h}{12}\right)^{0.3} = 0.7 \times \left(\frac{18.3}{12}\right)^{0.3} = 0.79 > 0.7$ For internal pressure: $C_e = 0.7 \times \left(\frac{0.5h}{12}\right)^{0.3} = 0.7 \times \left(\frac{0.5 \times 18.3}{12}\right)^{0.3} = 0.64 < 0.7 \rightarrow 0.7$	*Clause 4.1.7.1- Sentence 5*
Internal gust factor (C_{gi})	2.00	*Division B: Clause 4.1.7.1*
Internal Pressure Coefficient (C_{pi})	$-0.45 \rightarrow +0.30$	*Structural Commentary I: page I-21*
External Peak Composite Pressure-Gust Coefficient (C_pC_g)	Corner= -5.4 Edge= -2.5 Field= -1.8	*Low Slope* $\theta \leq 7°$ *Structural Commentary I: Figure I-9*
$C_eC_pC_g$	Corner= -4.27 Edge= -1.98 Field= -1.42	
$C_eC_{pi}C_{gi}$	$-0.63 \rightarrow +0.42$	
Design wind pressure (p)	Corner= -3.40 kPa (71.1 psf) Edge= -1.74 kPa (36.4 psf) Field= -1.33 kPa (27.8 psf)	
Roof zones	$a = min \begin{bmatrix} 0.1 \times 30.5 = 3.05m \\ 0.4 \times 18.3 = 7.32m \end{bmatrix} = 3.05m\ (1ft)$	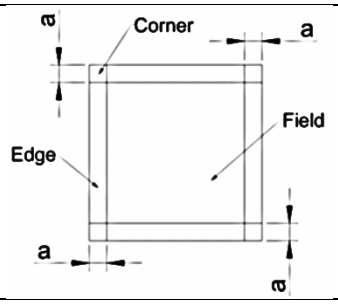

Table 3.3: Calculation of design wind loads based on ASCE7-10 (Case 1)

ASCE7-10 (Seattle, USA)- Low-rise Building		
Risk cat.	II	Table 1.5-1
Wind speed V	49 m/s (110 mph)	Fig. 26.5-1 B
Wind dir. factor K_d	1.00	No load combination Section 26.6, Table 26.6-1
Exposure cat.	Suburban	Section 26.7
Topographic factor K_{zt}	1.00	Not subjected to topo-graphic effect Section 26.8 and 26.8-1
Internal pressure coeff. GC_{pi}	$-0.55 \rightarrow +0.55$	Partially Enclosed Section 26.10 and 26.11 Table 26.11-1
Velocity pressure exposure coeff. K_h	0.85	Table 30.3-1
Velocity pressure q_h	$0.613 \times K_h K_d K_{zt} V^2 = 0.613 \times 0.85 \times 1 \times 1 \times 49^2 = 1.25\ kPa$	Equation 30.3-1 (ASCE7-10)
External pressure coeff GC_p	Corner= -2.8 Edge= -1.8 Field= -1.0	Gable with $\theta \leq 7^\circ$ Figure 30.4-2
Design wind pressure P	Corner= $1.25(-2.8 - 0.55) = -4.19\ kPa$ Edge= $1.25(-1.8 - 0.55) = -2.94\ kPa$ Field= $1.25(-1.0 - 0.55) = -1.94\ kPa$	Equation 30.1-1 (ASCE7-10)
Roof zones	$= min \begin{bmatrix} 0.1 \times 30.5 = 3.05m \\ 0.4 \times 18.3 = 7.32m \end{bmatrix} = 3.05m\ (1ft)$	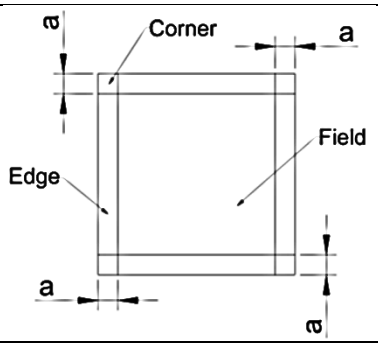

Similar procedures were followed for Case (2) and Case (3). Table 3.4 summarizes the calculated wind design loads as well as NBCC/ASCE ratios.

Table 3.4: Design wind loads for Case 1, Case 2 and Case 3

		NBCC2010 kPa (psf)	**ASCE7-10** kPa (psf)	**NBCC/ASCE**
Case 1	Corner	-3.4 (71.1)	-4.19 (87.6)	0.81
	Edge	-1.74 (36.4)	-2.94 (61.4)	0.59
	Field	-1.33 (27.8)	-1.94 (40.5)	0.69
Case 2	Corner	-2.53 (52.9)	-4.56 (95.3)	0.56
	Edge	-1.30 (27.2)	-3.20 (66.9)	0.40
	Field	-1.00 (20.9)	-2.11 (44.0)	0.48
Case 3	Corner	-2.32 (48.5)	-4.56 (95.3)	0.51
	Edge	-1.19 (24.9)	-3.20 (66.9)	0.37
	Field	-0.91 (19.0)	-2.11 (44.1)	0.43

The NBCC2010 code yielded fairly lower values than those of the ASCE7-10. The difference, as shown in Table 3.4, varies depending on the roof zone. The NBCC/ASCE ratio falls within a range of 0.51 to 0.81 for the corner zone, 0.37 to 0.59 for the edge zone and 0.43 to 0.69 for the field zone.

It is important to mention that NBCC requires the calculated design wind loads to be factored as **1.4** if combined with any other types of loads. The NBCC2010 includes five loading cases (NBCC's Table 4.1.3.2). For example, when wind load (W) is combined with dead (D), live (L) and snow loads (S), the total deign load is equal to:

(1.2D or 0.9D)+ 1.4W+ (0.5L or 0.5S)

An explanation for the variation in design loads between the NBCC and ASCE is further discussed through the parameter discussion presented in the next section.

3.3.2 Parameter Discussion of NBCC2010 and ASCE7-10

Sample calculations cannot just draw a clear picture of the dissimilarities between the NBCC2010 and ASCE7-10. Thus, it would be suitable to individually investigate the design parameters for a hypothetical building located in a border city. Such an investigation may reveal the contribution of each design parameter in producing different results by NBCC2010 and ASCE7-10. With this intention, the design equations are rearranged in form of three components as follows:

	Wind speed and importance	Density of air	Building and location parameters	Code source
NBCC2010	$I \times V^2$	$\frac{1}{2}\rho$	$C_e C_p C_g - C_{ei} C_{pi} C_{gi}$	See Section 3.1.1
ASCE7-10	V^2	0.613	$K_z \left(GC_p - GC_i\right)$	See Section 3.2

1. *Building and location parameters:* these parameters are theoretically less likely to influence the difference in the calculated loads as they are dependent on the geometry of the building and the surrounding terrain. However, each code uses different standards for estimating these parameters. Strictly speaking, such parameters are usually estimated by using wind tunnel tests and field measurements that may be conducted under dissimilar conditions. As a result, the parameters can vary between the two codes, resulting in different design values.

2. *Density of air:* for a certain ambient temperature, the density of air should be constant and not affecting the variation in the design loads.
3. *Wind speed and importance level:* the NBCC2010 and ASCE7-10 have different criteria for estimating the design wind speed and for taking into consideration the importance level of the building. Consequently, this part of the equations appears to be the cause of the gap between the two codes in terms of design wind loads.

The following sections discuss in detail how design wind speed affects the calculated design loads based on the NBCC2010 and ASCE7-10.

Measurement of Wind Speed

In fact, the process of estimating the design wind speed in both codes is subjected to the local regulations and standards. For instance, in the case of Victoria (Canada)/ Seattle (United States), the NBCC2010 and ASCE7-10 would estimate different wind speed values despite the fact that the two cities are located in the same geological area and affected by similar meteorological conditions.

Wind Speed Type

The NBCC2010 makes use of hourly averaged wind speed, whereas the ASCE7-10 uses 3-second gust wind speed (averaged over a period of three seconds). In fact, the 3-second gust wind speed is equal to 1.54 times the hourly averaged wind speed (Baskaran and Smith, 2005), which gives an additional rise to the design loads calculated by the ASCE7-10 in comparison with those calculated by the NBCC2010.

It is worth mentioning that 3-second gust wind speed seems more appropriate than the hourly averaged wind speed because claddings would be more sensitive to wind acting

over shorter periods (3 sec vs. 1 h). That is to say, the ASCE may produce more realistic design loads.

Importance/Risk Category and Return Period

As for the NBCC2010, the design wind speed is estimated based on a return period of 50 year. Furthermore, the design wind speed is modified for different importance level by multiplying V^2 by the importance factor; see Table 3.5. On the other hand, the ASCE7-10 estimates the design wind speed based on different return periods depending on the risk category of the building (corresponding to importance level in NBCC2010).

Table 3.6 shows the risk categories in the ASCE7-10 and the corresponding return periods.

Table 3.5: Importance factor as per NBCC2010

Importance Category	Importance Factor, I_w
Low	0.9
Normal	1
High	1.15
Post disaster	1.25

Table 3.6: Risk category and return period as per ASCE7-10

Risk Category	Return Period (years)
I	300
II	700
III and IV	1700

Due to the fact that the NBCC2010 and ASCE7-10 uses different approach to account for the importance level, the calculated design loads are further affected.

Efforts to identify the side-by-side dissimilarities between the NBCC2010 and the ASCE7-10 are rather difficult. First, the estimation process of the design parameters rises as one issue, where it is subjected to the local regulations of each country (Canada vs. the United States). Second, the design wind speed is technically adjusted to account for the importance/risk level of the building; however, different methods are adopted by the two codes. In addition, other factors such as using different lengths of historical data records, may contribute to the differences between the two codes in terms of the calculated wind design loads.

3.4 Wind Design Loads (Experimental Approach)

Sections 3.1, 3.2 and 3.3 presented a detailed review of calculating wind design loads on roof claddings. The design process, as discussed, relies on mathematical formulae that employ sets of design parameters and factors representing the building properties and location characteristics. Alternate options are also available instead of using the code values for the parameters. For example, field measurements can be conducted to estimate parameter values for more realistic design values.

Conducting field measurements at the site of a building would impose several difficulties such as instrumentation capability limitation, instrument installation, and/or weather conditions. This section presents an experimental approach which exclusively deals with two parameters: reference velocity pressure (q) and exposure factor (C_e). The rest of the parameters can still be calculated as per the NBCC2010.

As indicated in Section 3.1.1, the term $q.C_e$ represents the adjusted reference velocity pressure based on the roof's height and terrain roughness. Both q and C_e can be calculated through the tables provided by the NBCC2010. However, these parameters may be calculated experimentally. In this case, a three-step procedure is suggested to estimate the value of $q.C_e$ as follows:

1. Collecting wind speed data at the height of the building's roof.
2. The data are processed and prepared for statistical analysis.
3. As a statistical analysis, a probability distribution curve is fitted to the processed data in order to estimate the design wind speed (V) based on a return period of 50 years (as specified by NBCC2010).

After the design wind speed is obtained, the experimental value of the reference velocity pressure can be calculated as follows:

$$q_{exp} = 0.5\rho.(V^2)_{exp} \tag{3.1}$$

Because the wind speed measurements are performed at the roof's height level and the actual environment, the experimental reference velocity pressure does not require adjustment by the exposure factor, so one can consider$C_e = 1$. Figure 3.6 shows a schematic diagram of the suggested approach.

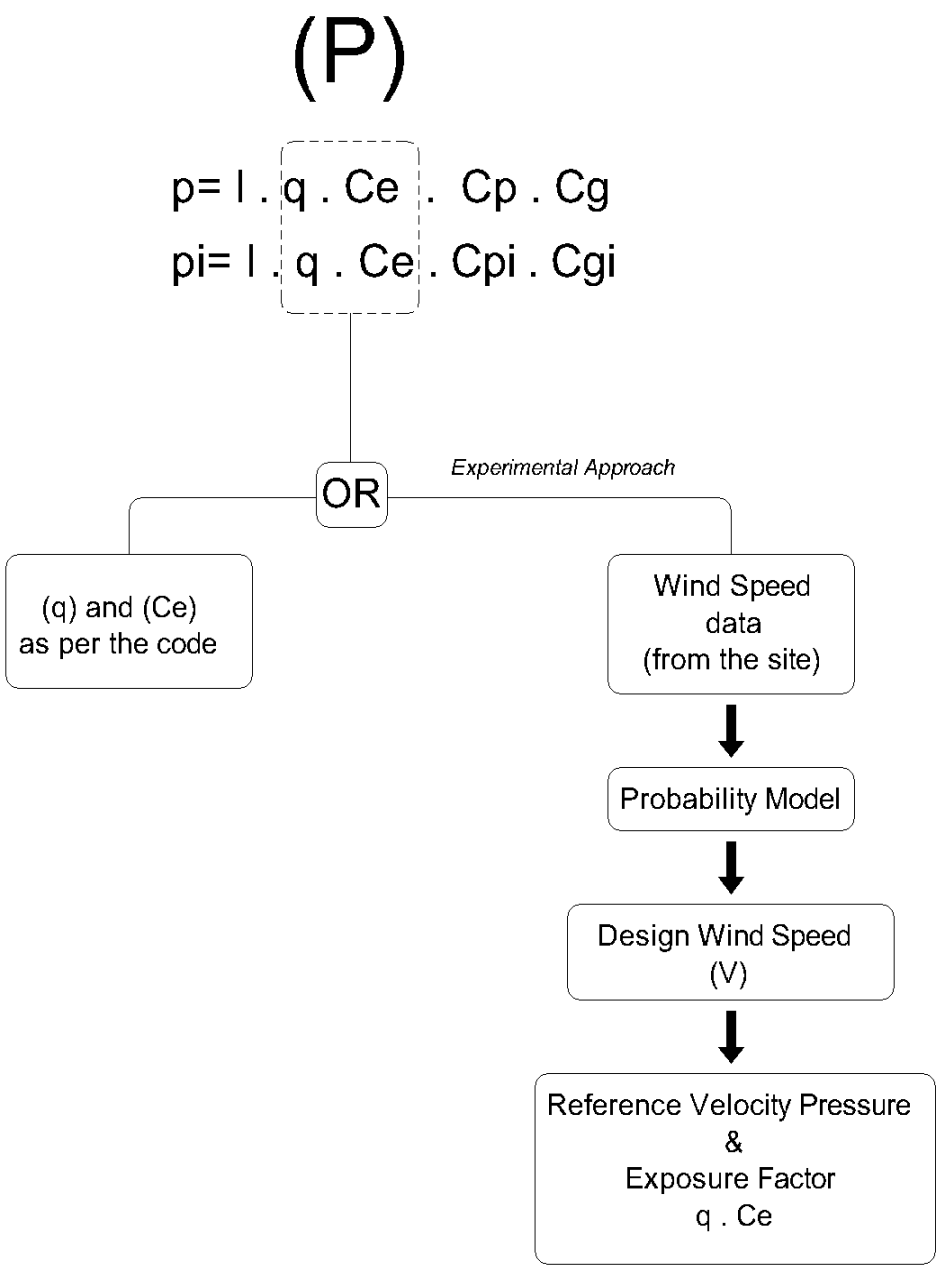

Figure 3.6: Experimental approach for estimating design wind loads

Figure 3.7 shows a hypothetical record of wind speed data collected over a period of fifteen (15) years from the location of the building used in the example discussed in Ta-

ble 3.1 (Case 1). The record includes 5478 points; each represents the maximum wind speed in one day (hourly averaged).

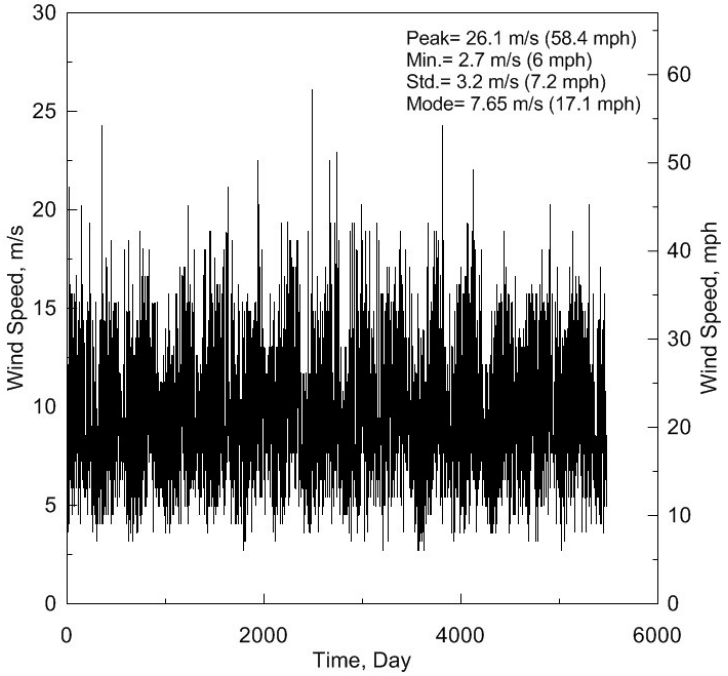

Figure 3.7: Wind speed record used to demonstrate the experimental approach (NIST)

3.4.1 Processing Wind Speed Data

This section is broadly discussed in Appendix (A).

3.4.2 Calculation of Design Wind Speed

With respect to the present example, the experimental design wind speed V_R was calculated based on different return periods: R= 50, 100, 150, 500, 1000 year to show the influence of the return period (Table 3.7) (The calculations can be found in Appendix A). However, only R= 50 year is considered for the design as it is the one used in the NBCC2010.

Table 3.7: Experimental design wind speed (experimental approach)

Return Period (years)	V_Rm/s (mph)
50	**26.05 (56)**
100	26.90 (58)
150	27.38 (59)
500	28.72 (62)
1000	29.45 (64)

3.1.1 Calculation of Design Wind Loads

Given the experimental design wind speed, the experimental reference velocity pressure based on a return period of 50 year can be calculated as follows:

$$C_e.q = 0.5 \times \rho \times (V_{50})^2 = 0.5 \times 1.29 \times 26.05^2 \times 10^{-3} = 0.44\ kPa\ (9.24\ psf)$$

As shown in Figure 3.6, by using code values for the parametersC_p, C_g, C_{pi} andC_{gi}, for the considered building. (See Table 3.1 and Table 3.2):

Roof zone	CpCg	Cgi	Cpi
Corner	-5.4	2.00	0.3
Edge	-2.5		
Field	-1.8		

The design wind load is given by:

$$P = p - p_i = I_w C_e C_p C_g - I_w C_e C_{pi} C_{gi}$$

The parameter C_e is calculated based on the full building's height in the case of the external pressure. However, in the case of internal pressure, C_e is computed by using half of the building's height (Table 3.3). In other terms, for the case of rough terrain (suburban):

External pressure: $C_e = 0.7 \times \left(\frac{h}{12}\right)^{0.3}$

Internal pressure: $C_e = 0.7 \times \left(\frac{0.5 \times h}{12}\right)^{0.3} = 0.7 \times \left(\frac{h}{12}\right)^{0.3} \times 0.812$

With respect to the present example, the parameter C_e is included in the reference velocity pressure (q); thus, C_e needs to be put out:

$$P = p - p_i = I_w . q . C_e . \left(C_p C_g - 0.812 \times C_{pi} C_{gi}\right)$$

Given that $q . C_e$= 0.44 kPa (9.24 psf), the design wind loads based on the experimental approach are:

$$Corner = 1.15 \times 0.44 \times (-5.4 - 0.812 \times 0.6) = 2.98\ kPa\ (62.3\ psf)$$
$$Edge = 1.15 \times 0.44 \times (-2.5 - 0.812 \times 0.6) = 1.51\ kPa\ (31.6\ psf)$$
$$Field = 1.15 \times 0.44 \times (-1.8 - 0.812 \times 0.6) = 1.16\ kPa\ (24.2\ psf)$$

Table 3.8 compares the experimental and NBCC2010 design loads:

Table 3.8: Wind design loads based on the NBCC2010 and the experimental approach (Case 1)

Roof Zone	NBCC2010 kPa (psf) (Table 3.2)	Experimental kPa (psf)	Ratio Exp./NBCC
Corner	-3.4 (71.1)	-2.98 (62.3)	0.88
Edge	-1.74 (36.4)	-1.51 (31.6)	0.88
Field	-1.33 (27.8)	- 1.16 (24.2)	0.87

In this example, the experimental approach yields lower design wind loads in comparison with those of the NBCC2010. Thus, the design loads calculated by the experimental approach can be used instead of those calculated purely by the code. In fact, the NBCC2010 permits, on the designer's responsibility, the use of an experimental approach to estimate the design loads, where they can be more realistic as they would represent the actual conditions of the considered building. It is of high importance to use high quality data for obtaining trusted wind design loads.

3.5 Conclusion

This chapter analysed the calculation procedure for wind loads as per the NBCC and ASCE in calculating design wind loads on roof claddings. By taking side-by-side cities along Canada-USA border, wind load calculations were performed to demonstrate the differences and similarities between the NBCC and ASCE. Even though both the NBCC and ASCE provide the essential tools for calculating design wind loads, they differ from each other in many aspects, such as the determination of design parameters. Consequently, attempts to compare the design parameters of each code appear to be complex. As a part of the current contribution, the existing version of the online Wind-RCI Calculator

was updated from NBCC2005 to NBCC2010 provisions. Additionally, to calculate design loads, an experimental approach for estimating some of the code parameters was presented. For this purpose, wind speed data were processed, and one of the reliable probability curves was fitted in order to obtain the design wind speed. Then, the reference velocity pressure, and therefore the design wind loads were calculated. In such a case, experimentally calculated deign loads can be used instead of those calculated based on the code.

Chapter 4. Experimental Methodology

Introduction

This chapter is dedicated to demonstrating the developed experimental methodology that has been designed to test and evaluate roof edge components for wind loads. Wind pressure was simulated and conducted in a lab environment by using full scale edge mock-ups. The experimental setup was designed based on the need for simulating the dynamic nature of wind loads. For this purpose, the test strategy was formulated by applying time-varying pressure uniformly on the structural components of the considered roof edge system. This chapter discusses the modules of the experimental setup, as follows:

1. Pressure chamber
2. Pressure simulator
3. Edge system
4. Instrumentation and data acquisition

4.1 Dynamic Roofing Facility (DRF- Mini)

The Dynamic Roof Facility (DRF) at the National Research Council of Canada (NRCC) was offered to develop the suggested experimental method. Figure 4.1 illustrates the layout of the experimental methodology which is composed of four modules. The following is a brief review of the test modules followed by a detailed description.

Module 1: Pressure Chamber

The pressure chamber represented by the edge substrate is responsible for building up the pressure and transferring it to the edge components. The pressure is transferred to the edge components through a pressurizable object (pressure plane) installed underneath the

metal. The pressure chamber is a hollow box which served as a nailer. The concept of the pressure chamber and the installation process are discussed in Section 4.4.

Module 2: Pressure Simulator

A regenerative air blower was employed to supply the pressure chamber with air to build up the required pressure in the pressurizable object (pressure plane). As a result, the expansion of the pressurizable object produces the simulated loads on the edge components. Also, a computer-driven flap was attached to one side of the pressure chamber. The purpose of the flap is to allow for pressurizing and depressurizing the pressure chamber by closing/ opening the flap in order to simulate loading/ unloading cycles by the pressure plane. The flap is also called the "gust simulator". The air blower and gust simulator are further discussed in Section 4.3.

Module 3: Edge Systems

This module represents the edge system considered for testing. The edge system included the coping, cleat/clip as well as the securing components. The installation process of the roof edge components and the pressure plane is explained in Section 4.4.

Module 4: Instrumentation and Data Acquisition

The pressure chamber was connected to a data acquisition system by pressure taps to read the pressure in the chamber. Furthermore, a computer was linked with both the air blower and the gust simulator in order to control the applied pressure. As for the response measurements, a set of laser sensors were used to monitor the deformations of the edge metal at various locations. The laser sensors were connected to the computer for data collections. The elements of this module are explained in Section 4.5.

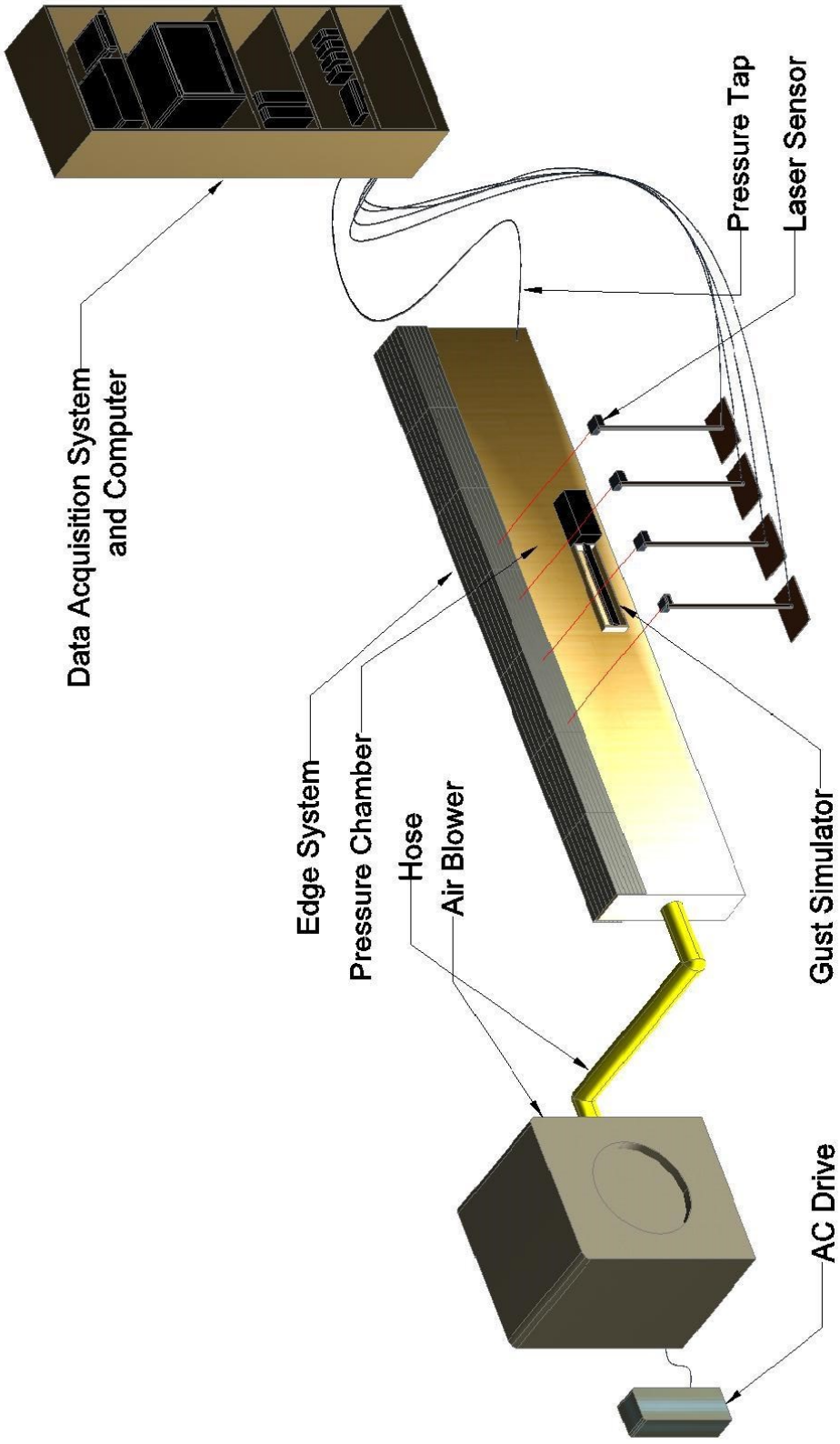

Figure 4.1: Experimental methodology (DRF-mini)

4.2 Pressure Chamber (Module1)

The need for a quick and easy installation process was the reason behind constructing the pressure chamber from hybrid materials. It was made of an aluminum framing assembly on which removable plywood sheets were installed forming the airtight pressure chamber. This was designed and manufactured in cooperation with the NRCC and the University of Ottawa. The edge substrate is also called "pressure chamber".

4.2.1 Pressure Chamber Construction and Installation

As shown in Figure 4.2, the aluminum framing of the pressure chamber assembly is composed of five 6 mm (0.25 in.) thick aluminum panels assembled by eight (8) frames, forming four (4) segments of 1.2 m (4 ft) long each. One end panel had a circular hole of 102 mm (4 in.) in diameter, representing the air intake (connection to air blower). In addition, each intermediate panel had a circular hole for air circulation between the segments; however the other end panel had no holes. Furthermore, 3 mm (0.125 in.) thick gasket strips were applied on the frames to ensure airtightness of the pressure chamber. The finished length of the aluminum framing was 4.9 m (16 ft). As for the plywood sheets, 13 mm (0.5 in.) thick plywood were installed on the aluminum assembly, in addition to wood nailer at the top to form the edge substrate. No. 10 screws and nuts were used for aluminum framing and substrate securement. The finished dimensions of the pressure chamber are: W: 254 mm (10 in.), H: 610 mm (24 in.) and L: 4.9 m (16 ft).

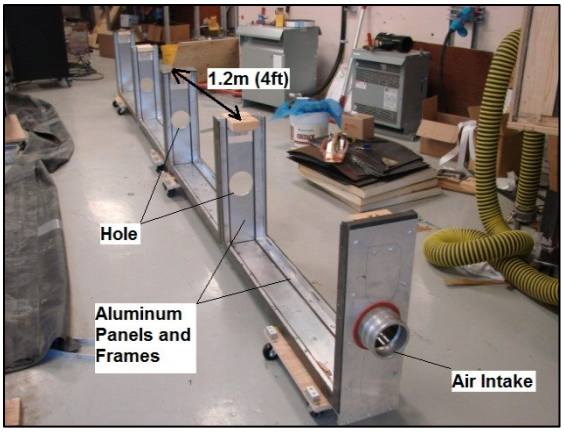

(a) Aluminum framing

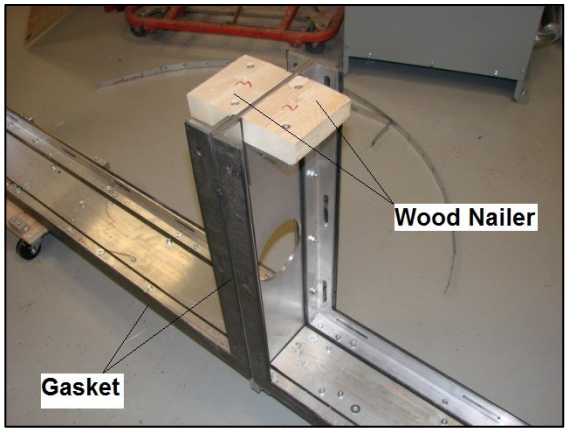

(b) Gasket and wood nailer

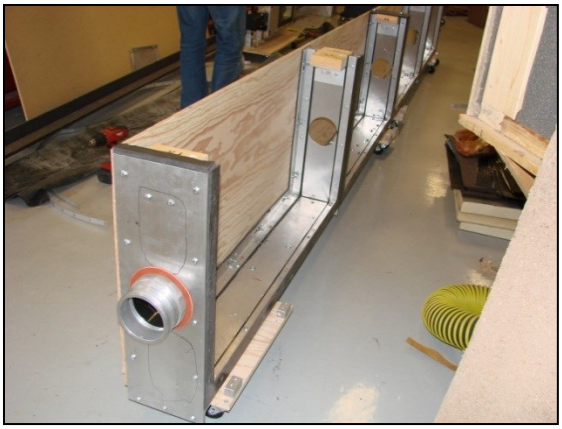

(c) Substrate installation

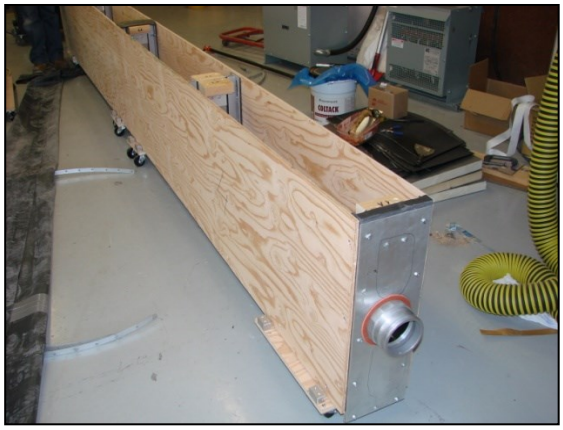

(d) Substrate installation

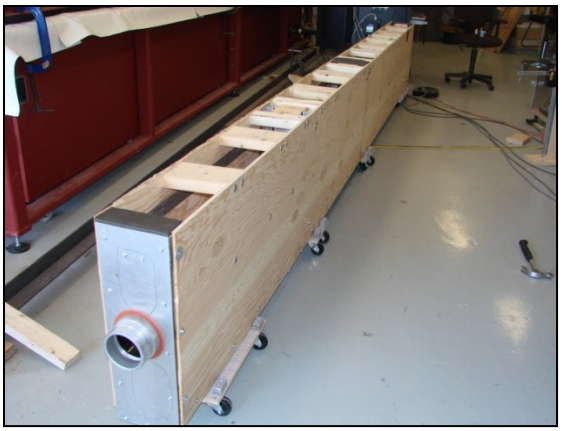

(e) Wood nailers

(f) Completed pressure chamber

Figure 4.2: Installation of pressure chamber

4.3 Pressure Simulator (Module2)

4.3.1 Gust Simulator

A device called the "gust simulator" was designed and manufactured by SAI Designs Incorporation. This device features a motor-driven flap built on a steel frame which was tightly secured to one side of the pressure chamber. The flap may take any position ranging from $\theta = 0^{\circ}$ to 90°: when the flap takes an angle of 90°, it means that the flap is fully close, corresponding to a fully enclosed pressure chamber (full pressurization). However, when the flap is fully open ($\theta = 0^{\circ}$), the pressure chamber becomes open, which corresponds to full depressurization of the pressure chamber. Any position between 0° and 90° of the flap causes partial pressurization/depressurization resulting in loading/unloading cycles. The position of the flap was controlled by a computer based on the selected test protocol which includes information about the pressure magnitude and timing. See Figure 4.3.

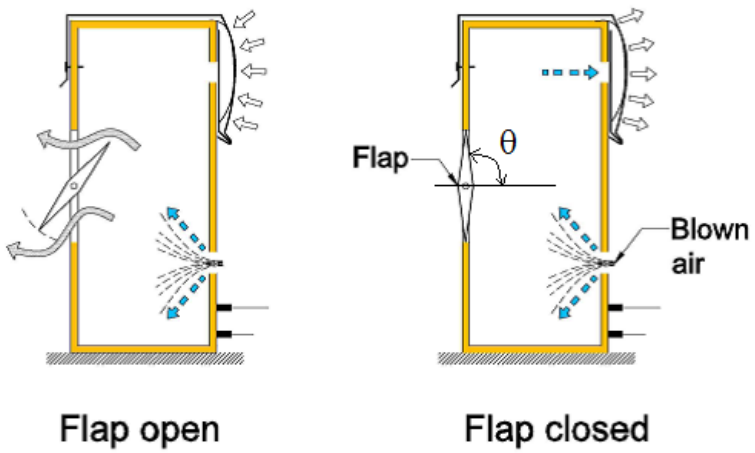

(a) Operation of gust simulator's flap

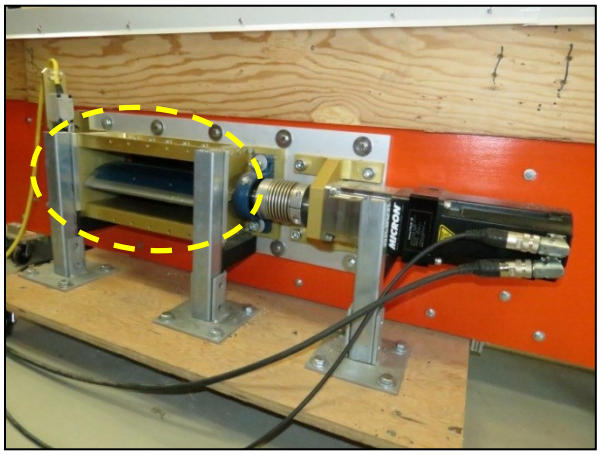

(b) Gust simulator installed

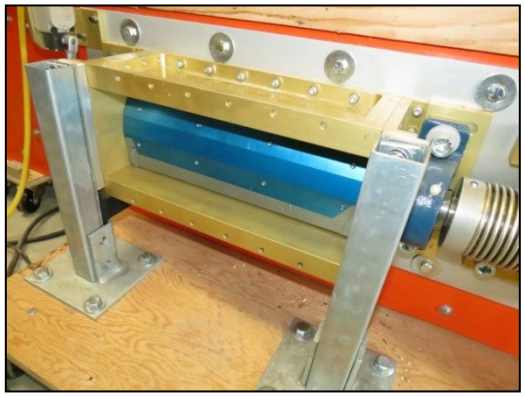

Flap closed- θ= 90˚ (loading)

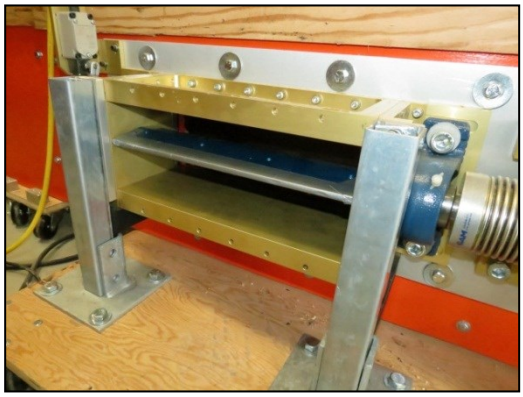

Flap open- θ= 0˚ (unloading)

Figure 4.3: Gust simulator

4.3.2 Air Blower

The air blower used in this study is a regenerative blower provided by Gast Regenair Inc. (Model No. R93150A; see Appendix B). This air blower has a maximum power of 15 HP (746 watts) at a frequency of 60 Hz which is sufficient to produce a maximum pressure of 31 kPa (650 psf). As schematically shown in Figure 4.4, a computer was connected to the air blower through an AC drive. The computer controls the air blower through the AC drive by varying motor input voltage and frequency. In turn, the air blower was connected to the pressure chamber by a flexible hose through the air intake (see Figure 4.1). The technical specifications of the air blower and AC drive can be found in the Appendix B.

Figure 4.4: Regenerative air blower and AC drive

4.4 Edge System Installation (Module 3)

Three configurations of edge systems were tested: Discontinuous cleat configuration (DCC), Continuous cleat configuration (CCC) and Anchor clips configuration (ACC). This section discusses the pressure plane installation as well as the installation of the considered edge system types.

Pressure Plane

The idea behind using a pressure plane was to replace the mechanical force produced by pistons in the ES-1 test method (Section 2.2.1). Thus, the required pressure was applied through a pressurizable object called "pressure plane" that was made of rubber membrane. The pressure plane was installed beneath the coping along the whole length of the pressure chamber. Furthermore, the pressure plane was secured against the pressure chamber by using batten bars and fasteners through the plywood to ensure airtightness of the installed pressure plane.

As for the performance of the pressure plane, air is pumped by the air blower into the pressure chamber (substrate) and therefore into the pressure plane through holes made on the plywood underneath the pressure plane. Accordingly, the pressure plane expands and exerts the required pressure on the coping (gust simulator's flap is closed or partially closed). However, when the pressure chamber is depressurized, the pressure plane also depressurizes, resulting in partial/full release of the load (gust simulator's flap is closed or partially open). This process is repeated in form of loading/unloading cycles as per the selected test protocol. Figure 4.5 shows the pressurization/depressurization process of the pressure plane. The installation of pressure planes varies depending on the type of the edge system installed.

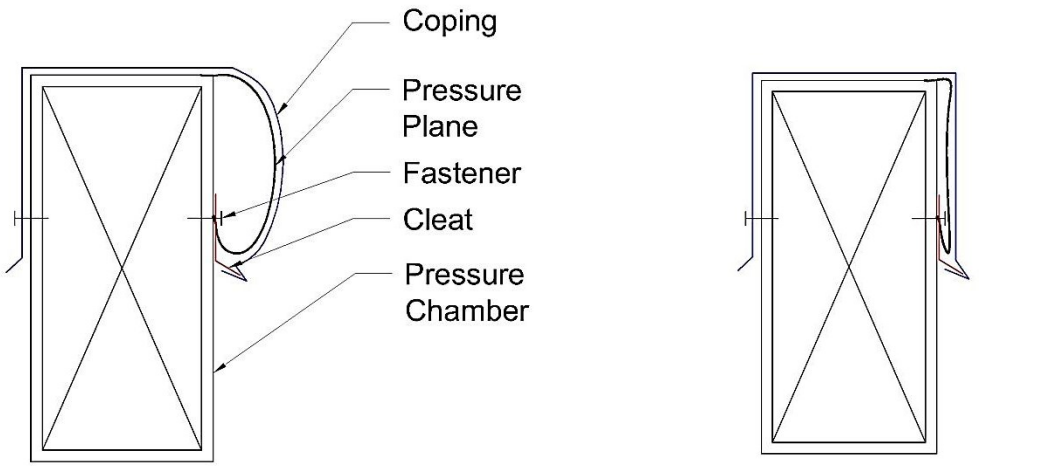

Figure 4.5: Performance of pressure plane

Test Segment of Coping

For all three edge systems, the edge coping was composed of three segments: two side segments (L_d), and the middle segment (L). Only the middle segment was of interest as it was a representative of an arbitrary coping segment with continuous boundary conditions (including coping joints), so it was referred to as "test segment". Observations and measurements were solely conducted for the test segment. The side segments were "dummy segments" (Figure 4.6). The type of joints between the coping segments depended on the type of the edge system installed.

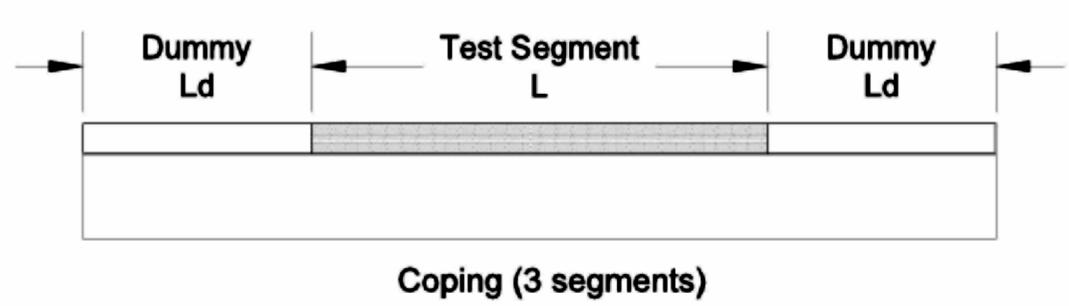

Figure 4.6: Test segment and dummy segments

Boundary Conditions

The boundary conditions of the tested edge systems were maintained such that both ends of the edge were clamped (fixed support) by bar clamps. Thus, the coping at the ends had no response (no deformation).

4.4.1 DCC (Discontinuous Cleat Configuration) Edge System

"DCC" refers to one of the edge system configurations that use discontinuous cleats. The roof edge system discussed herein is one of widely used roof edge systems as recommended by the Roofing Contractors Association of British Columbia (RCABC).

Geometry Details

As shown in Figure 4.7, the coping cross section has channel shape, featuring a 1016 mm (40 in.) long cleat located in the middle of the edge substrate (pressure chamber). The coping is secured at the front face by the cleat through clamping arrangement, whereas at the back face, it is secured by fasteners. As Figure 4.8 illustrates, the coping is composed of three (3) segments: side segments of 1.2 m (4 ft) each, and middle segment of 2.4 m (8 ft). The segments are joined together by using S-lock joints as shown Figure 4.9. Two

sets were tested, Set "A" and Set "B". The following is a detailed review of component installation.

1. Cleat Installation

As shown in Figure 4.10 (a) and (b), the cleat was positioned in the middle of the edge substrate and fastened by 25 mm (1 in.) long galvanized roofing nails spaced at 457 mm (18 in.) at the bottom.

2. Pressure Plane Installation

As shown in Figure 4.10 (c), (d), (e) and (f), a strip of rubber membrane of 0.3 m (1 ft) by 4.9 m (16 ft) was placed on the cleat, covering the edge substrate along its entire length, which formed the pressure plane. Even though the rubber strip was 0.3 m (1 ft) wide, it was installed over only the height of the cleat such that the excess of rubber was folded down to allow for adequate expansion. The pressure plane was air-sealed and secured around its perimeter by 3 mm (0.125 in.) thick gasket, batten bars and fasteners of No. 10 spaced at 38 mm (1.5 in.) through the plywood. After the pressure plane was installed, it was taped as preparation for the coping installation.

4. Coping and Joint Installation

As illustrated in Figure 4.11 (a), the middle segment of the coping was first mounted in the middle of the edge substrate by hooking it on the cleat at the front face. At both ends (joints), the middle segment was nailed at the top; see Figure 4.11 (b). Afterwards, as shown in Figure 4.11 (c), the side segments of the coping were installed by insertion into the S-lock joints. In addition, the coping was fastened at the back face by 38 mm (1.5 in.) long galvanized steel fasteners spaced at 305 mm (12 in.) through the plywood (Figure 4.11 (d)). The completed edge is illustrated in Figure 4.11 (e).

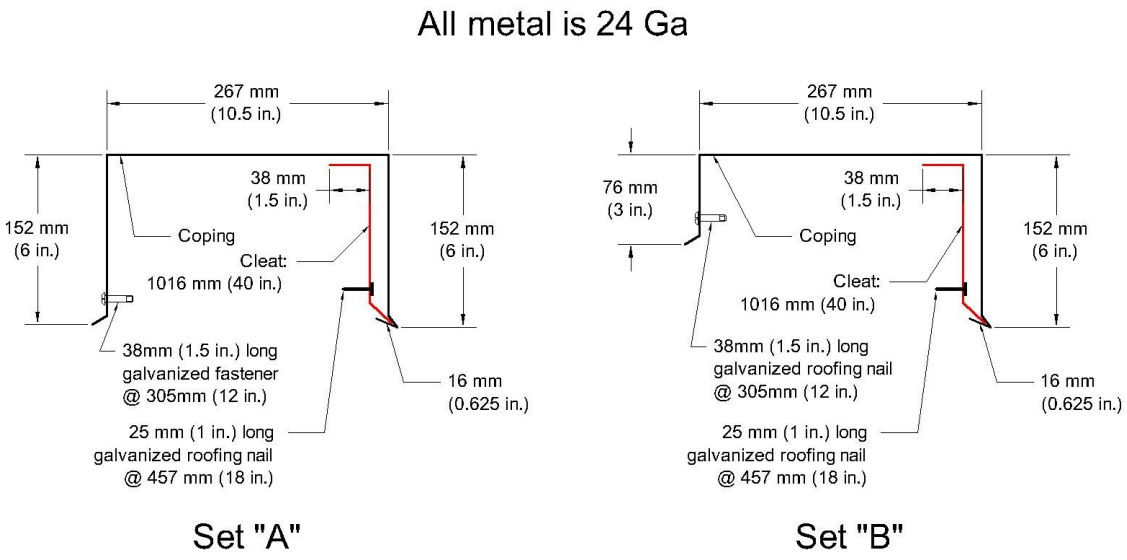

Figure 4.7: Cross section of DCC edge system (not to scale)

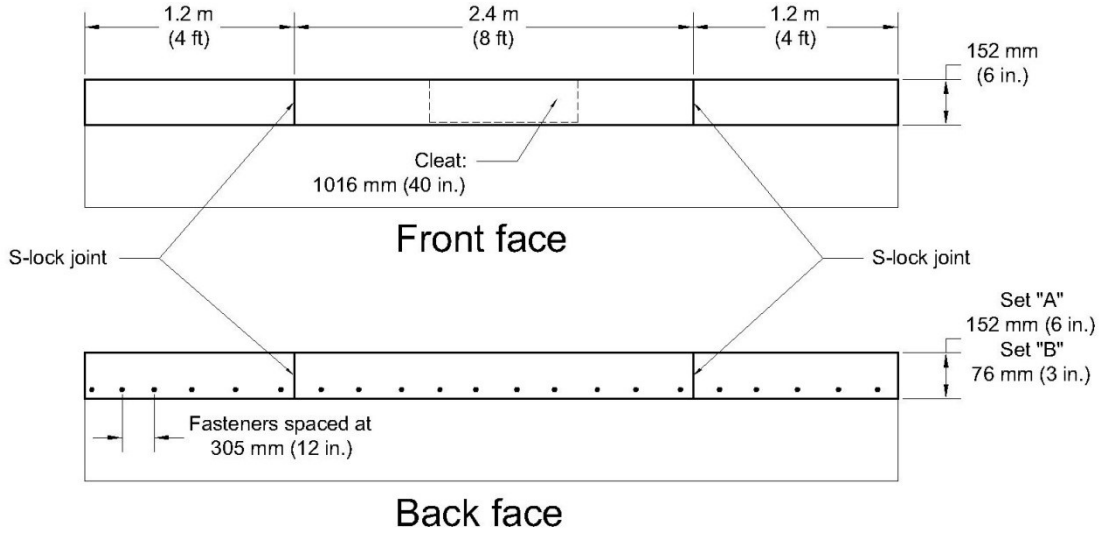

Figure 4.8: Front/back view of DCC coping (not to scale)

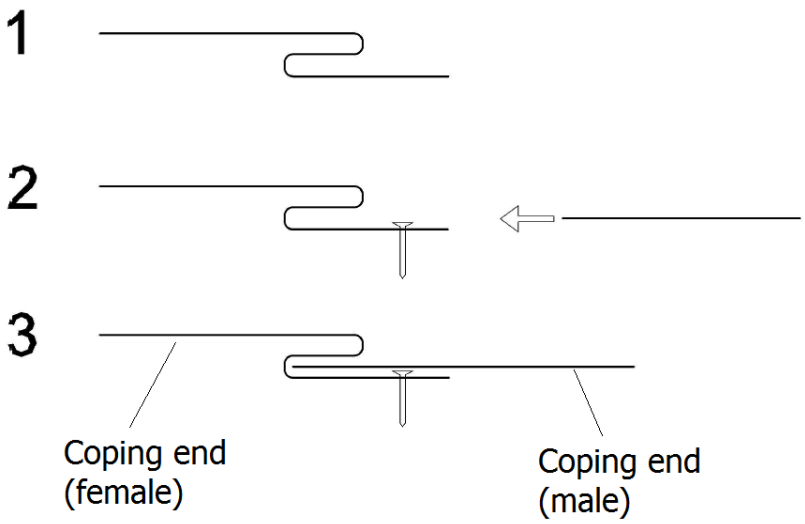

Figure 4.9: Mechanism of S-lock joint

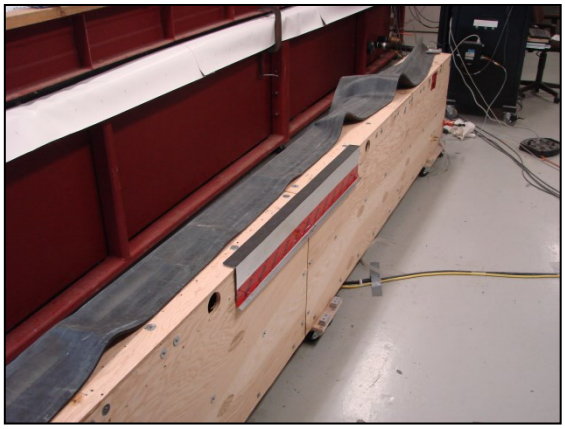

(a) Cleat and rubber strip

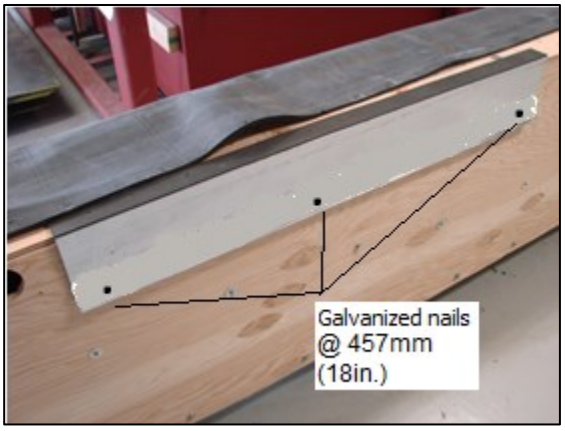

(b) Cleat installed

(c) Air sealing the pressure plane

(d) Securing the pressure plane

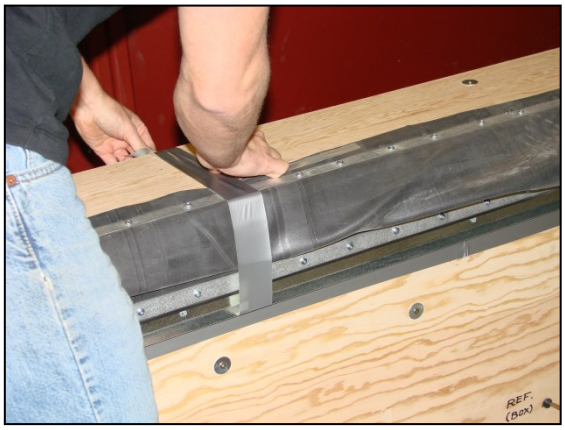

(e) Preparing the pressure plane

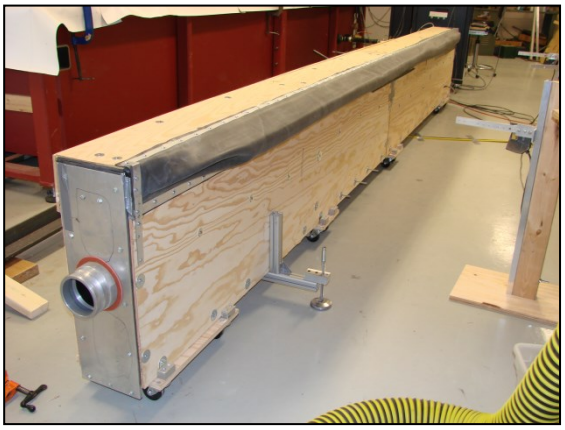

(f) Completed pressure plane

Figure 4.10: Installation of cleat and pressure plane for DCC edge system

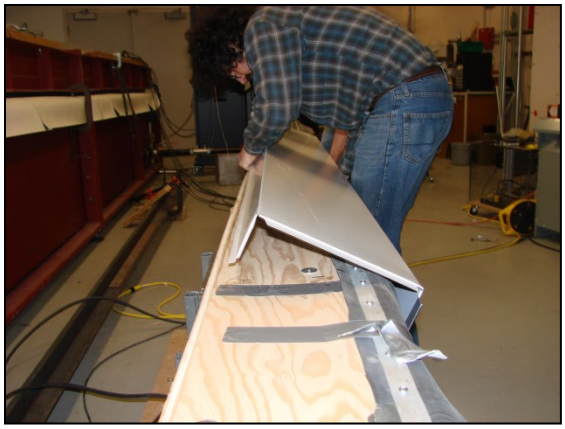

(a) Hooking the coping on the cleat

(b) Fastening middle segment at ends

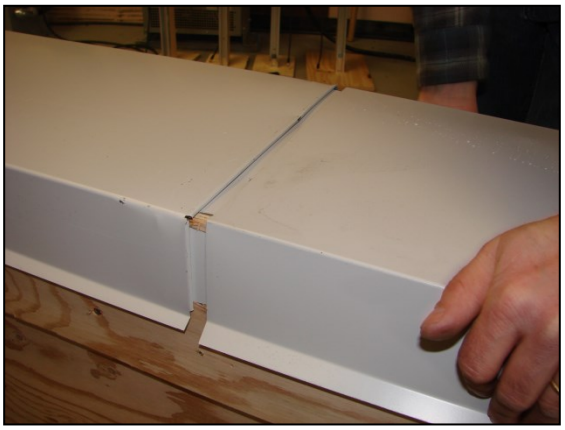

(c) Joining side segment (S-lock)

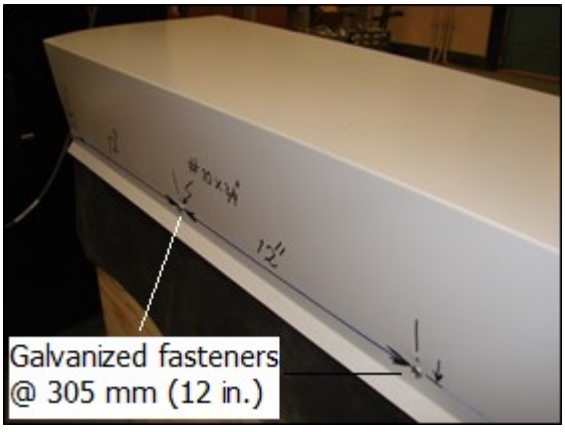

(d) Fastening the coping at back face

(e) Completed edge ready for testing

Figure 4.11: Installation of coping of DCC edge system

4.4.2 CCC (Continuous Cleat Configuration) Edge System

The edge system type being discussed herein is one of the approved roof edge systems by the National Roofing Contractors Association (NRCA) as specified in the technical notes of the NRCA, Sheet No. 3 (NRCA 5th edition construction details). A digital copy of the manual can be found at: http://www.nrca.net/rp/technical/details/ul.aspx.

Geometry Details

As shown in Figure 4.12, the coping cross section has a channel shape, featuring a continuous cleat along the whole length of the edge substrate. The coping is secured at the front face by the cleat through clamping arrangement, whereas at the back face, it is secured by fasteners. As Figure 4.13 illustrates, the coping is composed of three (3) segments: side segments of 1.2 m (4 ft) each, and middle segment of 2.4 m (8 ft) that are joined together by using S-lock joints as shown Figure 4.9. For this study, two sets were used: Set "A" and Set "B". The following is a detailed review of component installation.

1. Cleat Installation

The continuous cleat was fastened, using 25 mm (1 in.) long galvanized roofing nails spaced at 457 mm (18 in.) at the bottom as shown in Figure 4.14 (a) and (b).

2. Pressure Plane Installation

The pressure plane was installed in a similar manner as that of the DCC edge system. See Section 4.4.1 and Figure 4.14 (c), (d) and (e).

3. Coping and Joint Installation

The coping was installed in a similar manner as that of the DCC edge system. See Section 4.4.1 and Figure 4.11.

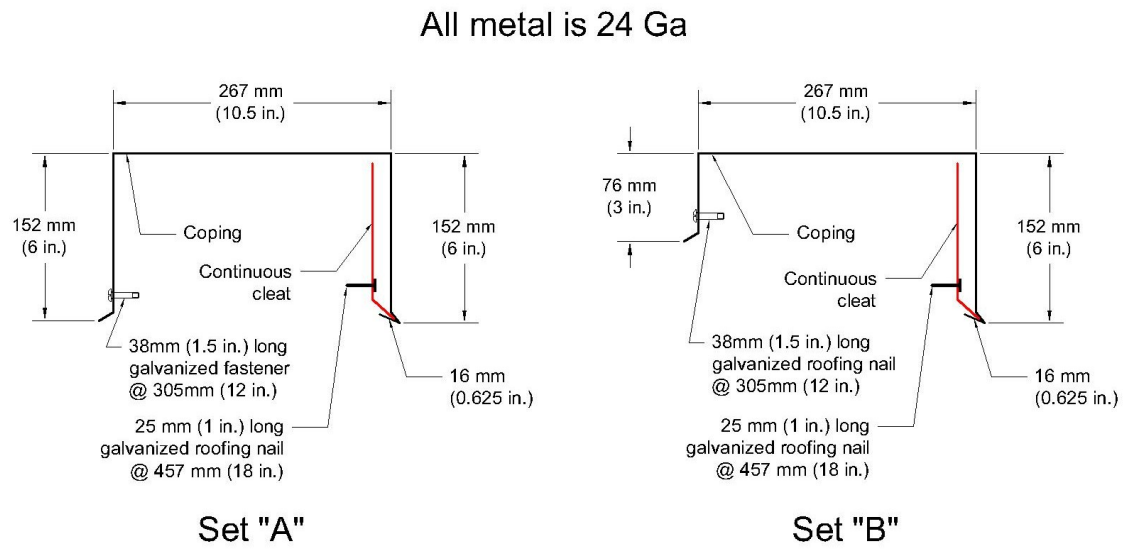

Figure 4.12: Cross section of CCC edge system (not to scale)

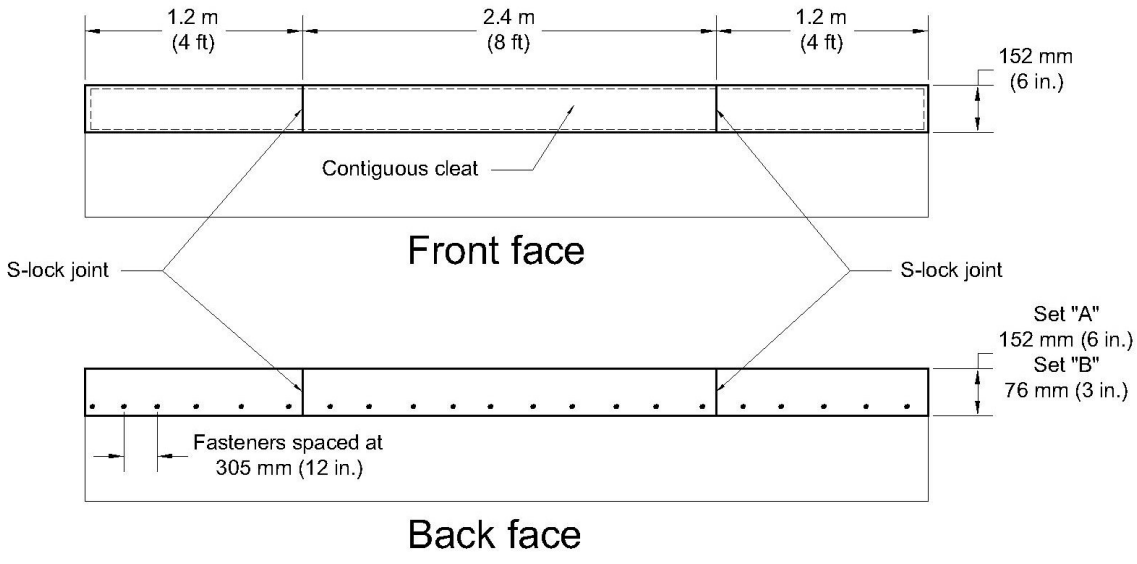

Figure 4.13: Front/back view of CCC coping (not to scale)

(a) Continuous cleat

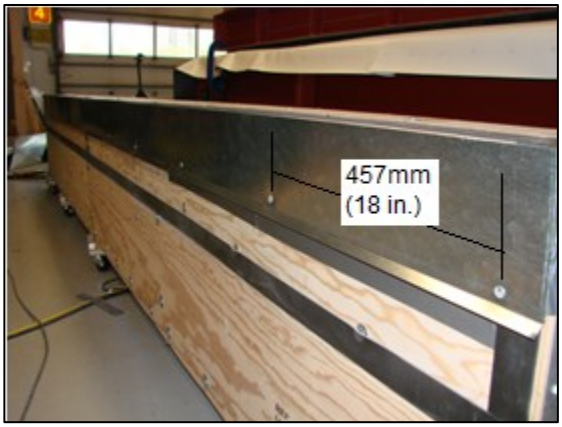

(b) Cleat installed

(c) Installing the pressure plane

(d) Air sealing the pressure plane

(e) Completed pressure plane

Figure 4.14: Installation of cleat and pressure plane for CCC edge system

4.4.3 ACC (Anchor Clip Configuration) Edge System

This type of roof edge system is manufactured by Metal-Era as one of their product line. It is called Perma-Tite Coping System as specified by Metal-Era Roof Edge Solutions (Metal-Era Product Catalogue can be found at http://www.metalera.com/Products.aspx).

Geometry Details

As shown in Figure 4.15, the coping makes use of a full snap-on design utilizing steel anchor clips with built-in stainless steel C-shaped springs. As shown in Figure 4.16, the coping is composed of three (3) segments: side segments of 1.2 m (4 ft) each, and middle one of 2.4 m (8 ft). The coping segments are joined by splice plates that replace the ordinary S-lock joints (Figure 4.17). Two sets were tested: Set "A" and Set "B". The installation of this edge system was done as follows:

1. Anchor Clip Installation

As shown in Figure 4.18 (a), (b) and (c), the anchor clips were mounted on the edge substrate 1.2 m (4 ft) apart such that stainless steel spring faced the back face of the coping. Four 38 mm (1.5 in.) long galvanized steel fasteners were used for securing each anchor clip only at the top.

2. Pressure Plane Installation

As indicated, the anchor clips did not allow fasteners on its face; thus, the pressure plane discontinued at the anchor clips. As a result, the pressure plane was in form of four (4) rubber membrane strips (each is 0.3 m (1 ft) by 1.2 m (14 ft)) that were air sealed, installed and secured by batten bars and No. 10 fasteners with a spacing of 38 mm (1.5 in.). Similar to the pressure planes of the CCC and DCC systems, the pressure planes were

installed over the height of the coping, i.e. 152 mm (6 in.) such that the excess rubber was folded down. See Figure 4.18 (d), (e) and (f).

3. Coping Installation

After the anchor clips and pressure planes were installed, two splice plates were positioned on the anchor clips located 1.2 m (4 ft) away from the edge substrate ends, where the coping joints would exist (Figure 4.19 (a)). As shown in Figure 4.19 (b), (c), (d) and (e), the coping segments were positioned and clipped on the anchor clips. In addition, at the splice plates, the coping segments were secured by the pre-applied adhesive. The completed edge is illustrated in Figure 4.19 (f).

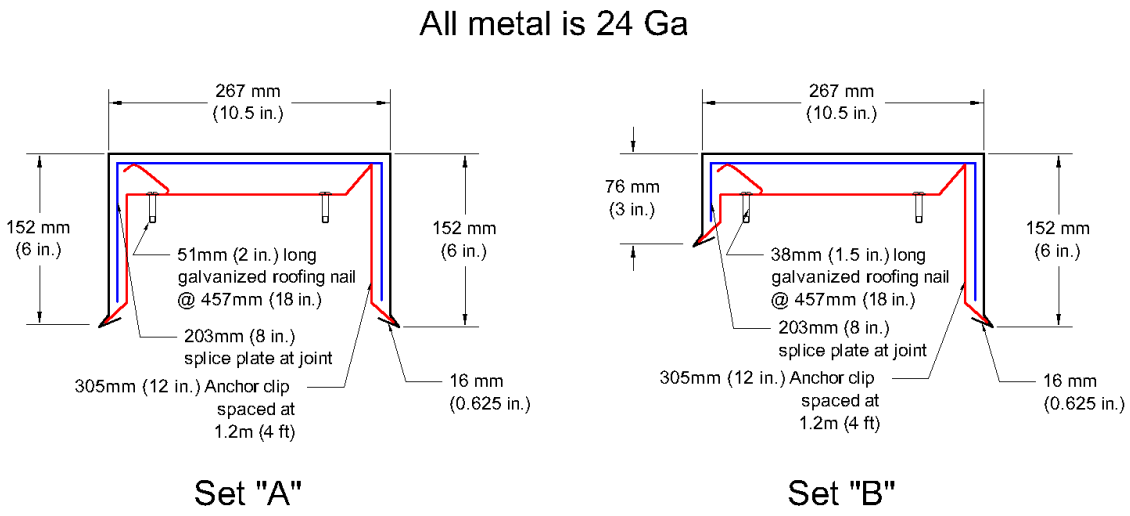

Figure 4.15: Cross section of ACC edge system (not to scale)

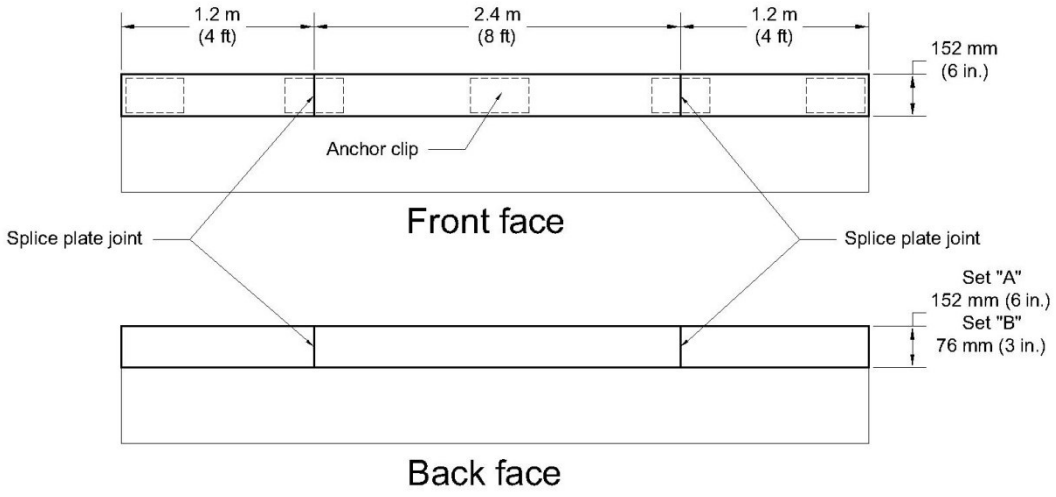

Figure 4.16: Front/back view of ACC coping (not to scale)

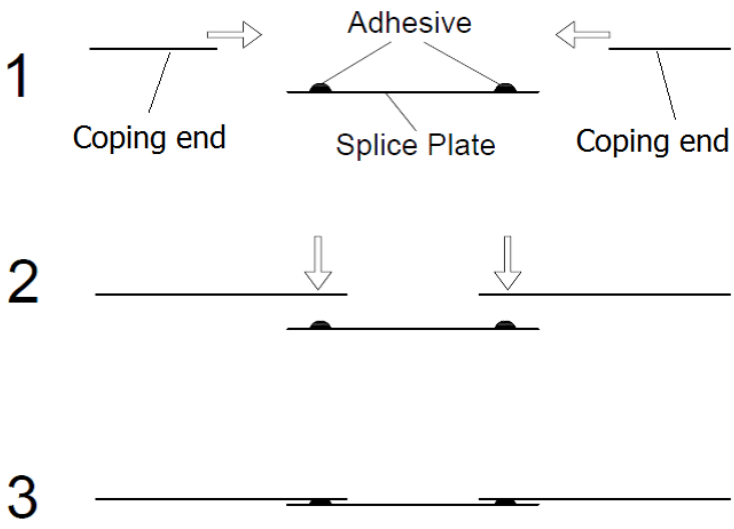

Figure 4.17: Mechanism of splice plate joint

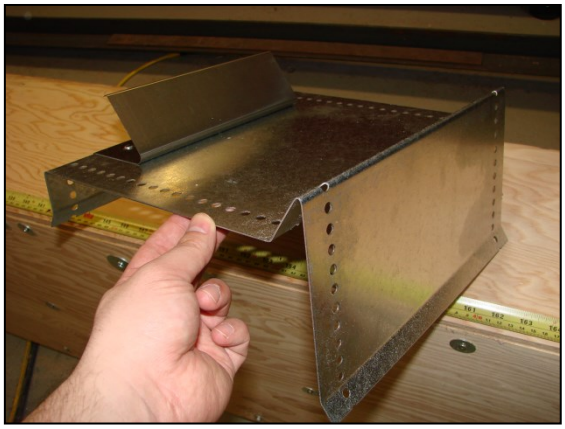

(a) Anchor clip

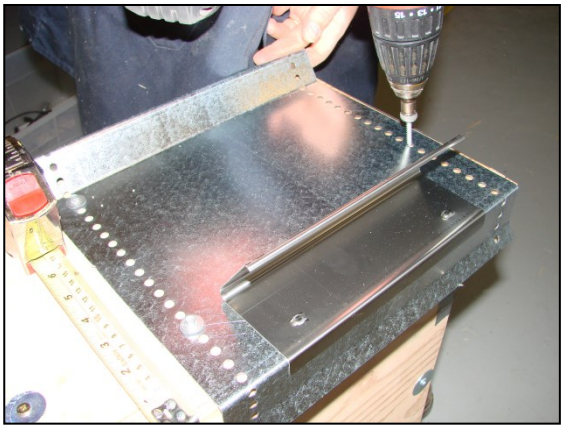

(b) Securing the anchor clip

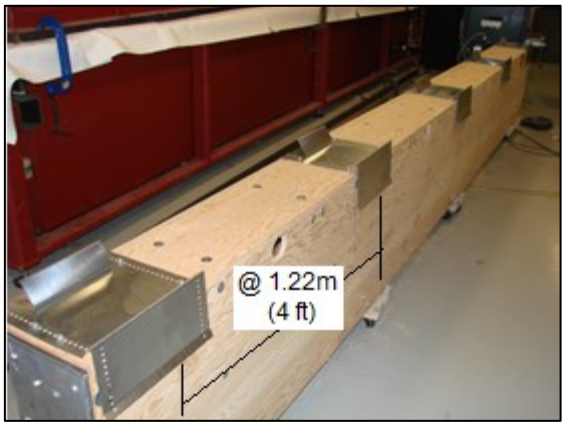

(c) Five anchor clips installed

(d) Air sealing the pressure plane

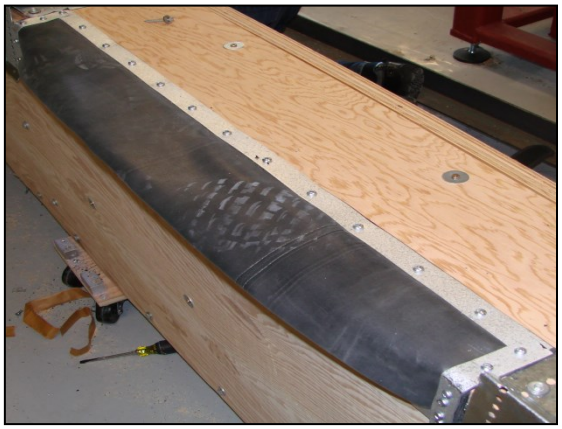

(e) Pressure plane installed

(f) Completed pressure plane

Figure 4.18: Installation of anchor clips and pressure plane for ACC edge system

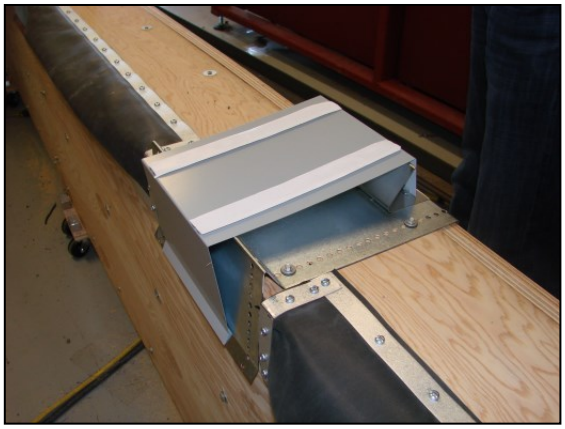

(a) Splice plate

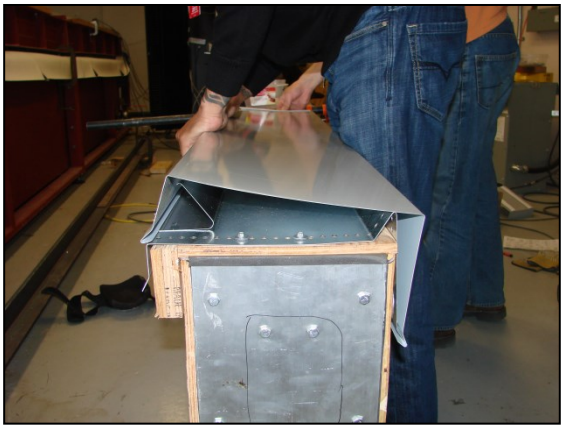

(b) Clipping the coping on anchor clips

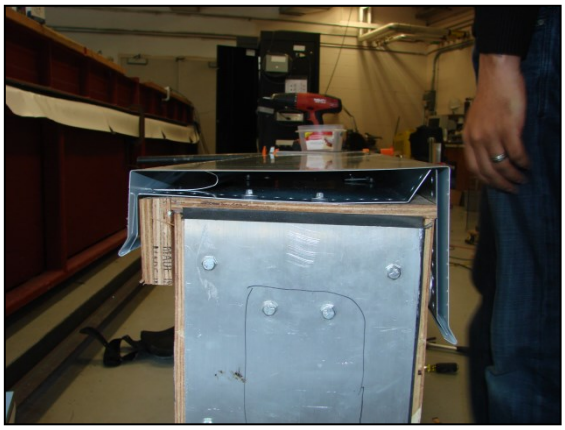

(c) coping clipped

(d) Side segment and splice plate installed

(e) Installing middle segment

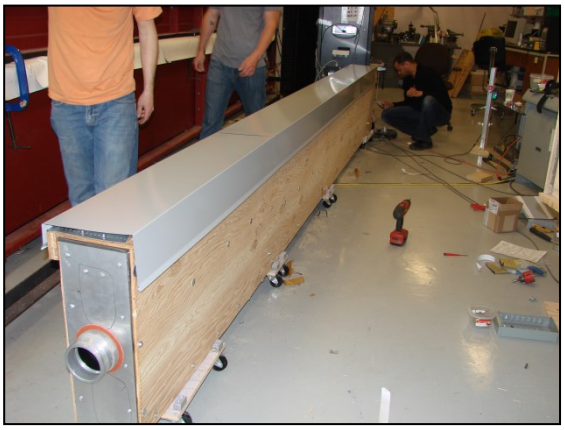

(f) Completed edge ready for testing

Figure 4.19: Installation of coping of ACC edge system

4.5 Instrumentation and Data Acquisition (Module 4)

4.5.1 Pressure Measurement

The pressure measurement was carried out by using a pressure tap in form of copper pipe of 6 mm (0.25 in.) in diameter that was connected to the pressure chamber to collect pressure data. In turn, the pressure tap was connected to a computer and the data acquisition system (DAQ). On one hand, the pressure data were used as feedback for the computer as a part of the operation process. On the other hand, the pressure data were collected and saved by the DAQ in form of time histories for further analysis. As for the pressure tap performance, the pressure tap was connected to a signal converter unit (transducer) that was connected to the VXI unit and then wired with the computer. The transducer translates the mechanical signal from the pressure tap to an electrical signal, whereas the VXI unit converts this signal to a digital signal displayed as a pressure reading on the computer. Figure 4.20 shows a schematic diagram of the pressure tap connection.

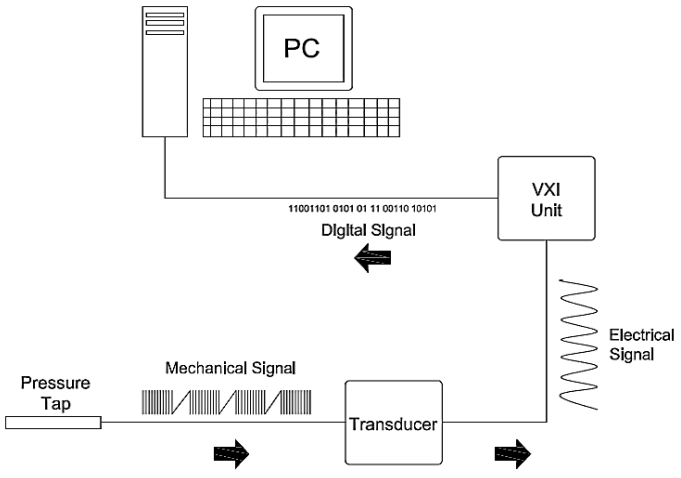

Figure 4.20: Pressure tap setup and connections

4.5.2 Deformation Measurement

The deformations of the test segment of the coping were recorded by laser-powered sensors at different locations: x= 0, L/2, L/4, 3L/4 and L of the test segment (Figure 4.21). As for the sensor connection, each sensor was connected to the controller unit, transducer, and the computer in series.

The sensor emits a laser beam to the point where the deformation is tracked. The beam is then reflected on the coping surface back to a receiver embedded in the sensor. The deformation is simply calculated based on the travelling time of the incident and reflected laser beam. The controller unit is responsible for calibrating the sensors as well as identifying the signals from each one. The transducer converts the signal to an electric signal that is transformed to a readable digital signal by the VXI unit. The deformation data from each sensor were collected and saved for further analyses (see Figure 4.22).

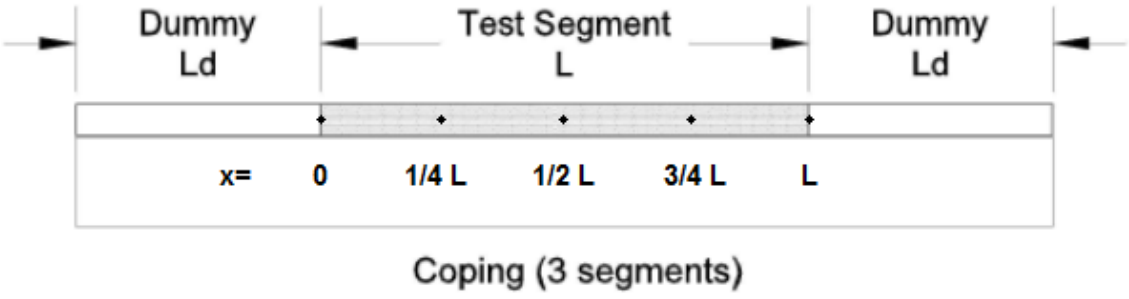

Figure 4.21: Laser sensor locations

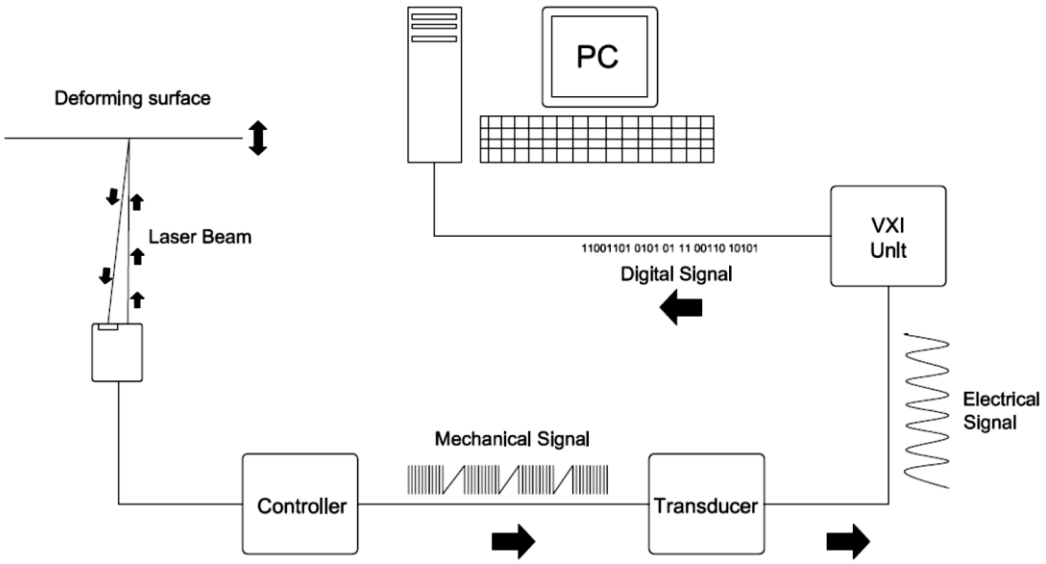

Figure 4.22: Laser sensor setup and connection

4.6 Test Protocols

The term "test protocol" actually stands for the pressure application pattern. The pressure intensity, and therefore the load magnitude, is directly related to the amount of air being pumped into the pressure plane. In addition, persistence of the load depends on persistence of the flow. Theoretically, any test protocol may be pre-programmed and used; however, only two test protocols were utilized in this study. Each will be described in the following sections.

4.6.1 Static Test Protocol

In this test protocol, the gust simulator's flap is fully closed, and pressure build-up is achieved by controlling the flow speed of the blower. As shown in Figure 4.23, the pressure starts at 1.44 kPa (30 psf), and that pressure is maintained for 60 seconds. At the end of this 60-second period, the pressure increases by a fixed increment of 0.72 kPa (15 psf) to reach a total pressure of 2.16 kPa (45 psf). The new pressure level is also maintained for 60 seconds. This process continues up to the failure of the edge system or as required by the test performer (FM Global, 2005).

According to the static test protocol, the edge system's wind uplift rating is determined by the pressure at the level preceding the level at which the structural failure occurs, such as fastener pull-out or coping-cleat disengagement. It is worth mentioning that the amount of deformation is not part of the failure determination. In other words, as long as the edge components structurally remain together, no failure is recorded, even though the edge system may experience a substantial amount of deformation. For example, a 51 mm (2 in.) deformation may lead to water intrusion into the roofing system. For the present study, deformations were monitored and recorded at all pressure levels.

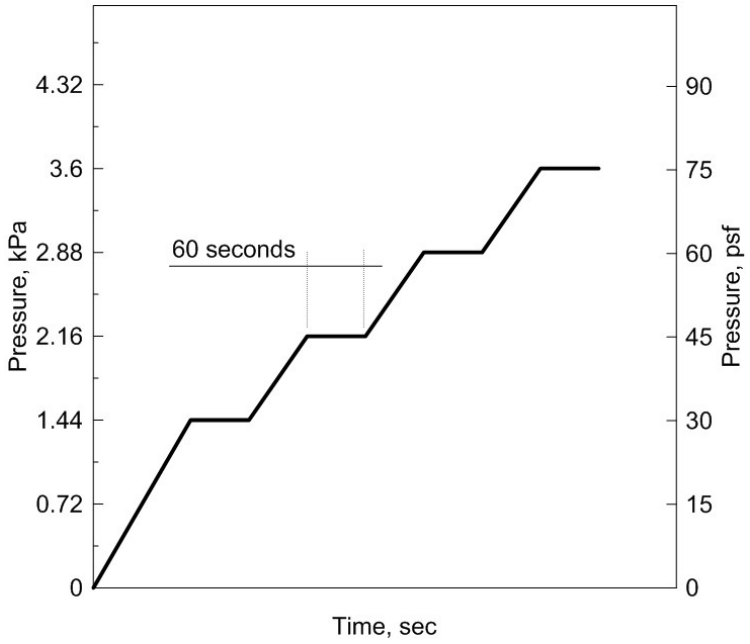

Figure 4.23: Static test protocol

4.6.2 Dynamic Test Protocol (CSA A123.21-10)

In this test protocol, the gust simulator flap closes and opens periodically to simulate wind loading (Figure 4.3). As shown in Figure 4.24, the protocol is composed of five (5) loading levels: A through E, and each level includes eight (8) sequences. In turn, each sequence contains a number of loading cycles (gusts) in form of loading/unloading phases. Throughout the sequence, the pressure fluctuates between two values that are a percentage of a pre-determined test pressure (PT). The total duration of the gust is 8 seconds approximately (Figure 4.25). The test pressure is selected by the test performer/designer based on the design wind pressure calculated by using the design code, such that the system being tested passes at some point the design pressure (CSA A123.21-10, 2010).

For example, code calculations yield a design wind pressure of 2.9 kPa (60 psf); thus, the test pressure is selected at 2.9 kPa (60 psf). The test starts at 25% of the test pressure, i.e.,

0.7 kPa (15 psf) at Level (A), and at the end of the level the pressure reaches 100% PT, i.e., 2.9 kPa (60 psf), where the system is subjected to the design pressure. The loading process continues up to the failure of the edge system or termination by user.

The edge's wind uplift rating is the maximum sustained pressure in the last loading level the edge fully passed. In the previous example, if the edge failed by either fastener pull-out or coping-cleat disengagement at sequence 6 of Level (C), Level (B) will be the last loading level the edge passed in full. As a result, the system rating is the maximum pressure in Level (B), i.e. 125% of PT= 3.63 kPa (76 psf).

Similar to the static test protocol, the dynamic test protocol does not rely on deformation-based failure criteria. In other words, whatever the amount of deformation is, the edge is not considered a failure unless a structural failure occurs. However, large deformations may result in poor weather protection for the roofing system.

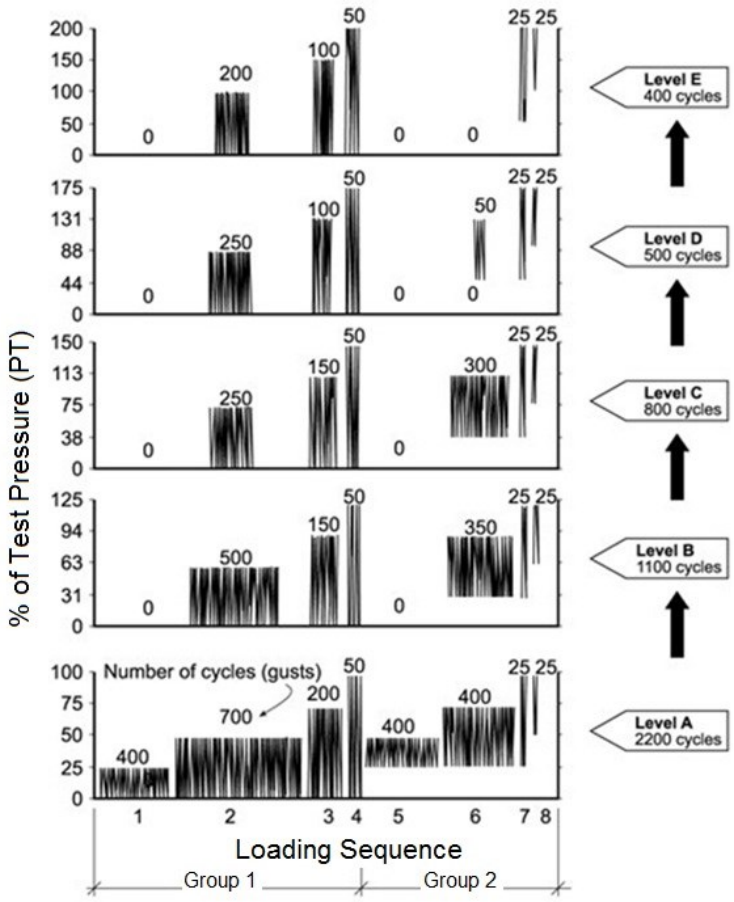

Figure 4.24: Dynamic test protocol (CSA A123.21-10)

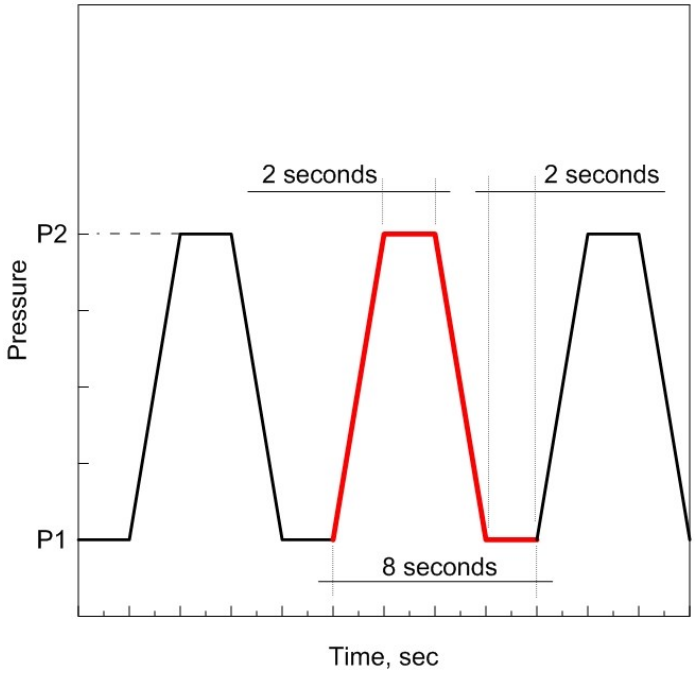

Figure 4.25: Gust duration (CSA A123.21-10)

4.7 Feedback Operation

After the edge system was installed, the operation of the test was done through steps as follows:

1. The blower was tightly connected to the pressure chamber by using a hose.
2. The gust simulator was connected to the controlling computer.
3. The gust simulator's flap was checked up for normal operation.
4. Pressure taps were connected to DAQ.
5. The laser sensors were connected to DAQ.
6. The type of test protocol was selected, and the test started.

The test process runs as follows:

The computer reads the pressure inside the pressure chamber, and based on the selected test protocol the computer sends signals to the blower through the AC drive to pump air into the pressure chamber at a specific speed. Instantaneously, the computer sends a signal to the gust simulator to take a position based on the required pressure as specified by the test protocol. This process is repeated based on the requirements of the test protocol until the test ends by component failure, termination by test performer or when the test protocol reaches its end. The data acquisition system collects and saves data of pressure and deformations of the coping.

Chapter 5. Results & Discussion

5.1 Introduction

A roof edge system is composed of different components that are integ1rated, using adhesive, fasteners or both to resist wind uplift forces. This chapter presents and discusses the performance of the three edge systems discussed in Section 4.4 under static and dynamic loading. In doing so, first the load transfer path through edge components is discussed and followed by a side-by-side performance comparison of the CCC and ACC edge systems. In a similar manner, a performance comparison of the CCC system and DCC system is also presented.

5.2 Geometry and Load Transfer Path

When an edge system is subjected to negative wind pressure, the load is transferred through the structural components of the edge system in a path called the "load transfer path". Every edge system establishes its own load transfer path depending on its structural components and integration. In this section, the discussion is limited to the tested roof edge systems, as follows:

1. **DCC Edge System:** The coping is secured by a discontinuous continuous cleat through clamping arrangement. In turn, the cleat is secured to the edge substrate by using nails. Besides, the coping is secured at the back face, using fasteners as no cleat exists. Furthermore, coping segments are connected by using S-lock joints; see Figure 5.1 (a).

   When the coping is exposed to negative pressure (suction), a resistance is produced in the coping in form of load which distributes along the coping through the coping

joints. Then, the load is transferred to the cleat through the clamping arrangement. As the last stage, the load is transferred to the edge substrate (nailer) by the cleat nails (Figure 5.1 (b)).

2. **CCC Edge System:** This system shares the same coping-cleat integration and S-lock joints with the DCC system. However, this system utilizes a continuous cleat; see Figure 5.2 (a).

   The load transfer path is similar to the one of the DCC system. However, due to the presence of a continuous cleat, the load transfers through the entire length of the cleat/coping (Figure 5.2 (b)).

3. **ACC Edge System:** Unlike, CCC and DCC systems, the ACC coping is secured by anchor clips through snap-on arrangement at both the front and back face. As for the anchor clip fastening, it is secured by fasteners only at the top. Contrary to the CCC system, splice plate joints replace S-lock joints when more than one coping segment is installed; see Figure 5.3 (a).

   When the coping is subjected to suction, a reaction load is produced and distributed along the coping through the splice plate joints and the built-in adhesives. Next, the load is transferred through the snap-on arrangement to the anchor clips. Finally, the load reached the edge substrate through the anchor clip fasteners (Figure 5.3 (b)).

In short, in order to sufficiently resist wind loads, the edge system shall maintain the load transfer path during its service life such that the load is properly distributed among the structural components of an edge. In fact, the developed experimental method is intended for evaluating roof edge systems through testing the ability of the edge components to establish and to maintain the load transfer path under static/dynamic loading.

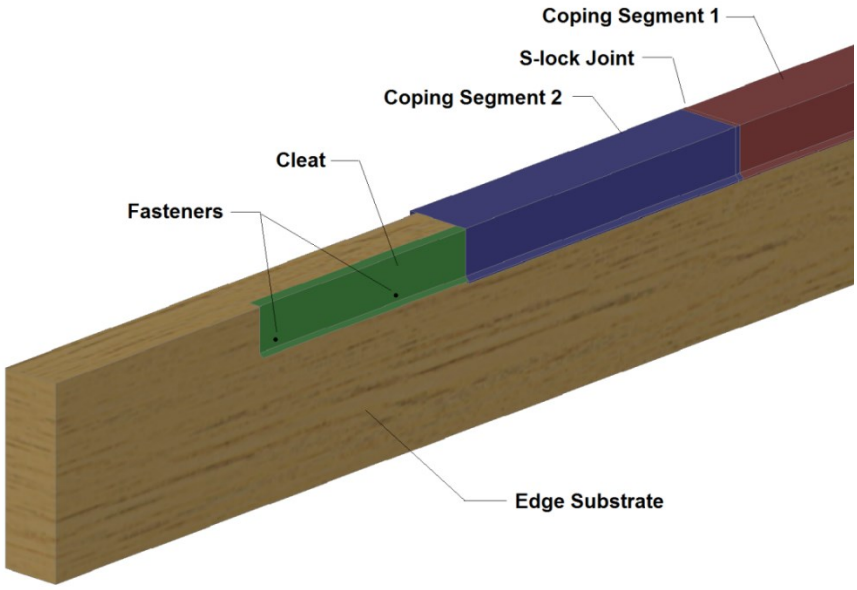

(a) Edge components

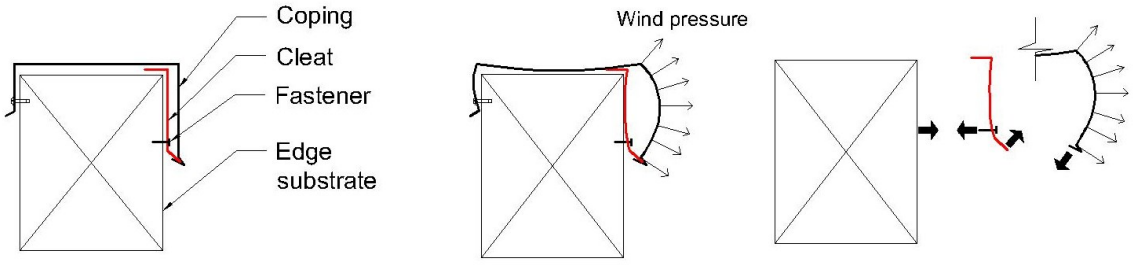

(b) Load transfer path

Figure 5.1: Components and load transfer path of DCC edge system

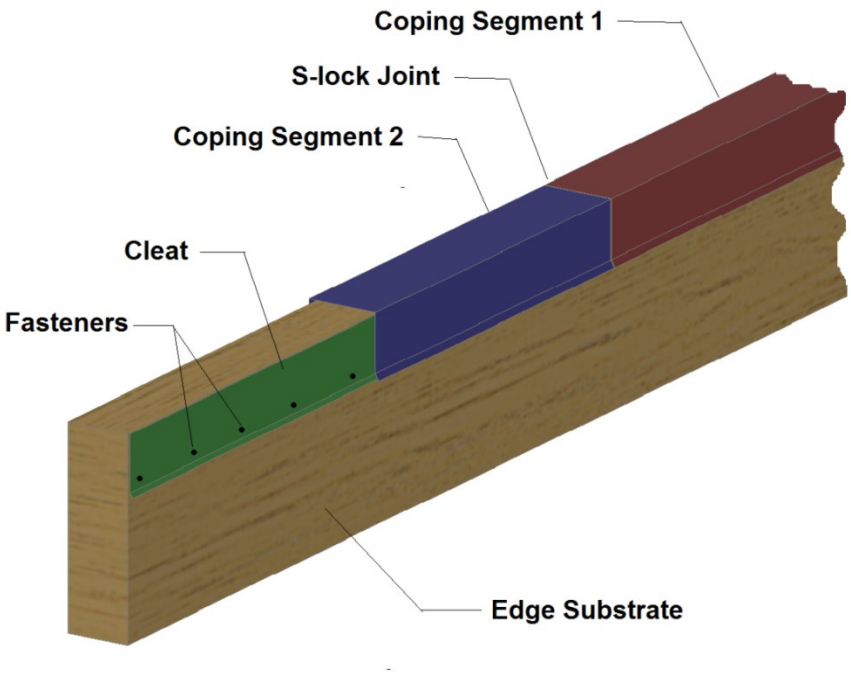

(a) Edge components

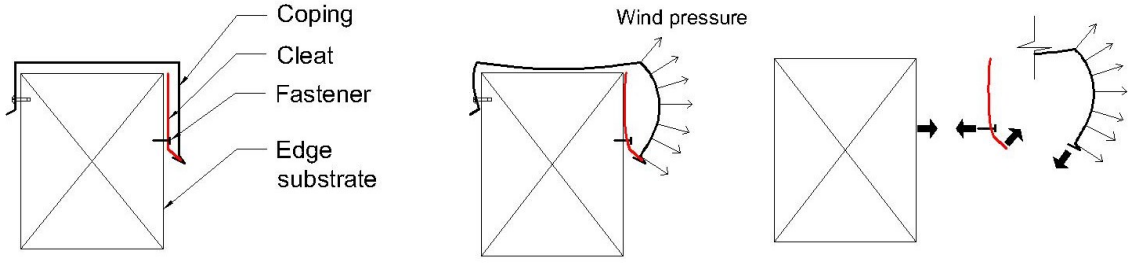

(b) Load transfer path

Figure 5.2: Components and load transfer path of CCC edge system

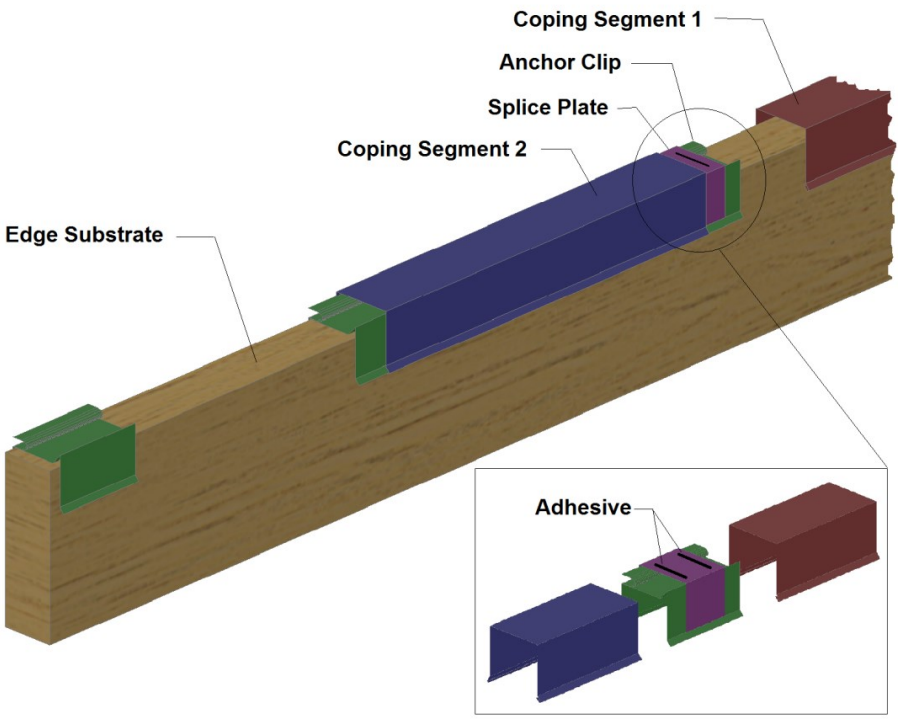

(a) Edge components

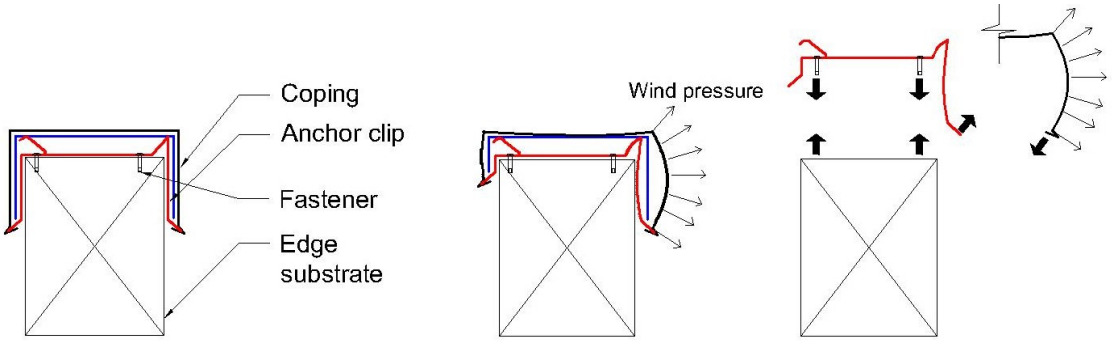

(b) Load transfer path

Figure 5.3: Components and load transfer path of ACC edge system

5.3 Test Array and Summary Results

As shown in Table 5.1, the three edge systems were tested under static and dynamic loading. As indicated in Section 4.4, two sets, A and B, were tested for each of the edge systems. The total number of tests conducted was eleven (11) tests. The two sets of the CCC system successfully completed the test with no structural failure. On the other hand, the coping of DCC system (Set "B") failed at 10 kPa (210 psf) corresponding to a sustained pressure of 9.6 kPa (200 psf). Similar to CCC, the two sets of ACC completely passed the test with no failure. In the next sections, the experimental observations and data analysis will be discussed but limited to Set "B" of each edge system since Set "A" and Set "B" produced very similar results.

Table 5.1: Test array of the roof edge systems by using the developed experimental method

Edge System	**Set**	**Sustained**		**Failed**		**Failure Mode**
		Dynamic kPa (psf)	*Static kPa (psf)*	*Dynamic kPa (psf)*	*Static kPa (psf)*	
CCC	A	14.35 (300) Level (E)	14.35 (300)	-	-	N/A
	B	14.35 (300) Level (E)	14.35 (300)	-	-	N/A
DCC	B	8.4 (175) Level (D)	9.33 (195)	9.6 (200) Level (E)	10 (210)	Coping-cleat disengagement
ACC	A	14.35 (300) Level (E)	14.35 (300)	-	-	N/A
	B	14.35 (300) Level (E)	14.35 (300)	-	-	N/A

5.4 Effect of Wind Load Simulation

In this section, the discussion focuses on the effect of wind load simulation on the performance of DCC edge system. For this purpose, two identical systems were tested: one by dynamic loading (CSA A123.21-10) and the other by static loading. Mainly, observations about the response of the coping under both loading scenarios are discussed. Further, the term "Rigidity Index" is introduced as an indication of the coping rigidity and therefore the reliability of the system.

5.4.1 Performance of DCC Edge System under Dynamic and Static Loading

Test Performance

As shown in Figure 5.4, under dynamic loading scenario, a test pressure of 4.8 kPa (100 psf) was selected. The pressure started at 1.2 kPa (25 psf) in Level (A) and ended at 9.2 kPa (200 psf) in Level (E), where the edge failed due to complete coping disengagement from the cleat. As a result, the system's rating was equal to the sustained load, **8.37 kPa (175 psf)**.

On the other hand, in the case of the static loading scenario, the pressure started at 1.44 kPa (30 psf) and incremented to the next level by 0.72 kPa (15 psf). Each incremental load was maintained for a period of 60 seconds. Eventually, the system failed at a pressure of 10 kPa (210 psf), and the rating of the system was equal to the sustained load, **9.33 kPa (195 psf)** (see Section 4.6 for more details about the test protocols).

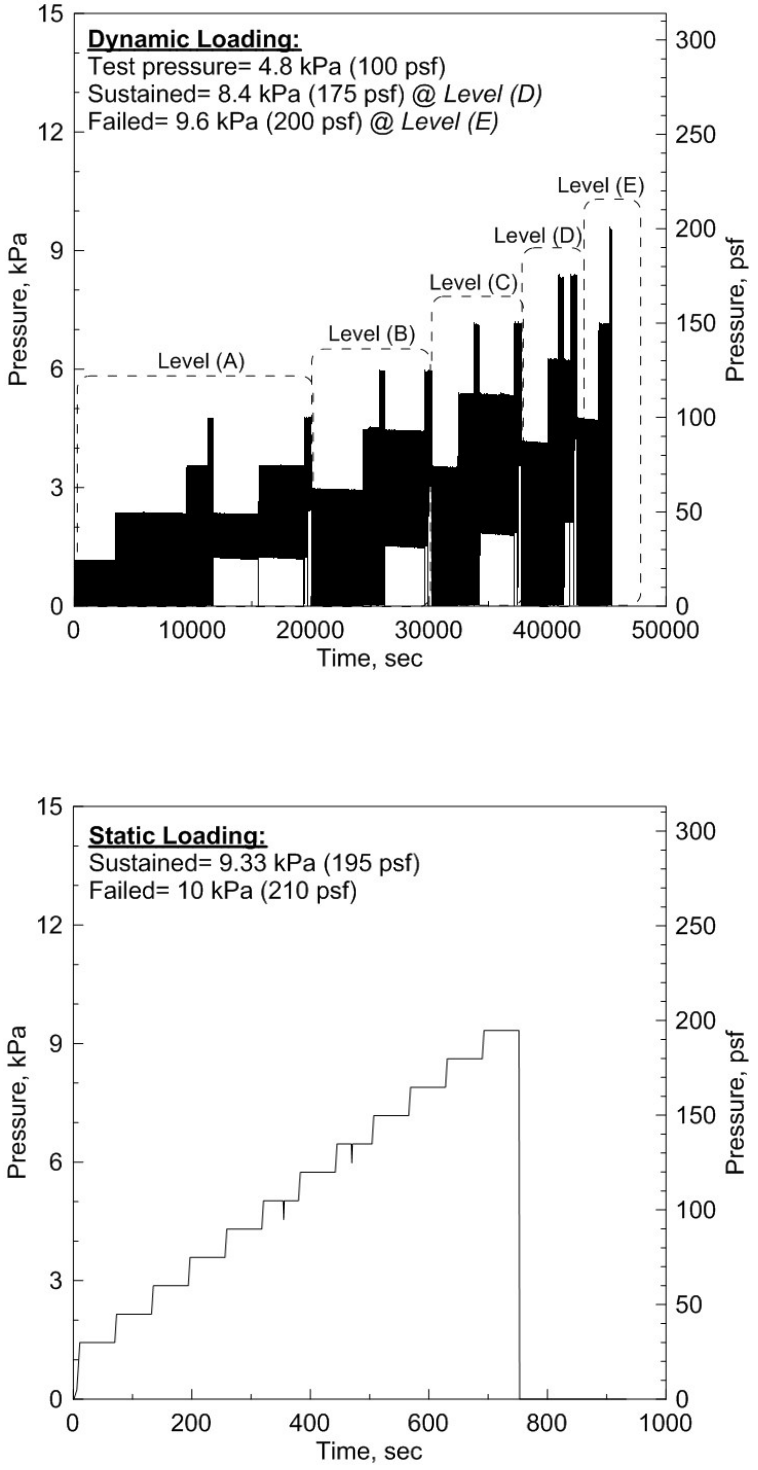

Figure 5.4: Effect of wind load simulation on DCC system

Failure Mode

Coping-cleat disengagement was the failure mode of the system under both loading scenarios (Figure 5.5). However, the system's rating based on the dynamic test protocol was evidently lower than that of the static test protocol. This is attributed to the fact that the dynamic test protocol typically performs 5000 cycles over a period of 13 hours, which takes into consideration the fatigue phenomenon.

Coping Performance

Figure 5.6 shows the performance of the coping under static and dynamic loading subjected to a pressure of 7.18 kPa (150 psf) and just before failure. During the loading process, the coping had very similar deformed shape under both scenarios. The common observation was that the deformations were minimal in the middle of the coping, whereas the coping greatly deformed at the joints.

Coping Joint Performance

Figure 5.7 shows the coping joint just before failure under both loading scenarios. Due to the presence of the discontinuous cleat, the coping joints (S-lock) were unsecured; therefore, they were able to deform more freely in comparison to the secured parts of the coping. Consequently, the coping segments were mostly deforming at the joints. It was also noted that the connected coping segments partially slipped apart at the joints. That was observed under both loading scenarios; it happened at Level (A) under dynamic loading and a pressure of 5 kPa (105 psf) under static loading.

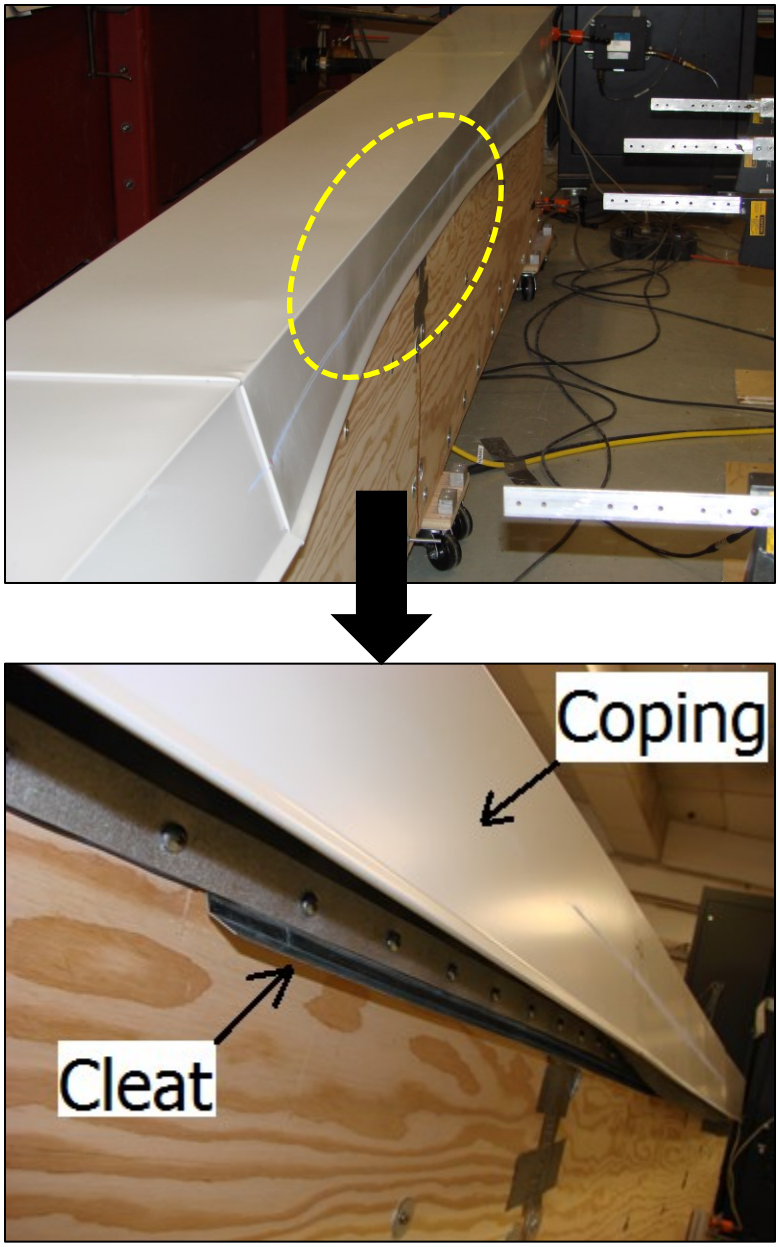

Figure 5.5: Failure mode of DCC edge system under dynamic and static loading

	Under dynamic loading	Under static loading
At 7.17 kPa (150 psf)	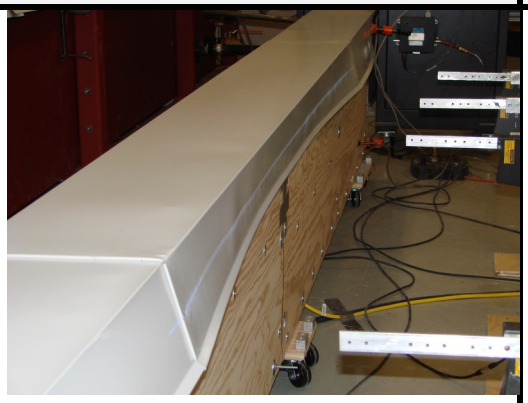	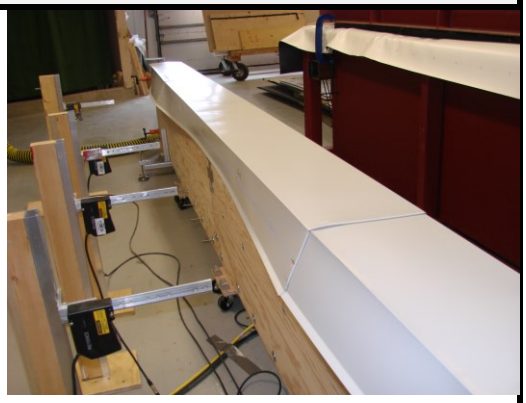
Just before failure	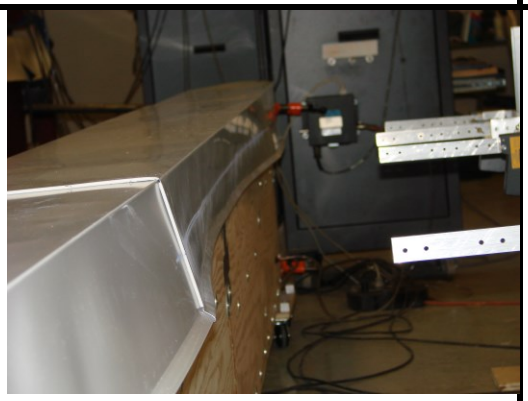	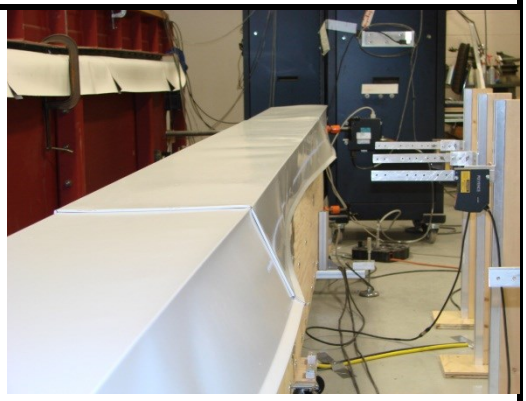

Figure 5.6: Performance of DCC coping under dynamic and static loading

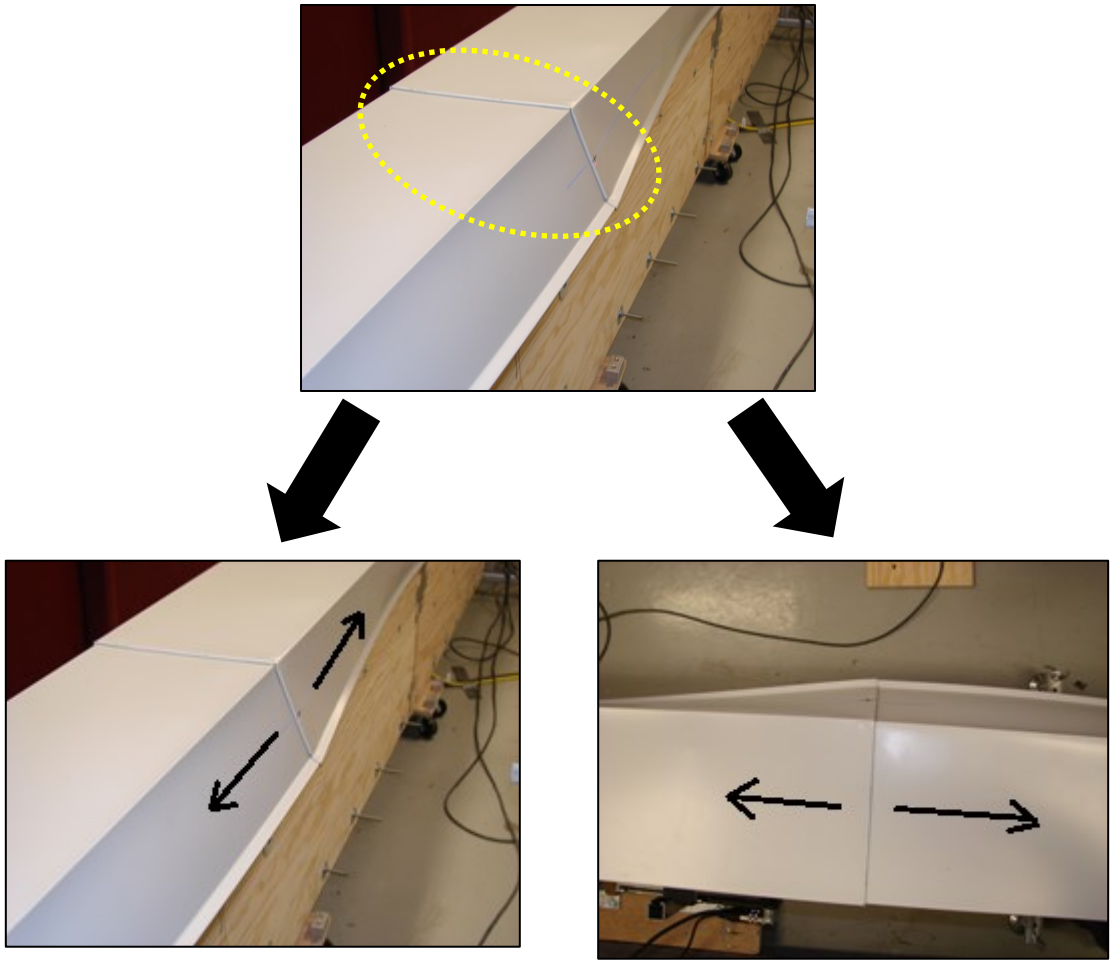

Figure 5.7: Performance of DCC coping joint under dynamic and static loading

5.4.2 Edge Response Analysis

It has been decided to validate the collected data from the experiments before presenting the response of the edge system. This has been done under two scenarios as follows:

1. Applied pressure vs. deformation
2. Symmetrical validation of deformation

Data Validation

Applied pressure vs. deformation. It was expected that the edge system would respond to the applied pressure in a harmonized fashion. This has been demonstrated in Figure 5.8 for both dynamic and static loading. The deformations of the coping increased as the applied pressure increased in the case of the static loading. With respect to the dynamic loading, the deformation behaved in a cyclic pattern similar to the applied loading.

Symmetrical validation of deformation. Given the uniformity of the applied load on the coping, coping joints should theoretically deform by the same amount (symmetry of system). However, due to installation conditions, the actual deformations may deviate from the ideal case. Thus, deformation data were checked against deviation from the perfect case. For this purpose, the deformation data of x= 0 (joint 1) and x= L (joint 2) were plotted versus each other. In the case of dynamic loading (Figure 5.9 (a)), the data were distributed along y= 0.91 x. On the other hand, y= 0.90 x fitted the deformation data under static loading; see Figure 5.9 (b). As shown in Figure 5.9 (b), two data points appear to fall out of the fit because the joints deformed suddenly and individually at those points. On the contrary, in Figure 5.9 (a), that incident did not happen clearly under dynamic loading. As an explanation, load cycling seemed to contribute to greater consistency in the way the two joints deformed.

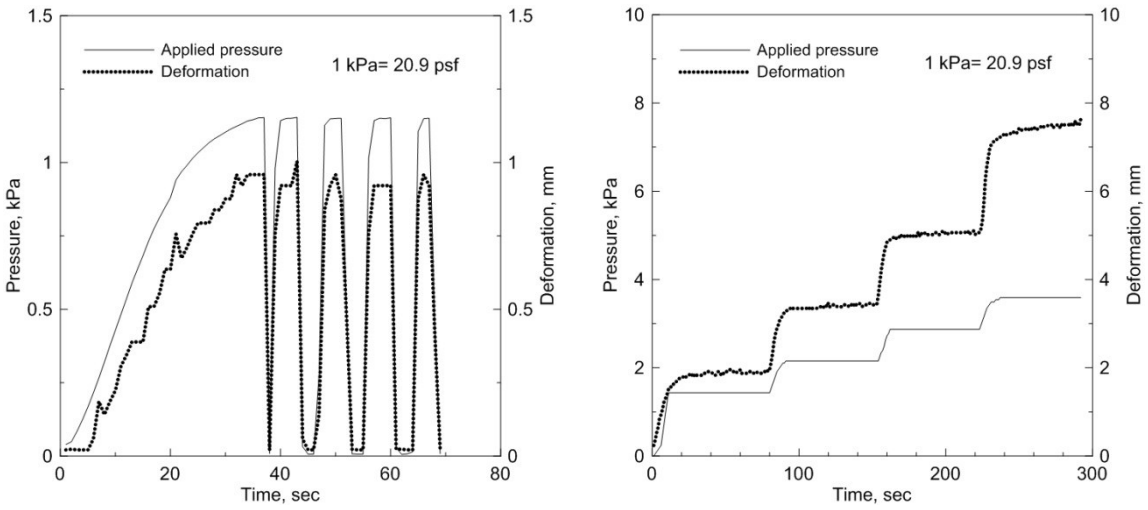

(a) Under dynamic loading (b) Under static loading

Figure 5.8: Validation of applied pressure vs. deformation data of DCC system

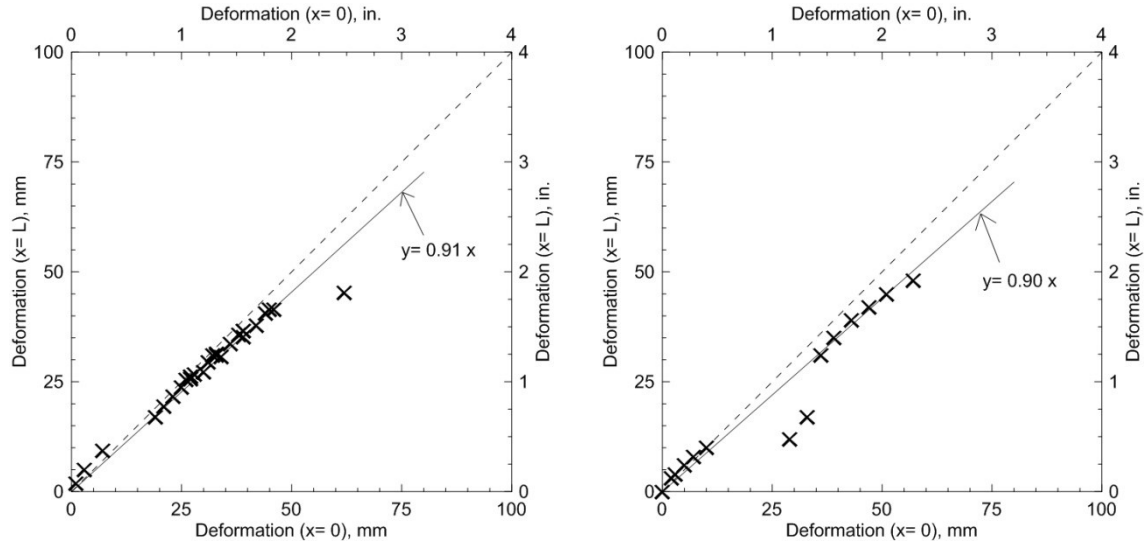

(a) Under dynamic loading (b) Under static loading

Figure 5.9: Symmetrical validation of deformation data of DCC edge system

Deformation of Coping

Figure 5.10 and Figure 5.11, show the deformation time history at x= 0 (joint) and x= L/2 (midpoint) under dynamic and static loading scenarios. In the case of dynamic loading, the deformation behaved cyclically in form of sequences and levels similar to the applied load. On the other hand, the deformation grew incrementally under static loading.

At x= 0 (Joint). The deformation reached a maximum of 62 mm (2.45 in.) under dynamic loading and 57 mm (2.25 in.) under static loading. Both plots in Figure 5.10 also show the excessive deformation (jump) of the joint that happened at t= 11000 sec (dynamic) and t= 380 sec (static). That is, as discussed earlier, attributed to the fact that the joints were not supported, resulting in sudden, large deformations. However, the excessive deformation of the joint appeared to be less noticeable under dynamic loading in comparison with the static loading scenario. This observation is attributed to the fact that the cyclic loading allowed the joint to restore some of the elastic deformation, where the load periodically dropped down to zero in every cycle. On the other hand, the static loading, which was continuously applied, did not permit restore of deformation. At the end of the test, the residual deformation of the joint was 18 mm (0.7 in.) under the dynamic scenario and 33 mm (1.3 in.) under the static one.

At x= L/2 (Midpoint). As shown Figure 5.11, the deformation was minimal under both loading scenario, where the largest deformation observed was 10 mm (0.4 in.) under dynamic loading and 5 mm under static loading. As the cleat secured only the central 1016 mm (40 in.) of the test segment of the coping, the secured area was restricted from movement due to the outward deformations of the unsecured joints at the sides of the test segment. This is further explained by the beam representation illustrated in Figure 5.12,

where the edge is represented by a three-span beam with hinges and fixed ends. The middle span of the beam represents the test segment of the coping, and the side spans represent the dummy segments. In addition, the cleat is symbolized by a roller located in the mid-span of the beam. Concerning the performance, when exposed to a uniformly distributed load Figure 5.12, the beam deforms insignificantly where supported by the roller. On top of that, the deforming hinges, as a result, produce negative bending moment in the middle that contributes to greater resistance to the applied load. This discussion is valid for the performance of the DCC coping under the applied load (pressure), where the coping joints are represented by the hinges.

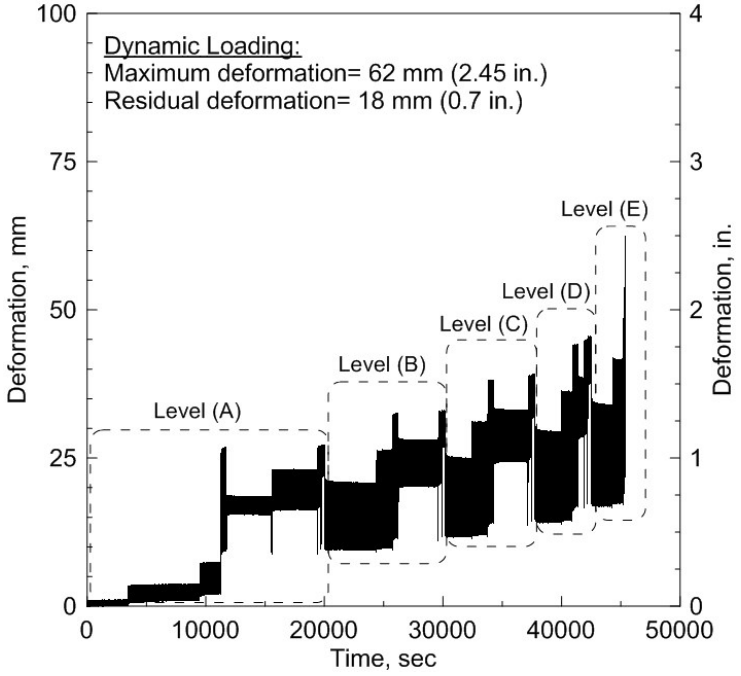

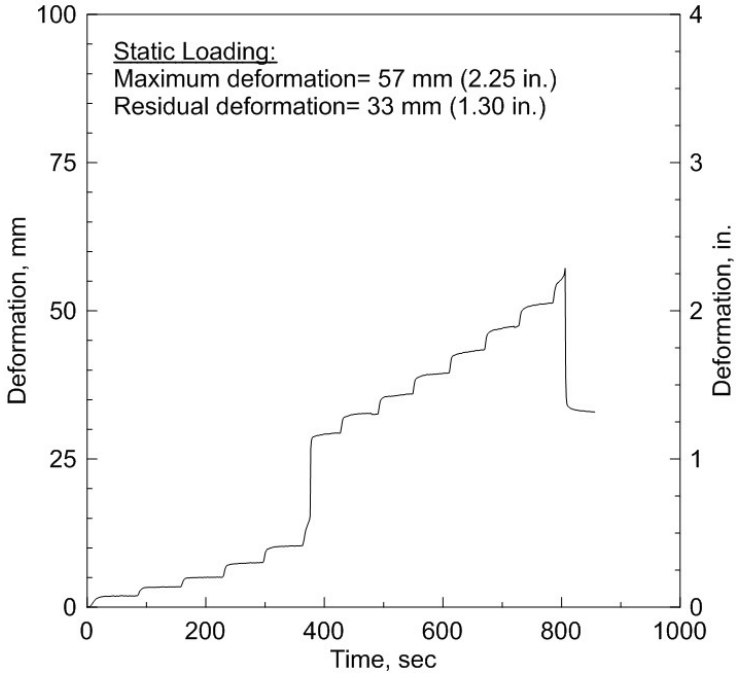

Figure 5.10: Deformation of DCC coping at x= 0

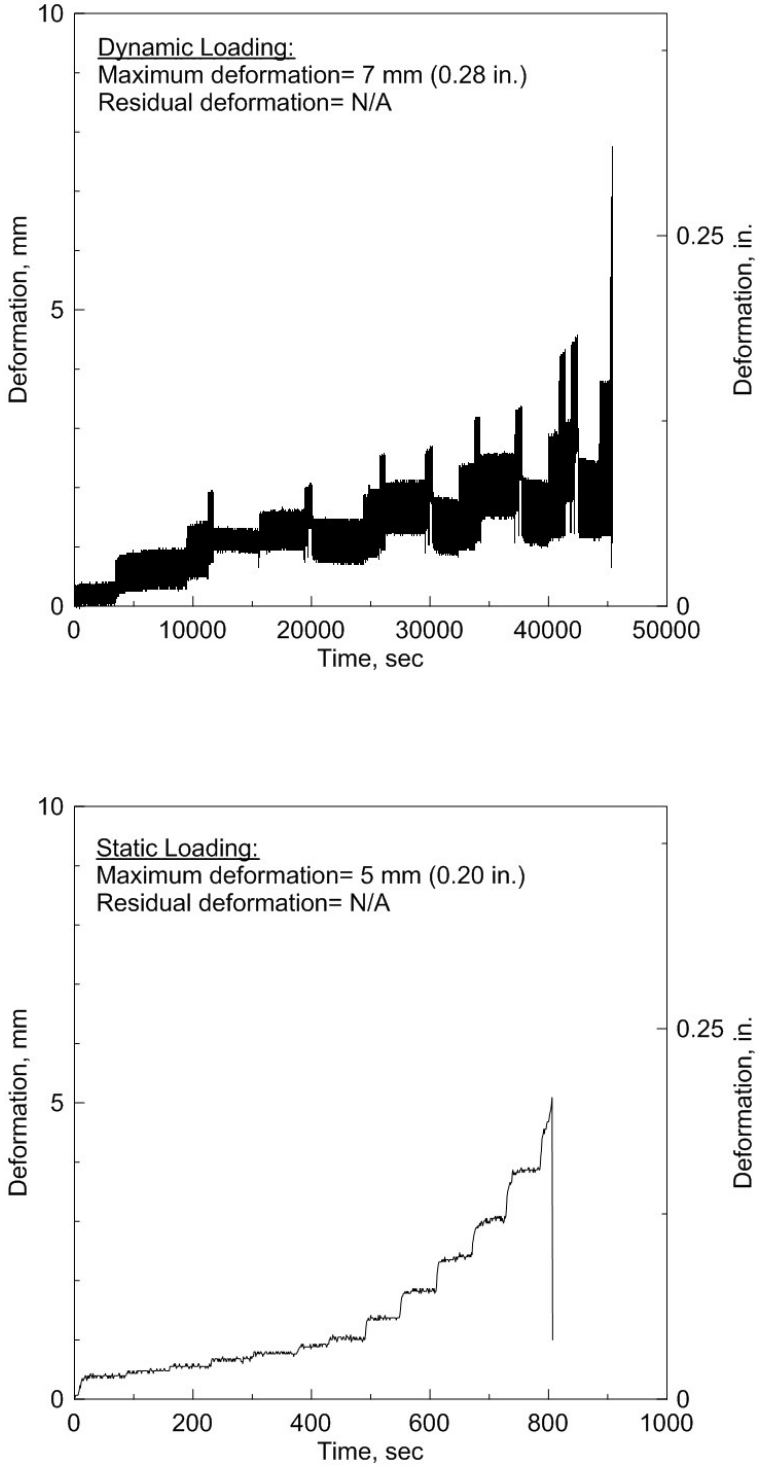

Figure 5.11: Deformation of DCC coping at x= L/2

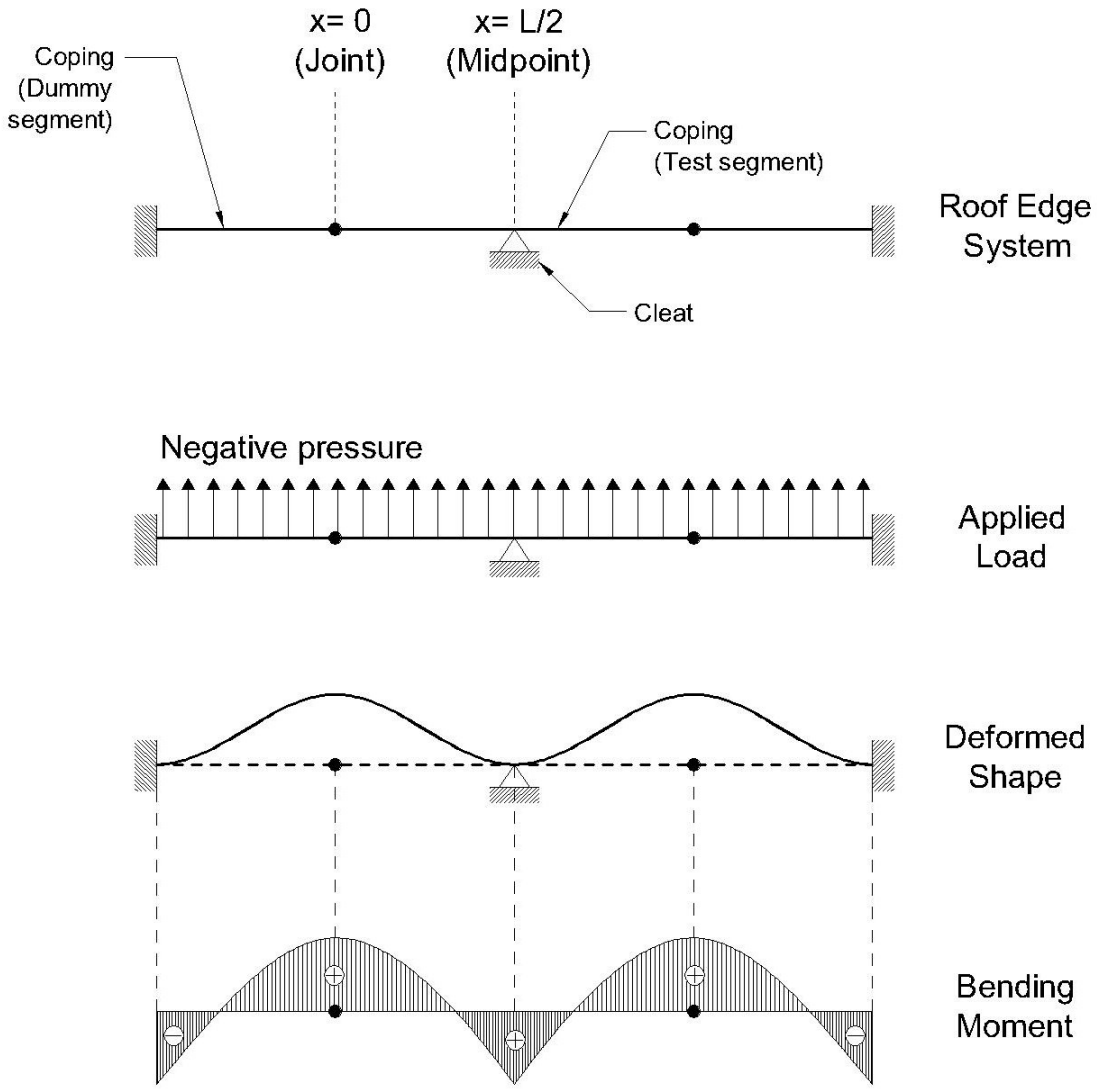

Figure 5.12: Beam representation of DCC edge system

5.4.3 Rigidity Index Analysis of Roof Edge System

In general, the overall response of an edge system depends on the response of its individual components. However, only the global response of the edge system can be evaluated such that it acts as one body. For this purpose, the term "Rigidity Index" was introduced as an indicator for the resistance of the coping against the applied load. The rigidity index, in definition, is the load required by the coping to deform the unit load. For instance, if the rigidity index of a coping is 0.5 kPa/mm (265.5 psf/in.), it means that the coping would deform 1 mm when it is exposed to 0.5 kPa (1 in. when exposed to 265.5 psf). As for the calculation of the rigidity index, it can be computed at any moment during the test through dividing the applied load by the respective deformation of the coping, as follows:

$$Rigidity\ Index = \frac{P}{D} \qquad \frac{kPa}{mm} \ \left(\frac{psf}{in.}\right)$$

In this section, the response of the DCC edge system is discussed with respect to the rigidity of the coping under both loading scenarios at x= 0 (joint) and x= L/2 (midpoint) in order to support the previously discussed observations.

At x= 0 (Joint). As shown in Figure 5.13 (a), under dynamic loading, the rigidity index started at 1.2 kPa/mm (637 psf/in.) and dropped to 0.19 kPa/mm (101 psf/in.) at a pressure of 2.4 kPa (50 psf) where the rigidity index stabilized until the failure of the system. In the case of static loading, the rigidity index started at 0.7 kPa/mm (372 psf/in.) and dropped to 0.19 kPa/mm (101 psf/in.) at a pressure of 5 kPa (105 psf). That is to say, under both loading scenarios, the rigidity index eventually stabilized; however, under dynamic loading, the minimum rigidity index had been reached at even lower pressure in comparison to the case of static loading.

At x= L/2 (Midpoint). As illustrated in Figure 5.13 (b), under dynamic loading, the rigidity index ranged between 1.5 kPa/mm (796 psf/in.) and 3 kPa/mm (1593 psf/in.). However, under static loading, the rigidity index started from 3.8 kPa/mm (2017 psf/in.) and reached a maximum value of 5.5 kPa/mm (2910 psf/in.) before it dropped to 2 kPa/mm (1062 psf/in.).

The load cycle affected the edge system by causing fatigue which was well translated by an early drop in the rigidity index. Under dynamic loading scenario, the rigidity index maintained lower values at low-to-medium load magnitudes compared to the results of the static scenario. This observation seems to be consistent with the fact that wind loads typically occur in low-to-medium magnitudes.

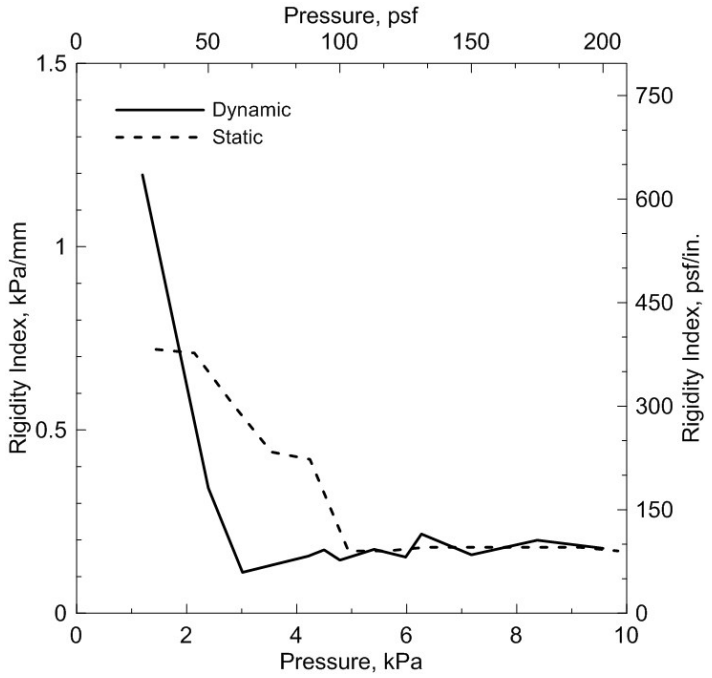

(a) x= 0

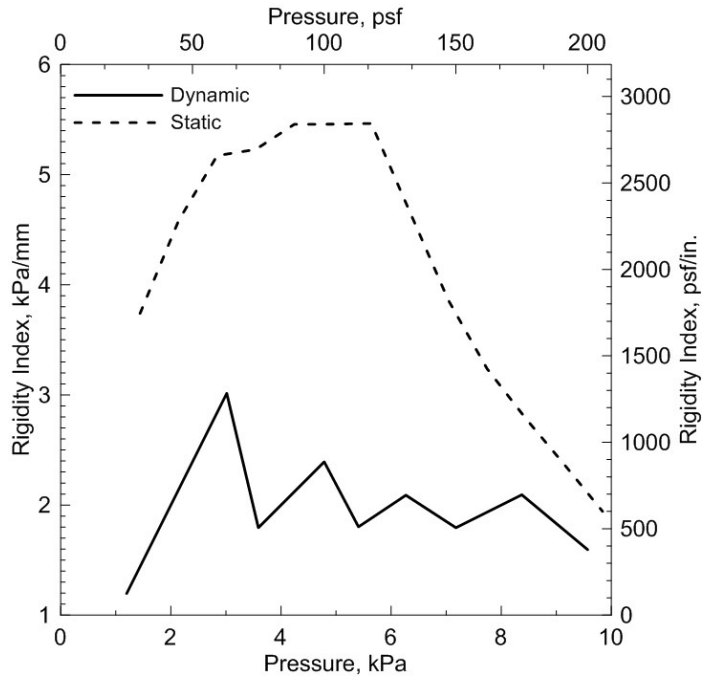

(b) x= L/2

Figure 5.13: Rigidity index of DCC edge system under dynamic and static loading

5.4.4 Discussion and Conclusion

This section presented and discussed the observations on the DCC edge system when tested under dynamic and static loading. Even though the failure load was the same under both scenarios, the rating of the system was expectedly lower when tested, using the dynamic test protocol in comparison with the static test protocol. In addition, the failure mode was the same in both loading cases. In terms of the response of the coping and joints, the edge system exhibited similar behaviour under both loading cases, where, the main observations were excessive deformation at the joints and minimal deformations at the midpoint of the coping.

Furthermore, the analysis of the coping rigidity index showed that lower values of rigidity index were reached at relatively lower loads under dynamic loading. On the contrary, the rigidity index unrealistically had larger values.

The performance comparison of the edge system under both test protocols showed that the dynamic test protocol would produce more effective evaluation of the tested edge system. The dynamic test protocol comes up as an adequate option for testing roof edge components under more realistic conditions.

5.5 CCC vs. ACC Edge System

CCC and ACC edge system were tested based on the dynamic test protocol (CSA A123.21-10). This section is dedicated to discussing and comparing the performance of the CCC and ACC edge systems under dynamic loading in terms of edge system response and rigidity analysis.

5.5.1 Performance of Edge System under Dynamic Loading

Test Performance

As Figure 5.14 depicts, for both edge systems the test pressure was selected at PT= 7.18 kPa (150 psf). The load, therefore, started at 25%PT= 1.8 kPa (38 psf) and ended at 200%PT= 14.35 kPa (300 psf). Both edge systems successfully passed all loading levels and completed the test with no failure. The observed response was solely limited to coping and joint deformations. Thus, the rating of both systems was **14.35 kPa (300 psf)**.

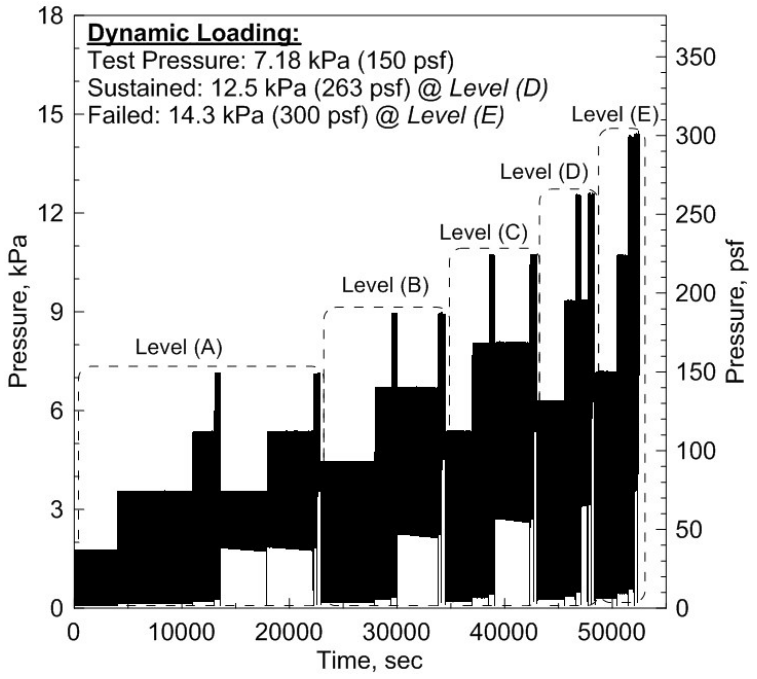

Figure 5.14: Test performance of CCC and ACC edge system under dynamic loading

Failure Mode

Neither the CCC nor ACC failed; hence, no failure mode was observed.

Coping Performance

Figure 5.15 graphically compares the performance of the CCC and ACC edge systems at the first loading level (A) and the last loading level (E).

Level (A). The CCC coping showed insignificant deformations due to presence of the continuous cleat, resulting in high resistance against the applied load. On the other hand, the performance of the ACC coping was entirely different. During this level, the coping could accumulate growing deformations as the load was increasing.

Level (E). The deformed shape of the CCC was extremely similar to the one in Level (A), where the deformations seemed to be very limited until the end of the test. As for the ACC coping, the deformations reached relatively much higher values. That was evidenced by the severely deformed shape of the coping. In addition, the largest deformations were observed at the end of the test.

The existence of the continuous cleat gave the CCC edge system considerably high resistance against the applied load throughout all loading levels. In comparison, the ACC coping experienced much larger deformations owing to the use of anchor clips that lacked securement at their face. For more details about the ACC coping configuration, see Section 4.4.3.

Coping Joint Performance

Figure 5.16 includes photos of the coping joint at the first level and the last level of the loading process.

Level (A). Whereas the CCC coping joints showed barely visible deformations, the ACC coping joints showed rapidly growing deformations. Furthermore, during this level, it

was noted that the ACC coping segments were moving apart at the splice plate joints, in addition to severe outward deformations.

Level (E). The CCC coping still maintained very minimal deformations and no visible difference was observed compared to Level (A). The ACC coping joints, however, experienced even larger deformations at higher loads. Additionally, during this level, the ACC coping segments at the joints severely moved apart, where adhesive failure was observed due to the exceedance of its shear capacity.

The continuous cleat had the greatest effect on the response of the coping joints by the minimal deformations the coping showed. Conversely, the ACC coping joints responded by much larger deformations. On top of that, the splice plate performed unsatisfactorily, where the adhesive failed due to excessive shear force acting in the plane of the splice plate.

	CCC System	ACC System
Level (A)		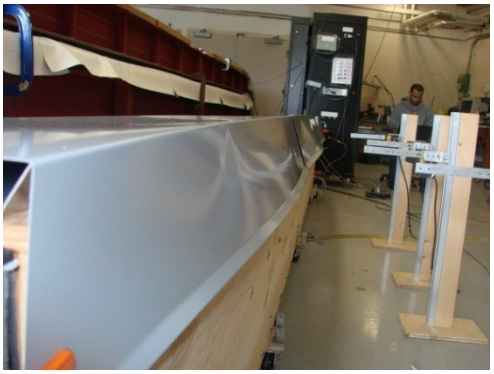
Level (E)		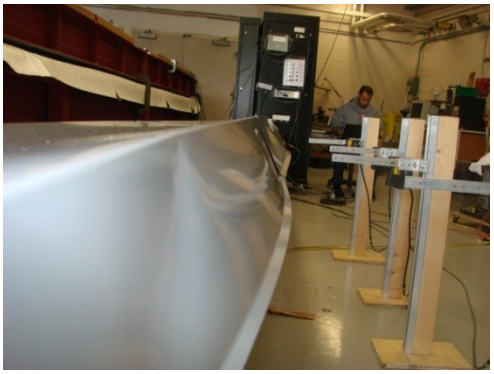

Figure 5.15: Performance of CCC and ACC coping under dynamic loading

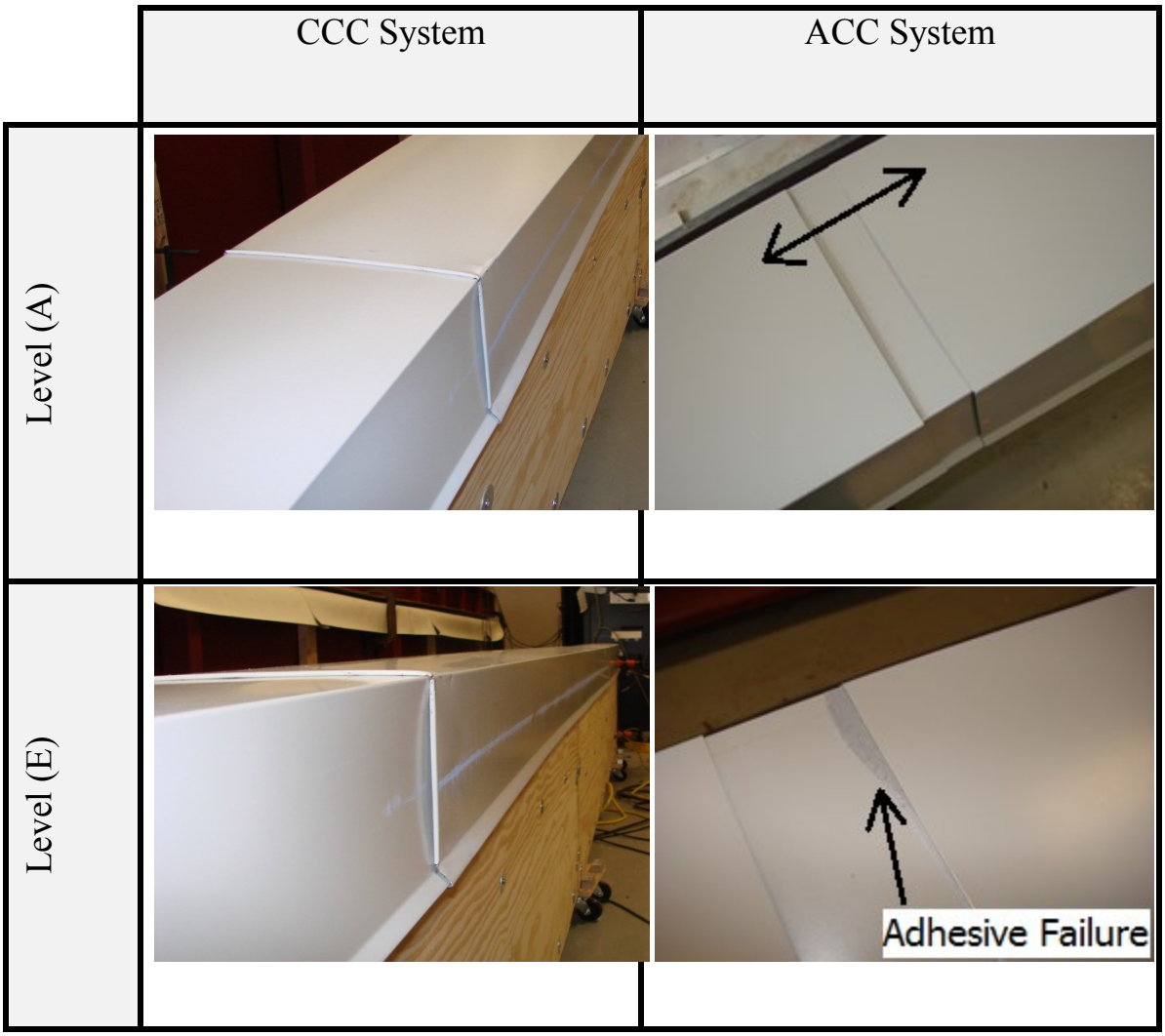

Figure 5.16: Performance of CCC and ACC coping joint under dynamic loading

5.5.2 Edge Response Analysis

Data Validation

The collected deformation data were further validated as shown in Figure 5.17 for both CCC and ACC edge systems. In the case of the CCC edge system, the deformation data of x= 0 (joint) and x= L were plotted against each other as illustrated in Figure 5.17 (a). The data points slightly deviated from y= x line as the equation of the best fit is y= 1.15. However, given that the largest deformation was 10 mm (0.4 in.), the deviation was only 1 mm (0.04 in.).

As for the ACC edge system (Figure 5.17 (b)), the deformation data of x= L/4 and x= 3L/4 were plotted. Unlike, the CCC edge system, the data points were perfectly consistent, and the best fit is y= 0.99 x, i.e. the deviation was only 1% from the y= x line.

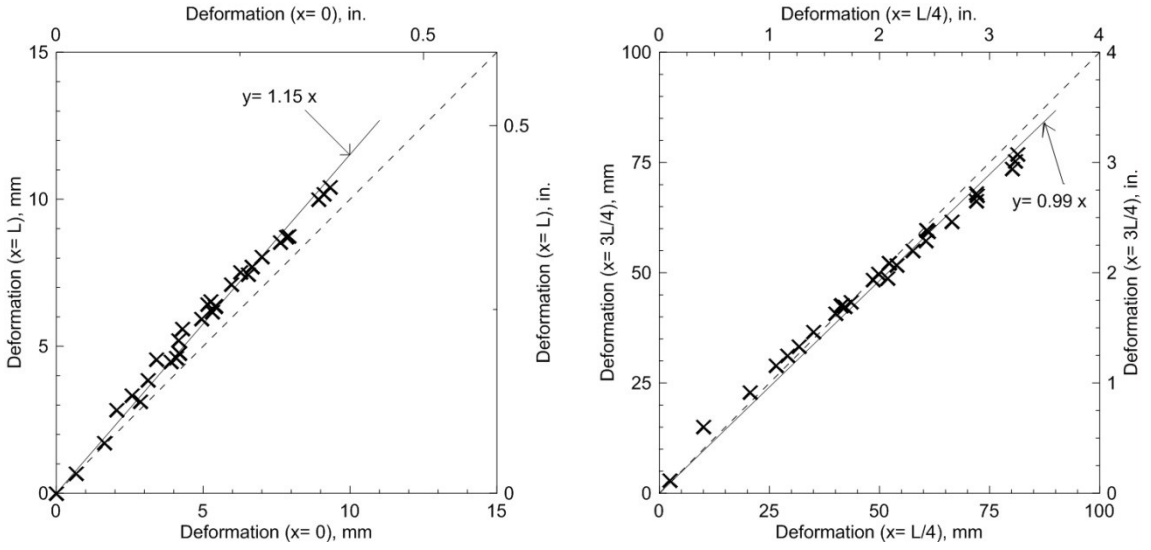

(a) CCC edge system (b) ACC edge system

Figure 5.17: Validation of deformation data of CCC and ACC edge systems under dynamic loading

Deformation of Coping Joint

Figure 5.18 demonstrates the coping deformation of both CCC and ACC edge systems at x= 0 (joint).

Level (A). The CCC coping maintained relatively small deformations as the largest value was only 4 mm (0.16 in.) at the end of this level. Conversely, the ACC coping deformation ranged from 2 mm (0.08 in.) to 26 mm (1 in.) during Level (A).

Level (E). The CCC coping deformation did not exceed 9 mm (0.35 in.) at the end of the level. On the other hand, the ACC coping could show deformations ranged from 38 mm (1.5 in.) to 62 mm (2.44 in.).

Even though the edge systems were subjected to the same loading with 5000 cycles, the CCC coping joint showed great resistance against the applied load. The high resistance was attributed to the continuous cleat which secured the coping and the joints along the whole length of the edge. The ACC coping joint, however, was unquestionably more flexible by almost six times, in comparison. As the ACC edge system used individual anchor clips that were only secured at the top, the coping was more vulnerable to high deformations.

Deformation of Coping

The coping deformation at midpoint (x= L/2) was also observed at Level (A) and Level (E) as shown in Figure 5.19.

Level (A). the CCC coping showed deformation ranged from 1 mm (0.04 in.) to a maximum of 6 mm (0.24 in.). On the contrary, the ACC coping deformed a minimum of 1 mm (0.04 in.) and a maximum of 32 mm (1.26 in.) during Level (A).

Level (E). The CCC coping still showed very small deformations, where the largest deformation observed at the end of the level was 14 mm (0.55 in.). The ACC coping deformations kept growing as they reached a value of 68 mm (2.68 in.) at the end of the test.

In fact the deformations of the CCC coping were greatly affected by the continuous cleat that, to a far extent, gave the edge system high rigidity against the applied load. Nevertheless, the ACC coping had much lower rigidity as the anchor clips only secured the coping by snap-on integration with no fasteners on the front face of the coping. Accordingly, the front face of the coping, where the load acted, was free to deform in response to the applied load.

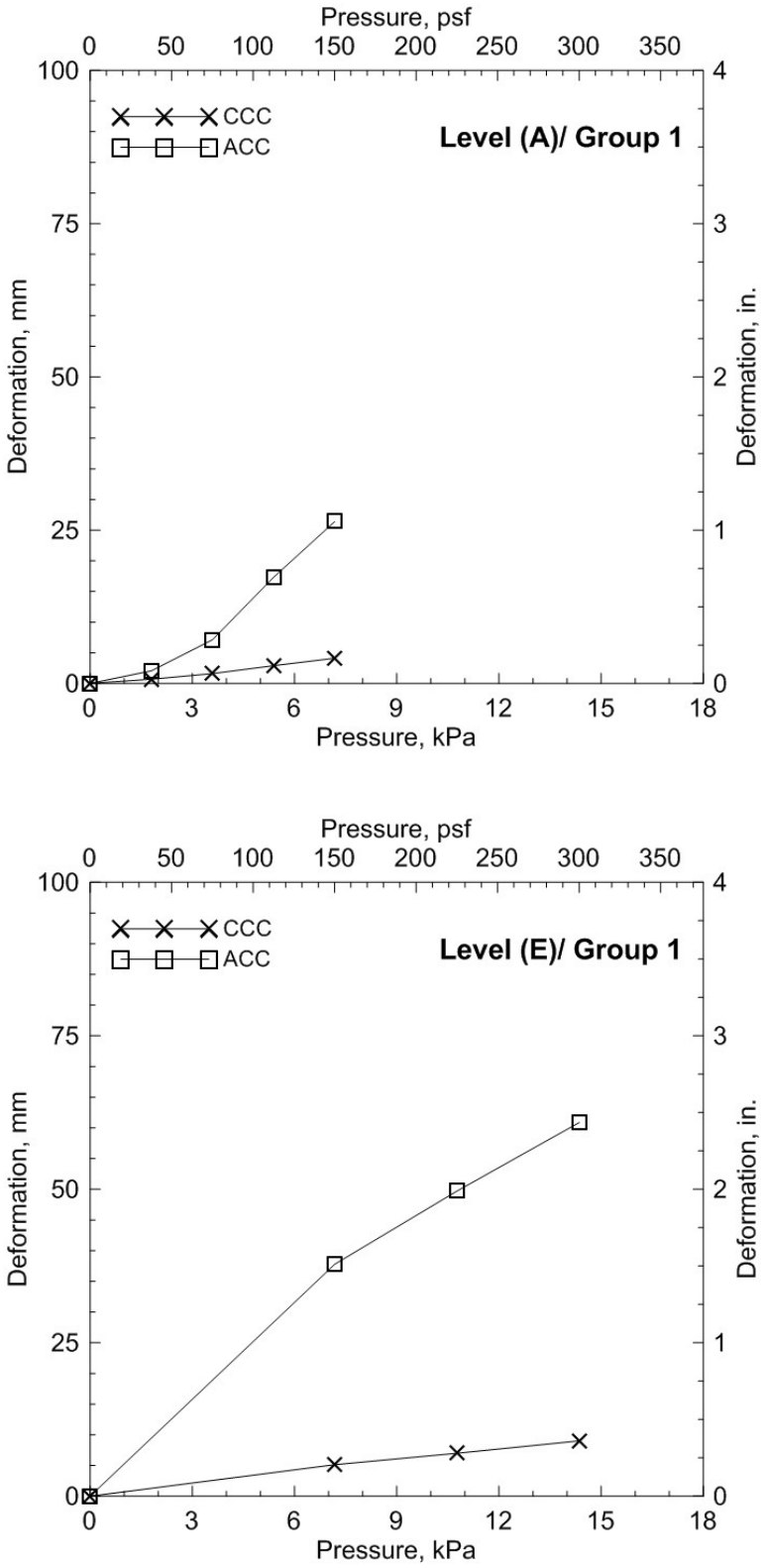

Figure 5.18: Deformation of CCC and ACC coping under dynamic loading at x= 0

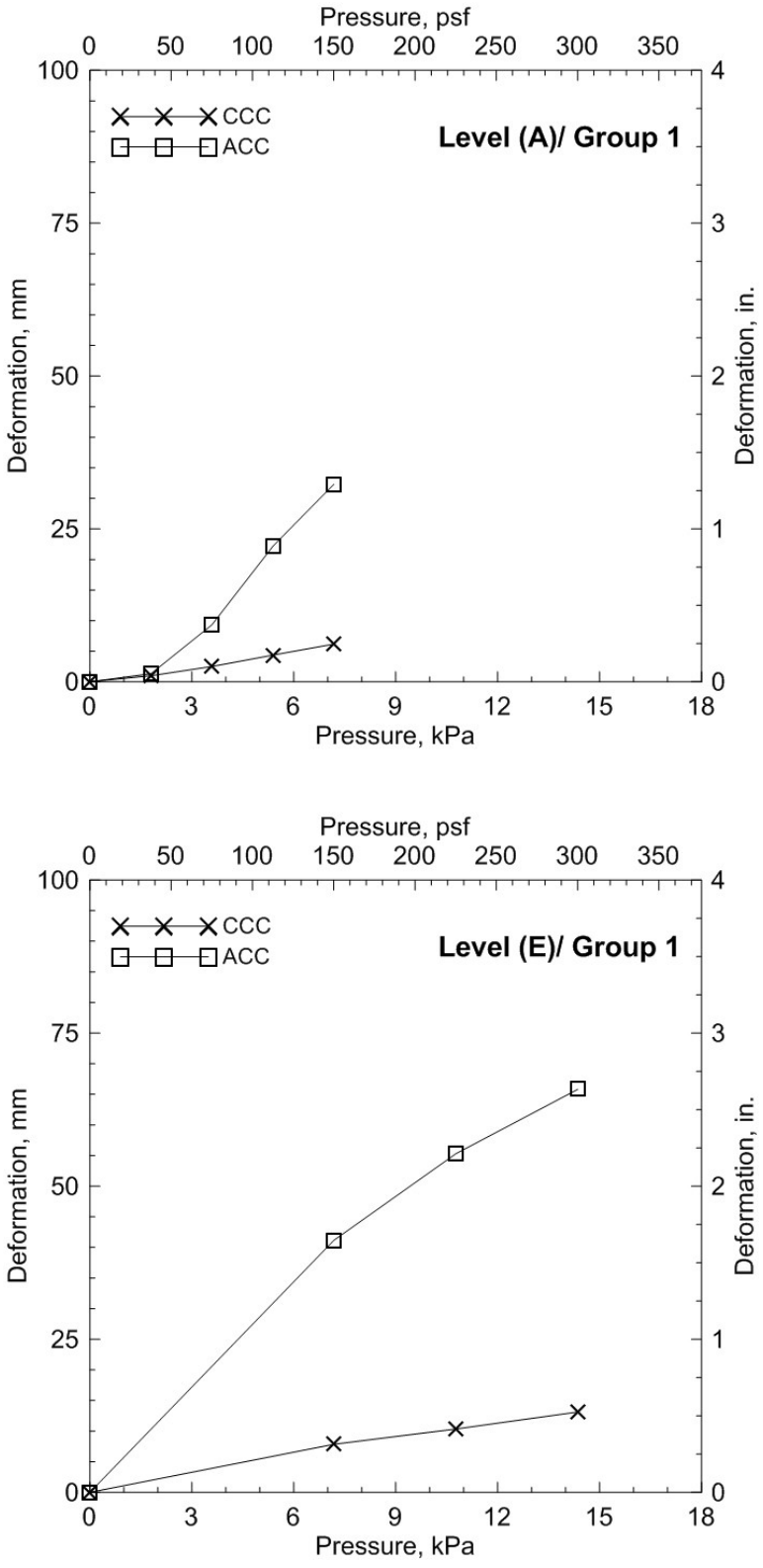

Figure 5.19: Deformation of CCC and ACC coping under dynamic loading at x= L/2

5.5.3 Rigidity Index Analysis of Roof Edge System

At x= 0 (Joint).

Figure 5.20 shows the rigidity index of the coping joint of CCC and ACC edge systems.

Level (A). The CCC had an initial rigidity index of 2.6 kPa/mm (1381 psf/in.). At the end of the level, the rigidity index dropped to a value of 1.7 kPa/mm (903 psf/in.), which was maintained until the end of the level. On the other hand, the ACC edge system showed much lower rigidity index, where it started at 0.9 kPa/mm (478 psf/in.) and went down to 0.3 kPa/mm (159 psf/in.).

Level (E). The CCC edge system maintained a rigidity index within a range of 1.4 – 1.6 kPa/mm (743 – 850 psf/in.). Similarly, the rigidity index of the ACC had a constant value of 0.2 kPa/mm (106 psf/in.) during the level.

At x= L/2 (Midpoint)

Figure 5.21 shows the rigidity index of the CCC edge system during Level (A) and Level (E) at x= L/2.

Level (A). During Level (A), the rigidity index CCC edge system started at a value of 1.8 kPa/mm (956 psf/in.) and dropped to 1 kPa/mm (531 psf/in.) at which the rigidity index stabilized until the end of the level. Similar behaviour was observed for ACC edge system, where the rigidity index started from 1 kPa/mm (531 psf/in.) and went down to 0.2 kPa/mm (106 psf/in.).

Level (E). Throughout the last level of the test (E), the rigidity index of CCC edge system maintained a value of 0.9 – 1.1 kPa/mm (478 – 584 psf/in.), whereas the ACC edge system showed a constant value of 0.2 kPa/mm (106 psf/in.).

Subjecting the edge system to dynamic loading revealed a crucial aspect that is the influence of load cycling on the rigidity of the system, which is system fatigue. As showed in Figure 5.20, for both edge systems, the rigidity index gradually dropped as the test progressed. However, the rigidity reached a minimum value at which it stabilized despite the progress of the test. A stable value of rigidity index means that the edge system would retain a minimum rigidity, where load cycling cannot cause more fatigue to the system. Whether exposing the edge system to a higher number of cycles would result in lower levels of rigidity remains an open question that is beyond the scope of this research.

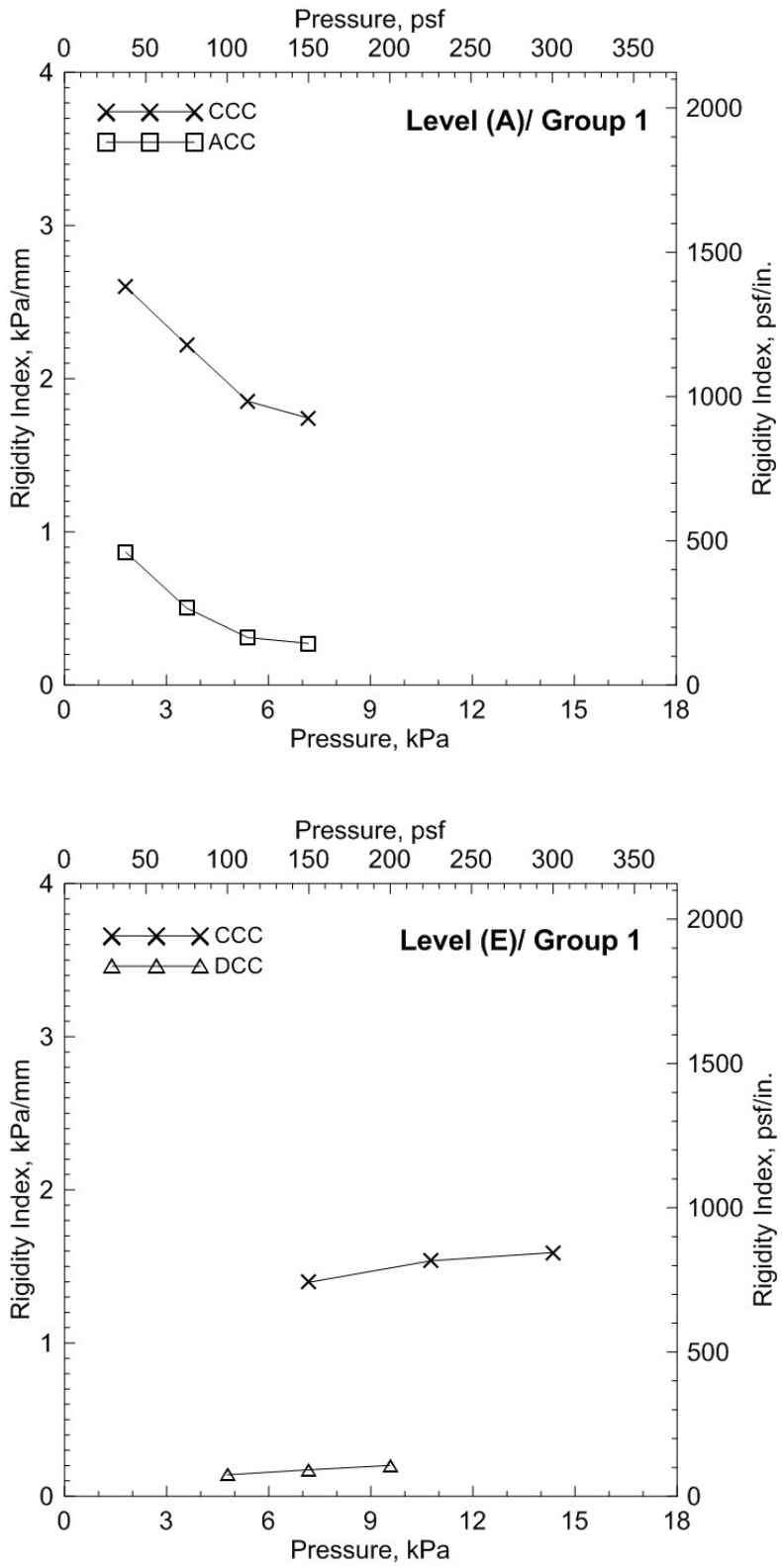

Figure 5.20: Rigidity index of CCC and ACC edge system under dynamic loading at x= 0

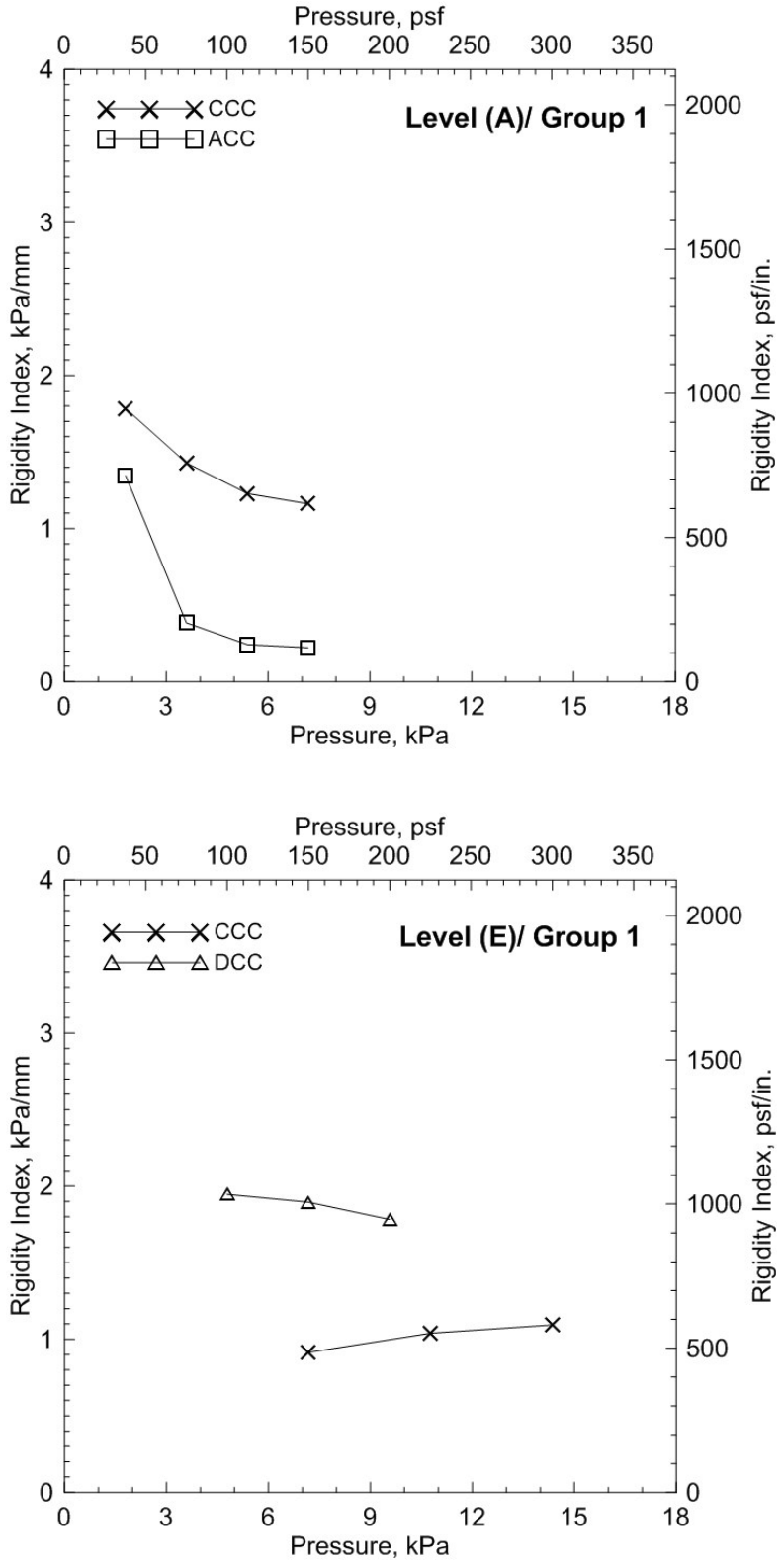

Figure 5.21: Rigidity index of CCC and ACC edge system under dynamic loading at x= L/2

5.5.4 Discussion and Conclusion

When tested by the dynamic test protocol, both CCC and ACC edge systems passed and completed the test with no failure; however, they responded very differently to the applied load. On one hand, the CCC coping did not show significant deformations, where the largest deformation did not exceed 14 mm (0.55 in.). On the other hand, the deformations of ACC coping reached much higher values.

In addition, the analysis of the rigidity index clearly reflected these observations as the CCC coping showed very large rigidity in comparison with ACC edge system. Also, both systems were sensitive to the number of loading cycles; they experienced drop in rigidity index after passing a certain number of loading cycles. That observation was a result of system fatigued due to the repetitive cycles under various load magnitudes. Though, the rigidity index of the CCC appeared to be less sensitive, where it could stabilize at relatively higher values.

To sum up, given the minimal deformations, the CCC edge system seemed to be a better solution due to the exceptional performance it showed compared to the ACC edge system. Such a performance would guarantee a roof edge system to have substantial resistance as well as adequate protection against issues such as water intrusion.

5.6 CCC vs. DCC Edge System

Section 5.5 showed a performance comparison for the CCC and ACC edge systems, where it was concluded that CCC edge system performed better compared to the ACC edge system under dynamic loading. This section similarly presents and discusses the performance of both the CCC and the DCC edge systems under dynamic loading in order to find out the best edge system among the available edge systems. The following sections include discussion of the observations, edge system response as well as the rigidity index.

5.6.1 Performance of Edge System under Dynamic Loading

Test Performance

As for the CCC edge system, a pressure of 7.18 kPa (150 psf) was selected as test pressure. Thus, the load started at 25%PT= 1.8 kPa (37.8 psf) and ended at 200%PT= 14.35 kPa (300 psf). The edge system passed all loading levels (A to E), undergoing 4800 loading cycles and successfully completed the test, where none of the edge components failed. Consequently, the system was given a rating of **14.35 kPa (300 psf)**. See Figure 5.14.

In the case of DCC edge system, the test pressure was selected at PT= 4.78 kPa (100 psf). The applied load, therefore, started at 1.2 kPa (25 psf) and continued up to 9.57 kPa (200 psf). Prior to the end of the test (at Level E), the coping suddenly disengaged from the cleat, and the test was automatically terminated. Consequently, the edge system was rated based on the maximum load at Level (D), i.e. **8.37 kPa (175 psf)**. See Figure 5.4.

Failure Mode

When subjected to dynamic loading, only the DCC edge system failed, whereas the CCC edge system successfully completed the test with no failure. As shown in Figure 5.5, the failure mode of the DCC edge system was coping-cleat disengagement, where the coping lost securement with the cleat. In other words, the load transfer path was blocked as the coping disengaged from the cleat. As a result, when failed, the coping was not able to transfer the load to the cleat. Moreover, severe deformations were observed near and at the coping joints prior to failure. It is worth mentioning to point out that this failure mode is the only possible mode, where the cleat was over-secured by the batten bars, securing the pressure plane. Consequently, cleat nail pull-out as a failure mode was not a possibility in this case.

Performance of Coping

Figure 5.22 illustrates the deformed shape of the CCC and DCC copings under the dynamic loading at Level (A) and Level (E). The deformations of the CCC coping were extremely small to the extent they were barely visible throughout the test.

On the contrary, the DCC coping differently responded to the applied load. At Level (A), the coping relatively showed large deformations in comparison with the ones of the CCC coping. Furthermore, at Level (E), the deformations became even larger, especially at the joints. Besides, the deformed shaped of the coping took a curvy profile, where deformations were minimal at the middle and maximal at the joints.

Performance of Coping Joint

Figure 5.23 shows the performance of coping joints of both CCC and DCC. Even though both CCC and DCC edge systems use S-lock joints, each one of them performed in a dif-

ferent way. While the joints of the CCC coping showed very minimal deformations, the DCC coping joints deformed greatly. In the case of CCC edge system, the coping joints were supported by the continuous cleat, which contributed to the high resistance of the coping against the applied load. On the other hand, the discontinuous cleat of the DCC edge system did not cover the joints, resulting in higher susceptibility to severe, growing deformations.

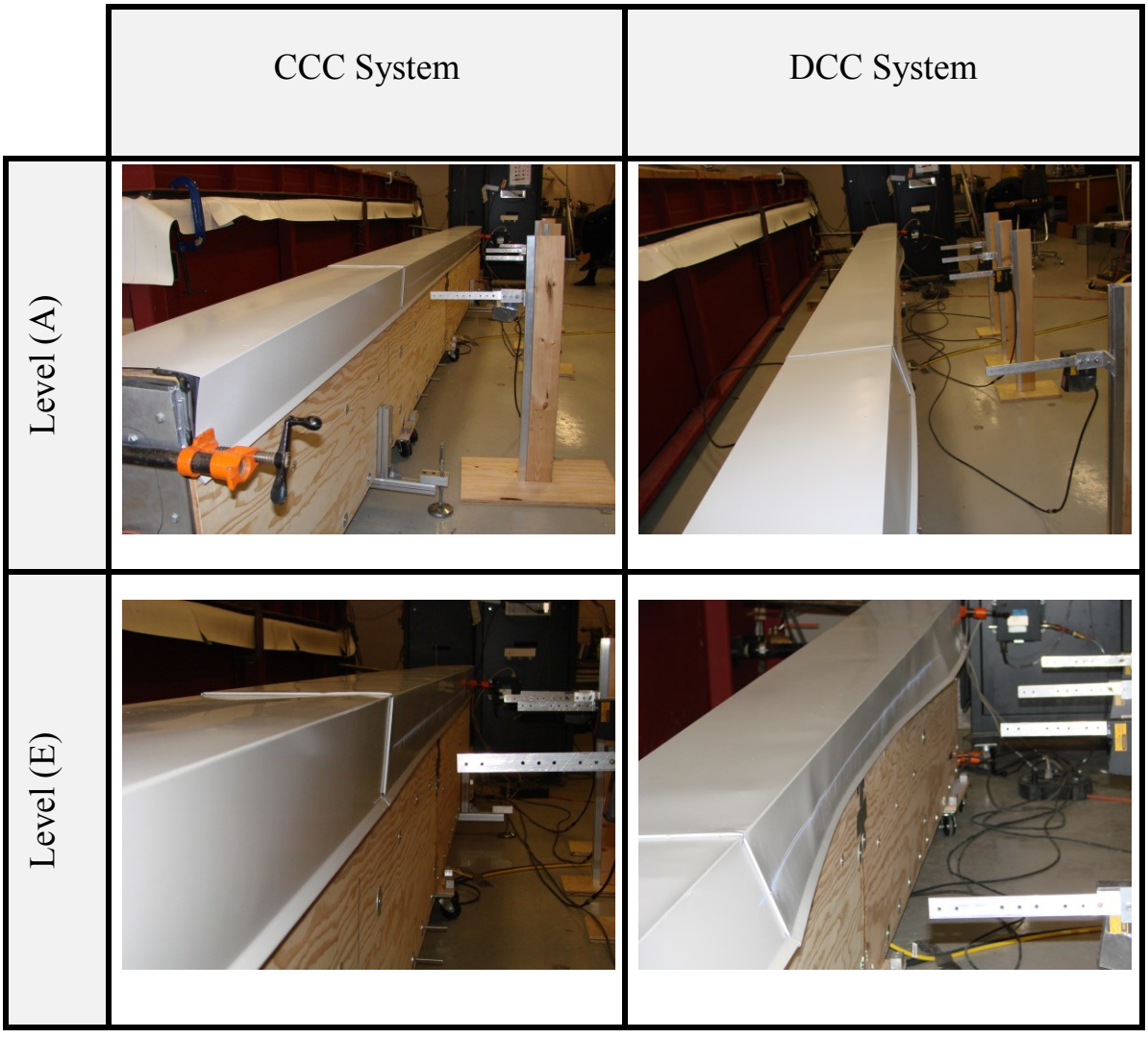

Figure 5.22: Performance of CCC and DCC coping under dynamic loading

	CCC System	DCC System
Level (A)		
Level (E)		

Figure 5.23: Performance of CCC and DCC coping joint under dynamic loading

5.6.2 Edge Response Analysis

Data Validation

Refer to Sections 5.5.2 and 5.4.2

Deformation of Coping at x= 0 (Joint)

Figure 5.24 presents a side-by side response comparison for the CCC and the DCC coping at Level (A) and Level (E).

Level (A). The CCC coping joint expectedly showed very small deformations with a maximum of only 4 mm (0.16 in.). However, the DCC coping joint deformation ranged between 1 mm (0.04 in.) and 27 mm (1.06 in.).

Level (E). The largest deformation observed at the CCC coping joint was 10 mm (0.4 in.). On the contrary, the DCC coping joint continued to deform increasingly, where it reached a maximum value of 57 mm (2.24 in.) at the end of the test.

In fact, the presence of the continuous cleat affected the deformation of the CCC coping joint as it demonstrated high resistance against the applied load. On the other hand, the joint of the DCC coping was considerably vulnerable to high deformations as the coping was not secured at the joints.

Deformation of Coping at x= L/2

In a similar fashion, Figure 5.25 shows deformations of both CCC and DCC copings at x= L/2 (midpoint) in Level (A) and Level (E):

Level (A). The CCC coping deformations grew from 1 mm (0.04 in.) to 6 mm (0.24 in.) at the end of the level, whereas the largest deformation of the DCC coping reached only 6 mm (0.24 in.).

Level (E). The CCC coping deformations started from 8 mm (0.31 in.) and ended at 14 mm (0.55 in.). In addition, the DCC coping seemed very resistant against the applied load with a minimum deformation of 2 mm (0.08) and a maximum of 7 mm (0.28 in.).

Yet, the effect of the continuous cleat clearly translated into small deformations of the CCC coping. However, the DCC coping showed even smaller deformations at the mid-point (x= L/2). Given that the joints of DCC coping were not secured by a cleat, their deformation caused the area near the midpoint to show resistance against outward deformation; see "Beam Representation of DCC system" (Figure 5.12). Base on the observations, the resistance of the coping at x= L/2 (midpoint) was continuously increasing with the increasing deformation of the joints. In the higher loading levels, the coping started some growing deformations, where the applied load seemed to have a greater effect.

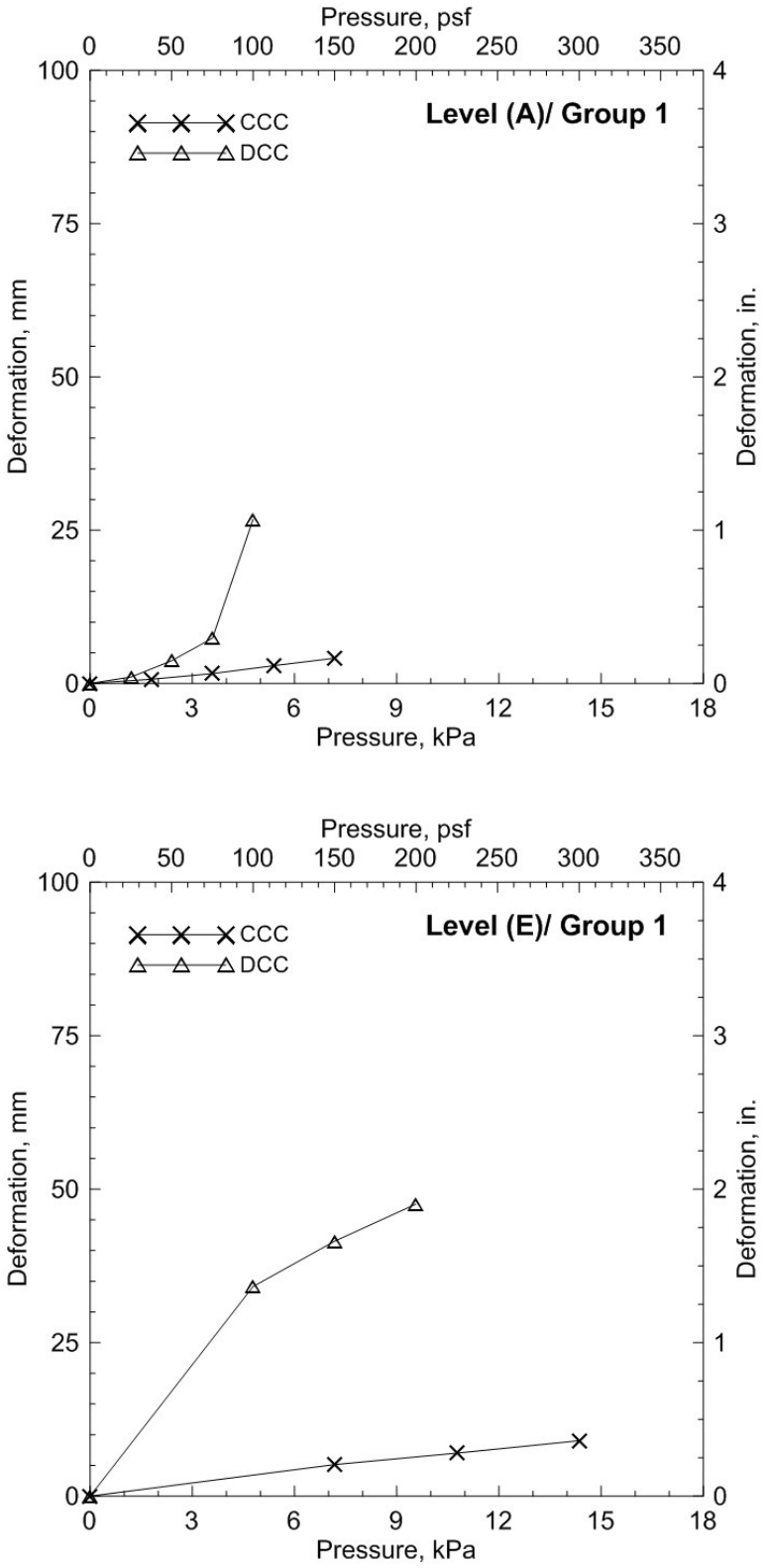

Figure 5.24: Deformation of CCC and DCC coping under dynamic loading at x= 0

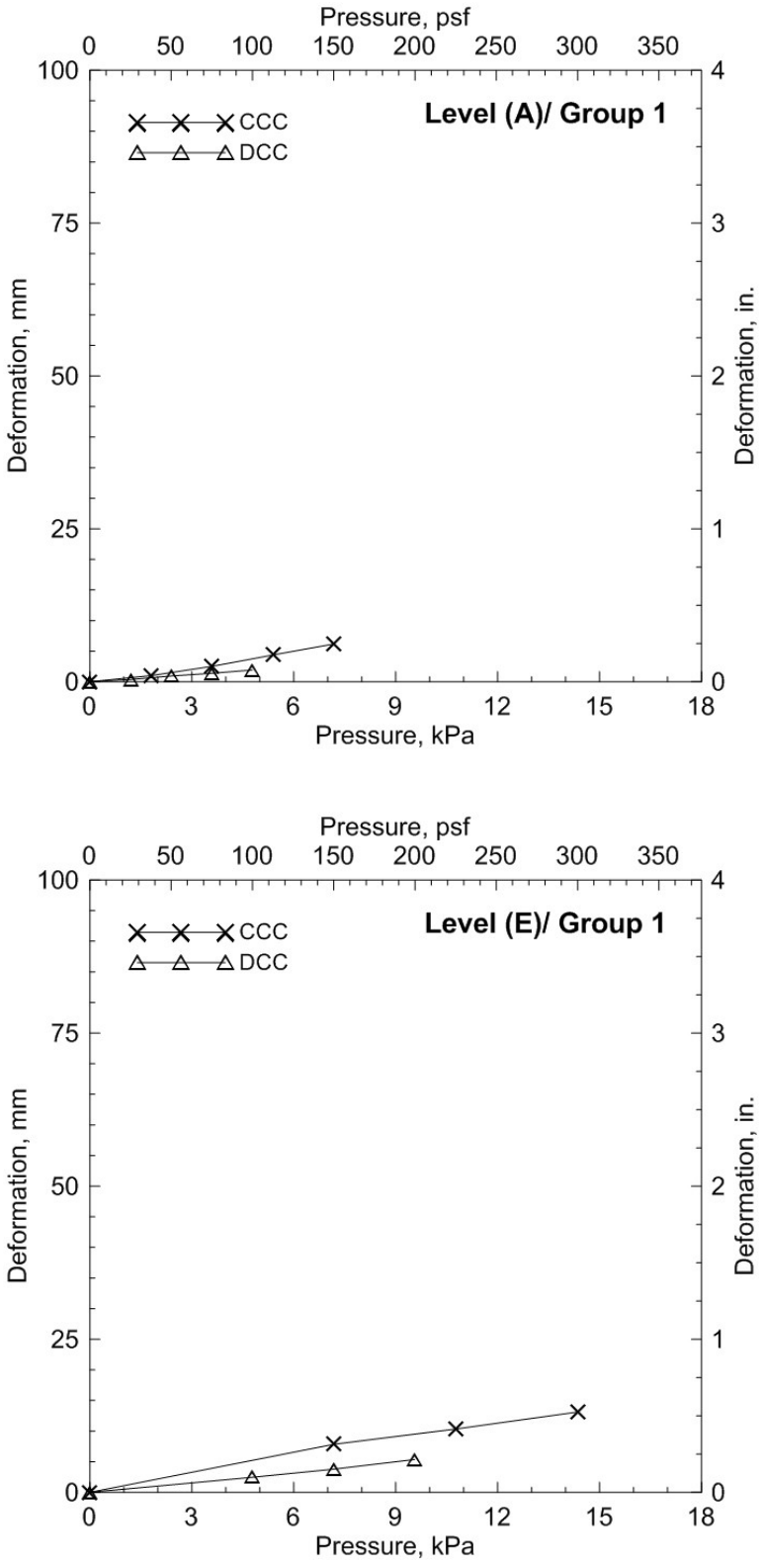

Figure 5.25: Deformation of CCC and DCC coping under dynamic loading at x= L/2

5.6.3 Rigidity Index Analysis of Edge System

The response of the edge systems to dynamic loading was further studied by investigating the rigidity index of the coping during the test:

Rigidity Index at x= 0

Figure 5.26 shows the rigidity index of the system at x= 0 (joint) during Level (A) and Level (E):

Level (A). The rigidity index of CCC coping had its largest value of 2.6 kPa (1381 psf/in.) at the beginning of the level. However, it dropped to 1.7 kPa/mm (903 psf/in.) and then stabilized at that value until the end of the level. With respect to the DCC edge system, the rigidity index started from 1.1 kPa/mm (584 psf/in.) and dramatically dropped to 0.13 kPa/mm (69 psf/in.) at the end of the level.

Level (E). The rigidity index of the CCC coping decreased to range between 1.4 kPa/mm (743 psf/in.) and 1.6 kPa/mm (850 psf/in.). Furthermore, the DCC coping maintain almost the same rigidity index value as Level (A), where the value fluctuated between 0.14 kPa/mm (74 psf/in.) and 0.2 kPa/mm (106 psf/in.).

Both the CCC and DCC copings showed relatively high rigidity index at the beginning of the test. However, after a while, it gradually dropped under the effect of the repetitive loading cycles, resulting in system fatigue.

Rigidity Index at x= L/2

Figure 5.27 illustrates the rigidity index of the system at x= 0 (joint) during Level (A) and Level (E):

Level (A). In the case of CCC coping, the rigidity index had its largest value at 1.8 kPa (956 psf/in.); however, it gradually decreased to 1.1 kPa/mm (584 psf/in.) and stabilized until the end of the level. On the other hand, the rigidity index of the DCC coping started at from 3.2 kPa/mm (1700 psf/in.) at the beginning of the level. Afterwards, it to 2.5 kPa/mm (1328 psf/in.) and kept fluctuating in a range of 1.9 kPa/mm (1009 psf/in.) – 2.5 kPa/mm (1328 psf/in.).

Level (E). The rigidity index of CCC coping conserved almost a stable value of 1.1 kPa/mm (584 psf/in.) during this level. However, the DCC coping continuously decreased in rigidity index from 1.9 kPa/mm (1009 psf/in.) to 1.3 kPa/mm (690 psf/in.).

The effect of load cycling was evident, where the rigidity of the CCC edge system decreased as the system had suffered from fatigue. However, the rigidity stopped decreasing and stabilized the point where fatigue seemed to have a limited effect. As for the DCC edge system, the rigidity index experienced fluctuations in value, but later, fatigue seemed to impose a greater effect as the rigidity index steadily decreased until the end of the test.

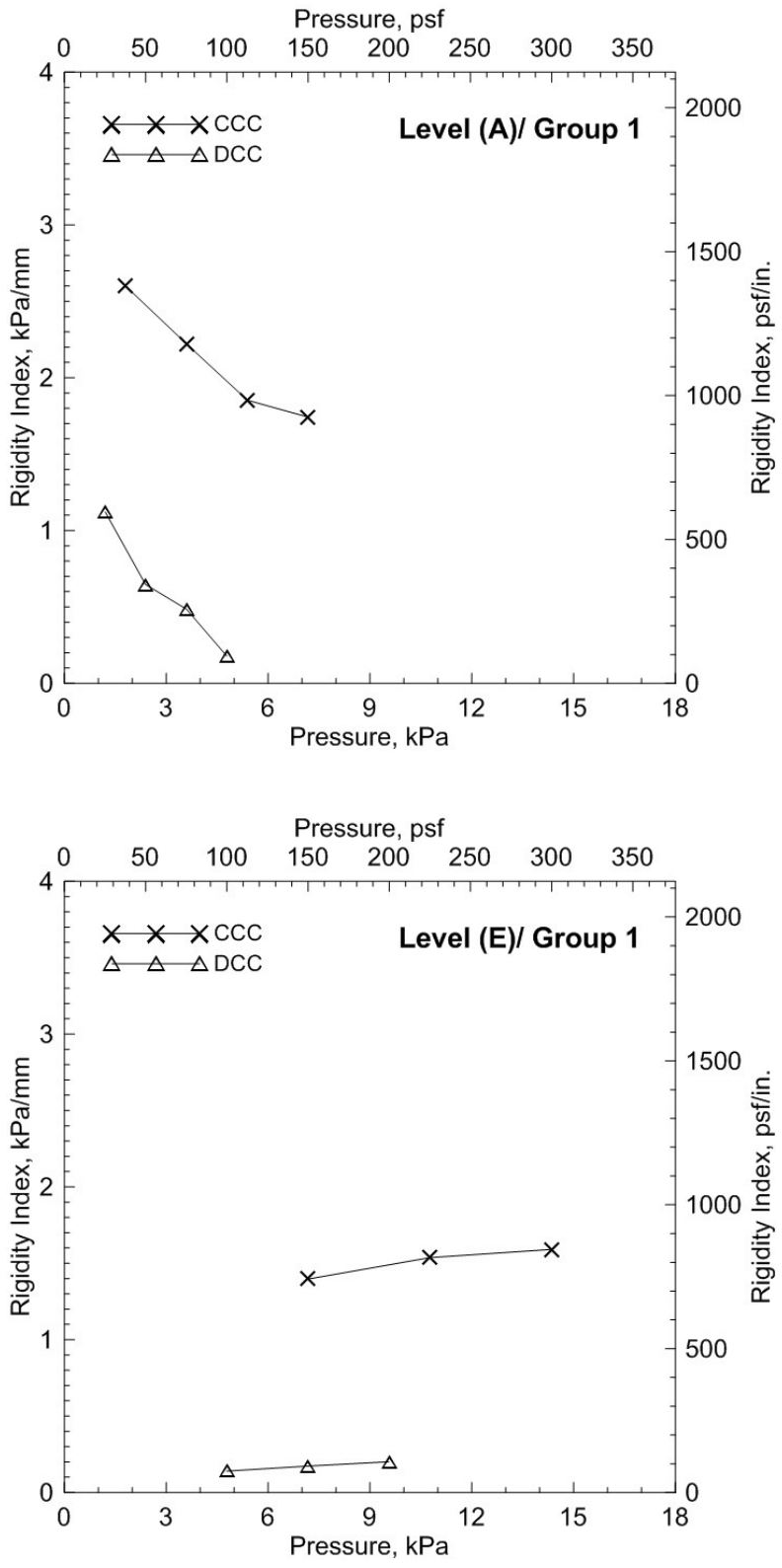

Figure 5.26: Rigidity index of CCC and DCC edge system under dynamic loading at x= 0

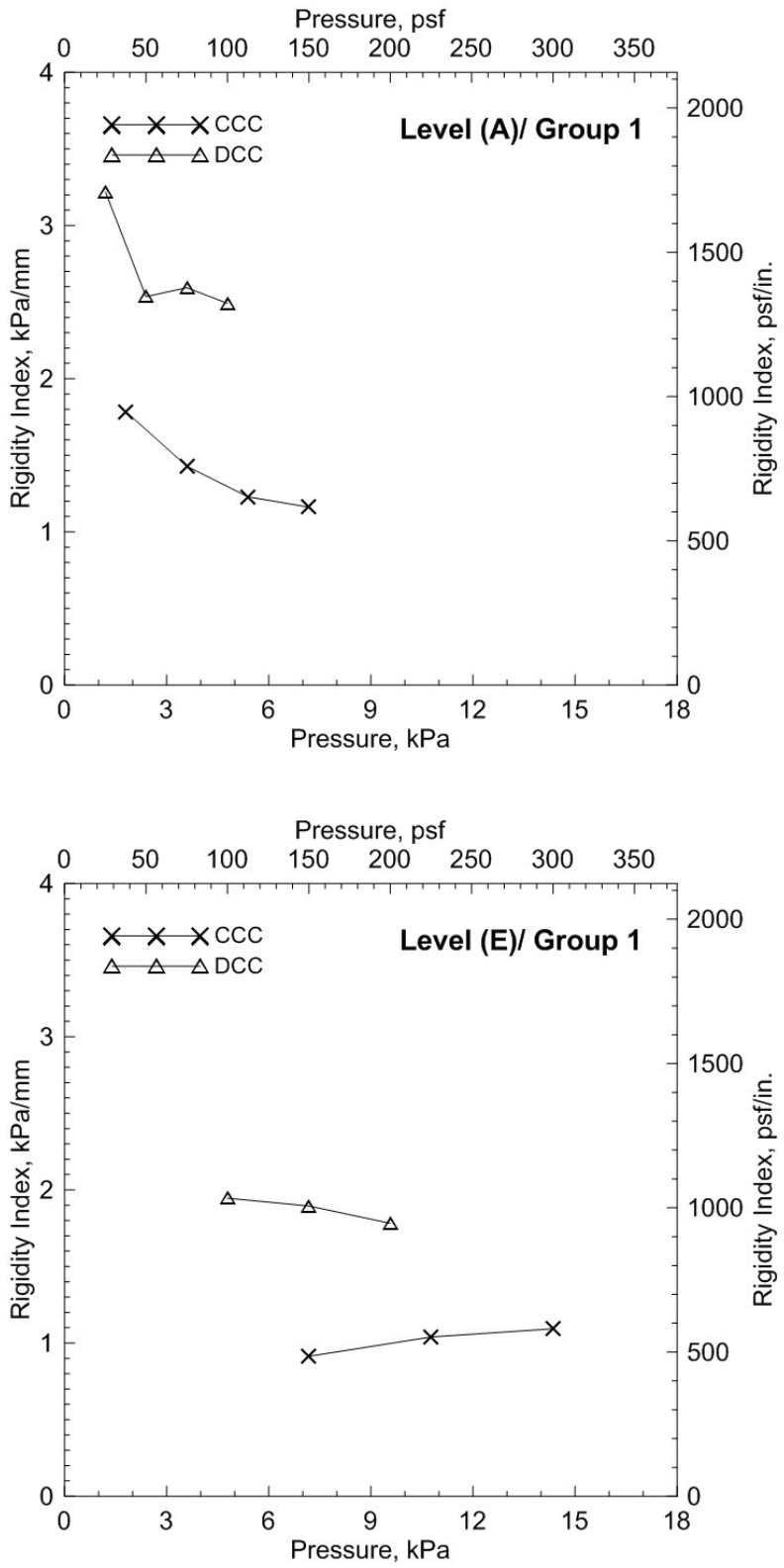

Figure 5.27: Rigidity index of CCC and DCC edge system under dynamic loading at x= L/2

5.6.4 Discussion

In fact the load transfer path of CCC edge system and DCC edge system share the same components with some differences in the contribution of each component. In other words, the size of the cleat, in the case of CCC edge system, provides a full load transfer from the coping to the edge substrate. In the case of the DCC edge system, however, the load is transferred only through the length of the discontinuous cleat.

Under dynamic loading, the CCC and DCC edge systems behaved differently. The CCC coping showed very minimal deformations throughout the test compared to the DCC coping which deformed greatly, especially at the unsupported joints. Furthermore, at the middle of DCC coping, the deformations were comparably maintained at the lowest intensities, where the cleat installed.

Analysing the rigidity index provided a concrete support to the experimental observations. That is to say, the rigidity of the CCC coping was relatively high in comparison with the DCC coping. In addition the analysis showed that the joints were the weakest part of the coping, which needs further attention in the design process.

Due to the minimal deformations compared to DCC edge system, the CCC edge system proved its ability to provide better weather protection. As for the DCC edge system, the issue of the unsupported joints contributed to a weaker performance and higher deformations that can lead to poorer weather protection.

5.7 Conclusion

Figure 5.28 shows the performance of the three edge systems (CCC, DCC and ACC) under dynamic loading. As for the coping joint, the deformations of both ACC and DCC

copings occupied higher values, whereas the CCC coping maintained significantly smaller deformation. On the other hand, at the midpoint, ACC coping had the highest deformation compared to the CCC and DCC.

From a practical point of view, it is not sufficient for a roof edge system to only resist the design load, but it needs to maintain a minimum level of weather protection to the roofing system. Such a protection can be achieved by using a roof edge system that shows minimal deformation in order to avoid issues such as water intrusion. In other words, based on the foregoing discussion, the CCC edge system evidently appeared as an adequate solution, in comparison with the DCC and ACC edge systems.

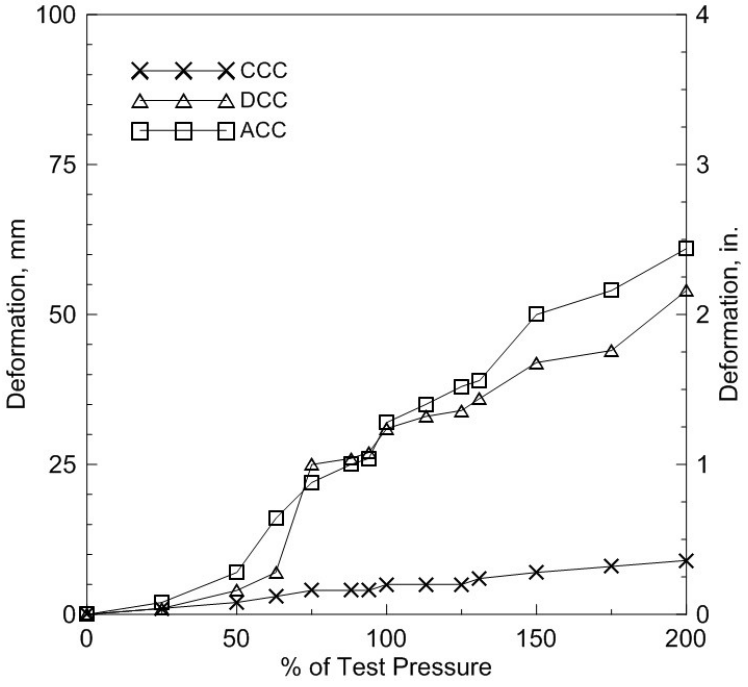

(a) x= 0

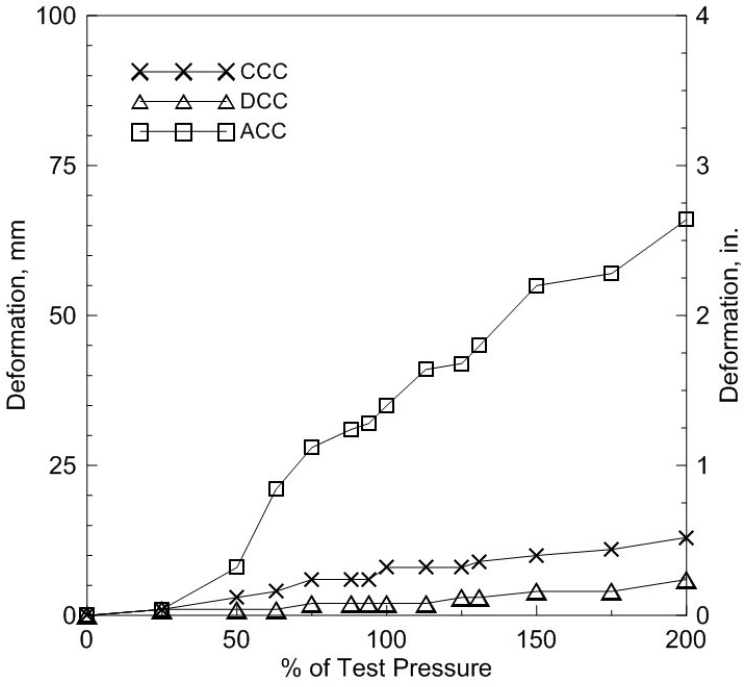

(b) x= L/2

Figure 5.28: Performance of CCC, DCC and ACC edge systems under dynamic loading

Chapter 6. Enhanced Experimental Setup

Introduction

Chapter 4 and 5 presented and discussed an experimental method for investigating roof edge systems by simulating static and dynamic wind pressure. The developed experimental setup relies on the use of pressure planes to apply the required pressure on the components of an edge system. The existing experimental setup is further enhanced to improve its applicability and efficiency. This chapter presents the enhancement and its superiority by comparing the experimental results of two roof edge systems, CCC and DCC.

6.1 Experimental Setup Enhancement

The main purpose of testing a roof edge is to make sure that the edge system is capable of resisting the design wind loads. As discussed Section 5.2, the loads acting on an edge system are transferred to the structural components of the edge following a path called the load transfer path. As shown in Figure 6.1 (a), when the coping of an edge is exposed to negative pressure (suction), the coping transfers the pressure to the cleat through the coping-cleat integration (Zone 1). In turn, the cleat resists the load by the securing nails that transfer the load to the edge substrate (Zone 2). In general a test method should evaluate the resistance of Zone 1 and Zone 2.

In reviewing the existing experimental setup, it is clear that securing the pressure planes by batten bars and fasteners results in an over-secured cleat. Accordingly, only Zone 1 of the load transfer path is evaluated. To evaluate simultaneously both Zone 1 and Zone 2 and to identify the weakest link on the resistance chain (Figure 6.1 (b)), the experimental

method needed enhancement. This has been achieved by the use of pre-manufactured bags instead of the pressure planes. These bags are referred to as “pressure bags”; they are intended to play the same role as pressure planes in simulating the required pressure. The following is a detailed review of the enhancement and its advantage over the existing one.

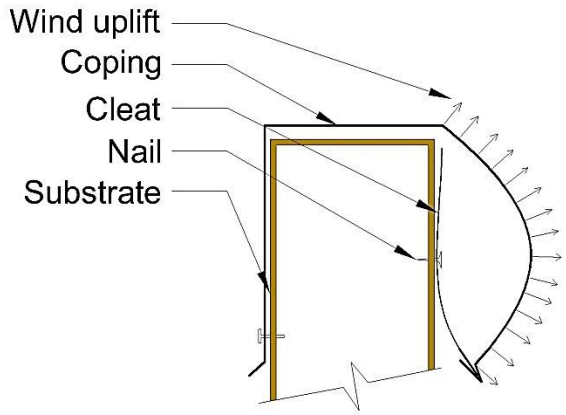

(a) Load transfer path of roof edge system

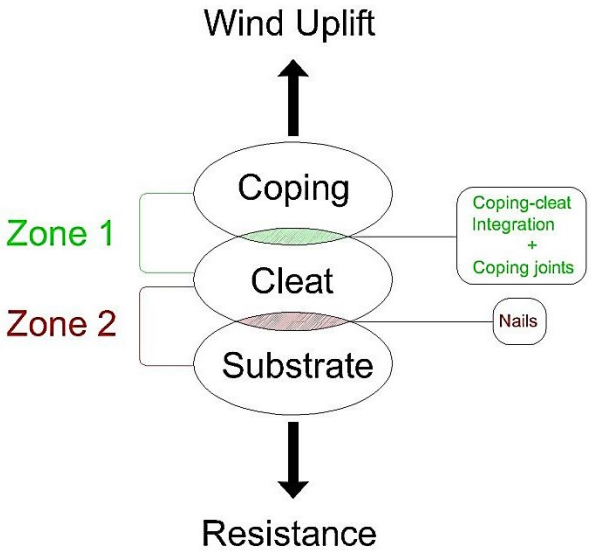

(b) Resistance chain of roof edge system

Figure 6.1: Load transfer and resistance chain of a roof edge system

6.1.1 Enhanced Experimental Setup and Test Operation

Figure 6.2 shows a schematic diagram of the enhanced experimental setup layout:

1. A pipe called the "pressure pipe" was installed inside the pressure chamber (edge substrate) along the whole length. One end of the pressure pipe was connected to the air blower, whereas the other end was closed.
2. The pressure pipe was connected to the gust simulator at the middle.
3. After the installation of the cleat, the pressure bags were installed and connected to the pressure pipe by using hoses that feed them with blowing air.
4. At the final step, the coping was mounted and secured on the edge substrate.

Unlike the existing experimental setup, the pressure chamber does not contribute to the test itself, rather it serves as a container of the pressure pipe and hoses and as a nailer for the edge components (see Figure 4.1).

The air blower pumps air into the pressure pipe that, in turn, transfers the air to the pressure bags through the hoses. When the gust simulator's flap is closed, the pressure builds up in the pressure pipe, causing the pressure bags to balloon and to apply pressure on the components. On the other hand, once the flap opens, the air evacuates from the pressure pipe and the bags, releasing the load. This process creates pressurization/ depressurization cycles simulating loading/ unloading cycles. Depending on the test protocol the process is repeated at specific timing and intensity to expose the edge system being tested to the required pressure. Next section discusses in detail the preparation of an edge to be tested by using the enhanced experimental setup.

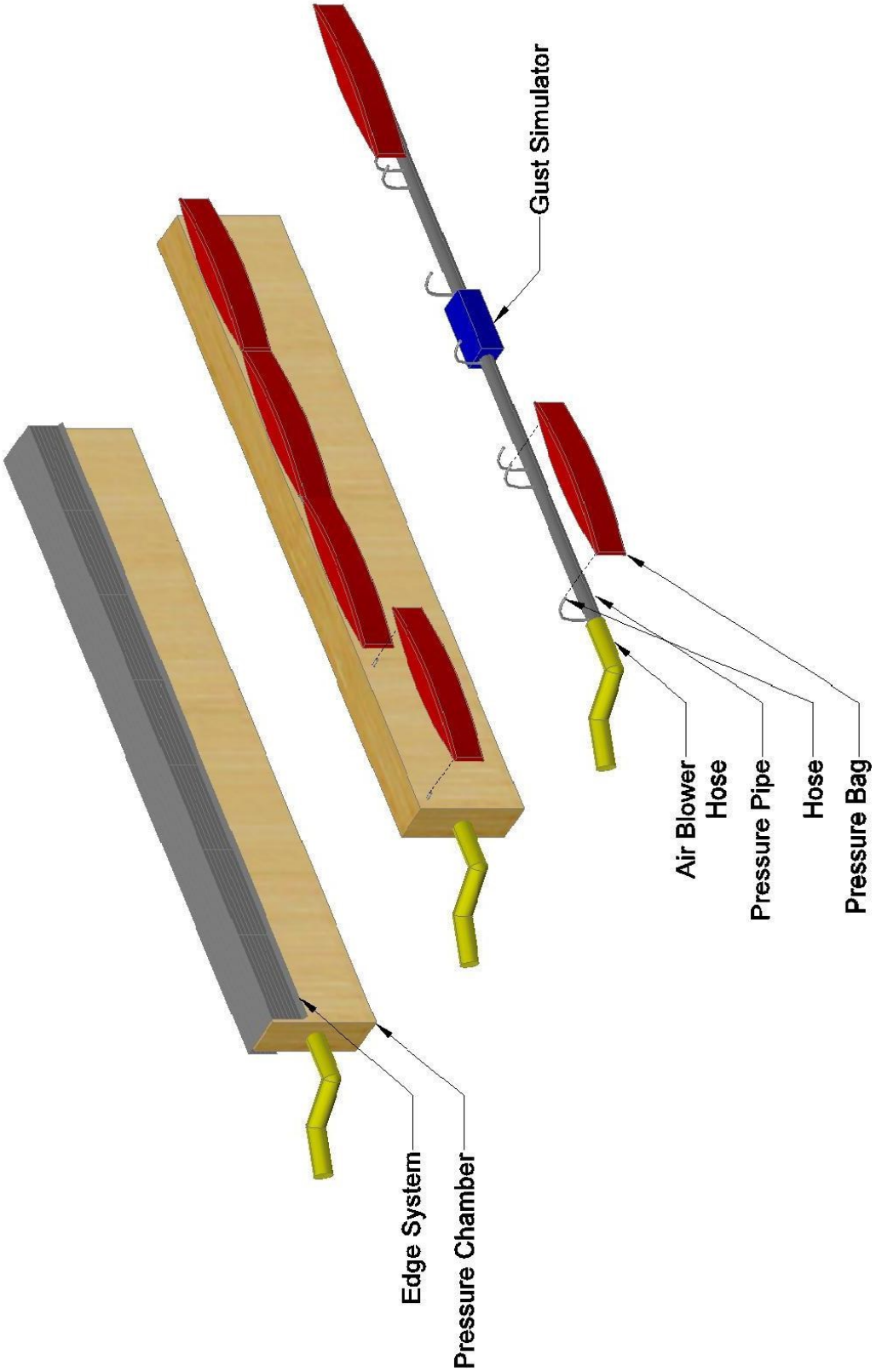

Figure 6.2: Enhanced experimental setup

6.1.2 Preparing a Roof Edge for Testing by the Enhanced Experimental Setup

Cleat and Pressure Bag Installation

As shown in Figure 6.3 (a), (b), (c), (d), (e) and (f), a PVC pipe (pressure pipe) of 76 mm (3 in.) in diameter was installed inside the edge substrate along its entire length from which hoses were branched to connect the pressure bags. At one end, the pressure pipe was connected to the air blower hose that feeds the pressure pipe with the air, whereas it was closed at the other end. At the middle of the pressure pipe, the gust simulator was connected through an air tight box. As for the cleat attachment, it was secured to the edge substrate (pressure chamber) by nails. Further, holes were drilled through the cleat to pass the hoses connecting the pressure bags with the pressure pipe. Four pressure bags (each is 1220 mm long) were installed along the entire length of the edge. They were securely connected to the feeding hoses by using ring clamps.

Coping Installation and Boundary Conditions

After the pressure bags were installed, the coping was mounted on the edge as shown in Figure 6.3 (g), (h), (i) and (j). The coping installation process and the edge boundary conditions are the same as discussed in Sections 4.4.1and 4.4.2.

(a) Pressure pipe and feeding hoses

(b) Installation of edge substrate

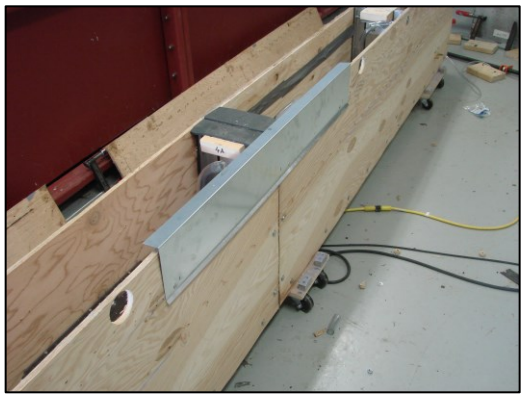

(c) Installation of cleat

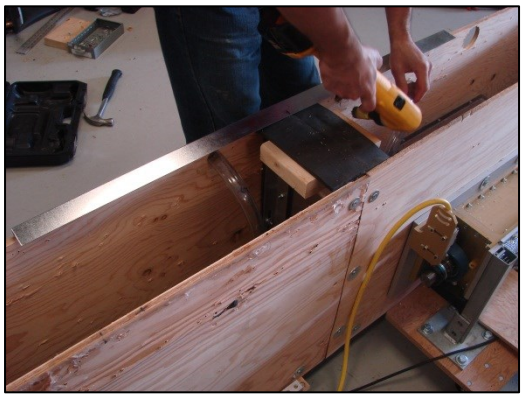

(d) Holes to install pressure bags

(e) Typical pressure bag

(f) Installation of a pressure bag

Figure 6.3: Installation of edge system using enhanced experimental setup

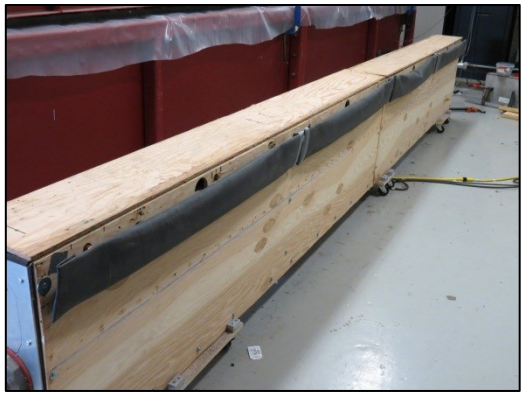

(g) Pressure bags installed along entire edge length

(h) Installation of coping

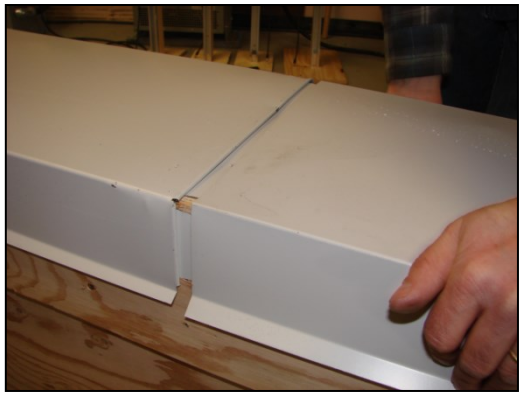

(i) Installation of coping joint

(j) Edge system ready for testing

Figure 6.3: Installation of edge system using enhanced experimental setup

6.2 Testing Roof Edge Systems using the Enhanced Experimental Setup

Two types of edge system were tested with the enhanced experimental setup: DCC and CCC. Only Set "B" of each edge system was tested (see Sections 4.4.1 and 4.4.2)

6.2.1 Response of DCC Edge system

Applied Pressure and Failure Mode:

As shown in Figure 6.4, the test pressure of 4.8 kPa (100 psf) was selected. The edge system successfully passed Levels A and B but failed at Level C. Cleat nail pull-out and coping-cleat disengagement were observed as a failure mode (Figure 6.5). The edge system was rated at **6 kPa (125 psf)**.

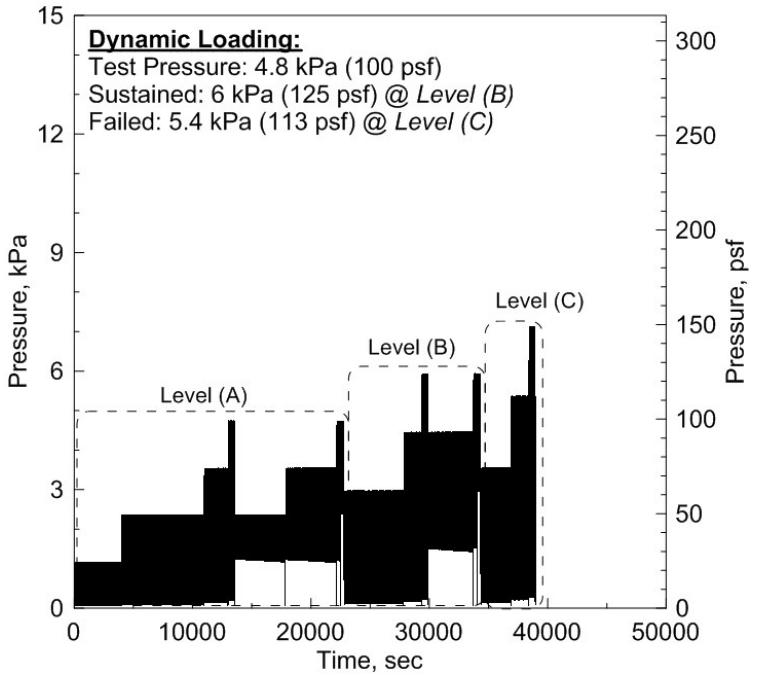

Figure 6.4: Test performance of DCC edge system under dynamic loading (Enhanced experimental setup)

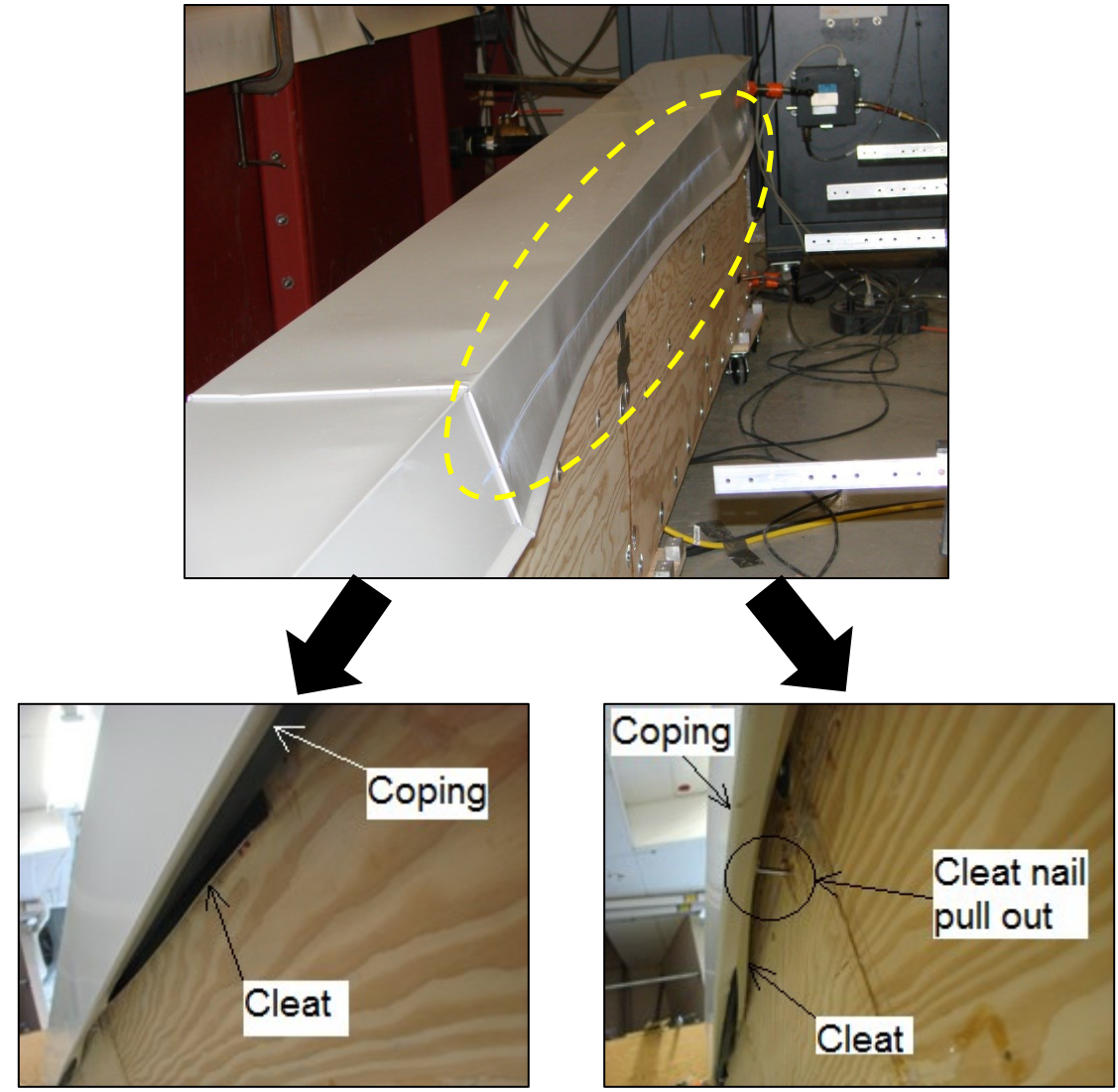

(a) Coping failed by disengagement from cleat

(b) Cleat nail pull-out

Figure 6.5: Failure mode of DCC edge system under dynamic loading (enhanced experimental setup)

Figure 6.6 shows a plot of the pressure data versus the deformation data at the coping joint. One can observe that the joint behaved in a linear way, where a line could expectedly be fitted through the data points. The highest deformation recorded was 33 mm (1.3 in.). In this case, the coping seemed susceptible to high deformations since it was not supported, i.e. no cleat was installed. On the other hand, the deformation at the midpoint was almost zero due to movement restriction at the middle; see Section 5.4.2 and Figure 5.12 for more details about this phenomenon.

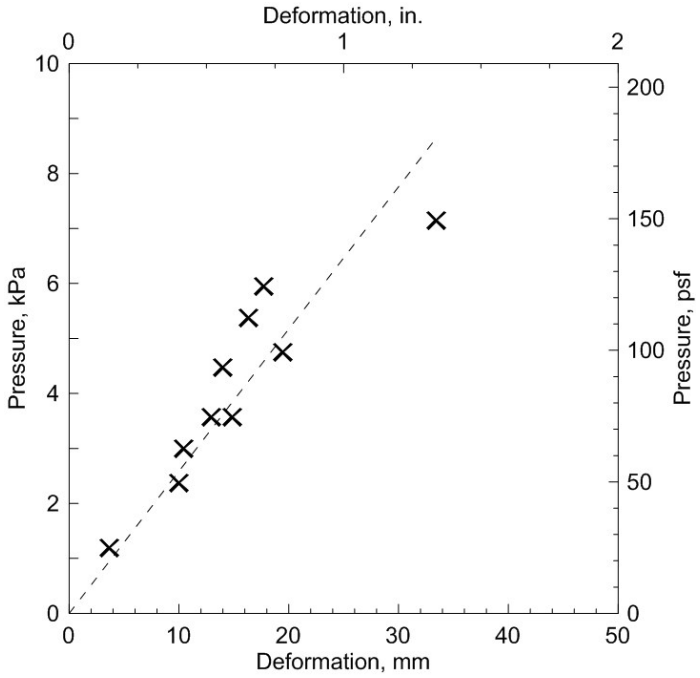

Figure 6.6: Deformation of DCC edge system coping at x= 0 (enhanced experimental setup)

6.2.2 Response of CCC Edge system

Edge Specification and Installation

All specifications, geometry and installation process are the same as presented in Section 4.4.2

Applied Pressure and Failure Mode

As illustrated in Figure 6.7, the test pressure was set at 7.14 kPa (150 psf). The edge could maintain satisfactory performance at Levels A, B, C and D; however, the edge system failed at Level E at a pressure of 14.3 kPa (300 psf). The failure mode was similar to the one of DCC edge system, where both coping-cleat disengagement and cleat nail pull-out occurred as shown in Figure 6.8. The edge system was rated at **12.5 kPa (263 psf)**.

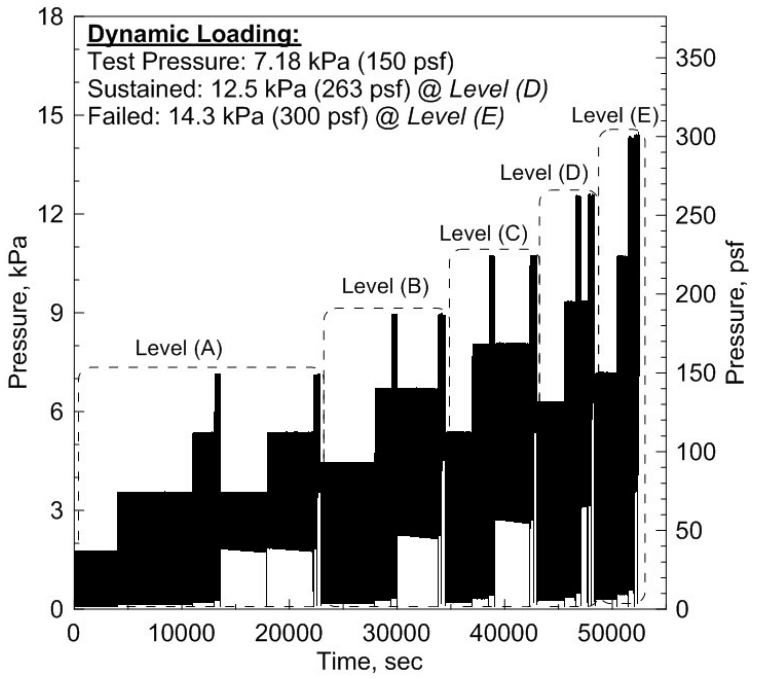

Figure 6.7: Test performance of CCC edge system under dynamic loading (enhanced experimental setup)

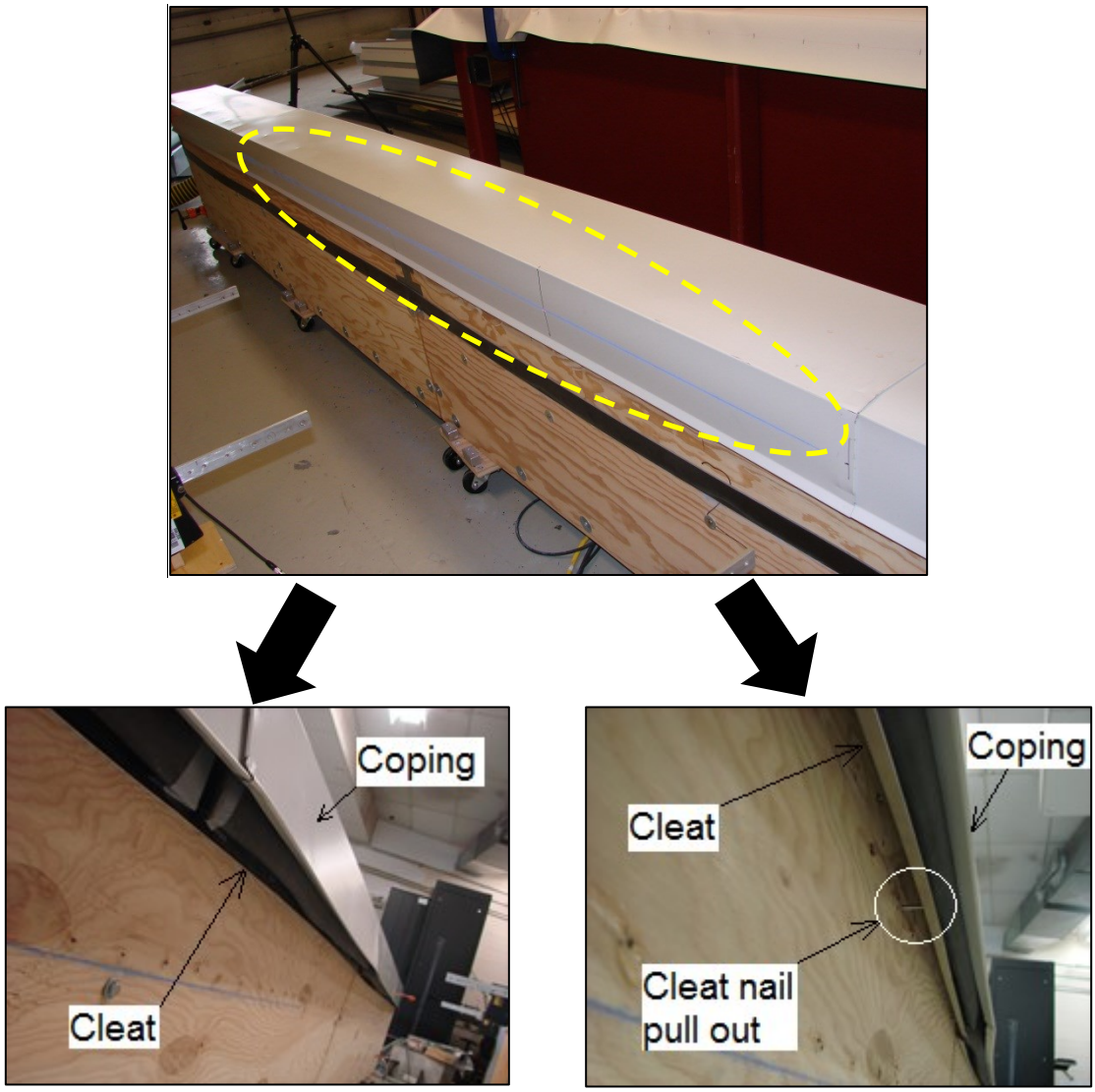

(a) Coping-cleat disengagement (b) Cleat nail pull-out

Figure 6.8: Failure mode of CCC edge system under dynamic loading (enhanced experimental setup)

Coping Deformation

As shown in Figure 6.9, the pressure data were plotted versus the recorded deformations. One can see that the coping deformations behaved linearly. This observation applies to both x= 0 (joint) and x= L/2 (midpoint). However, with respect to x= 0 (joint), the highest

deformation recorded was only 2 mm (0.1 in.) due to the high rigidity of the S-lock joint. On the contrary, at x= L/2 (midpoint), the deformation relatively recorded higher values, where the maximum was about 6 mm (0.2 in.). Overall, the coping experienced extremely low deformations due to the presence of a continuous cleat securing the entire coping.

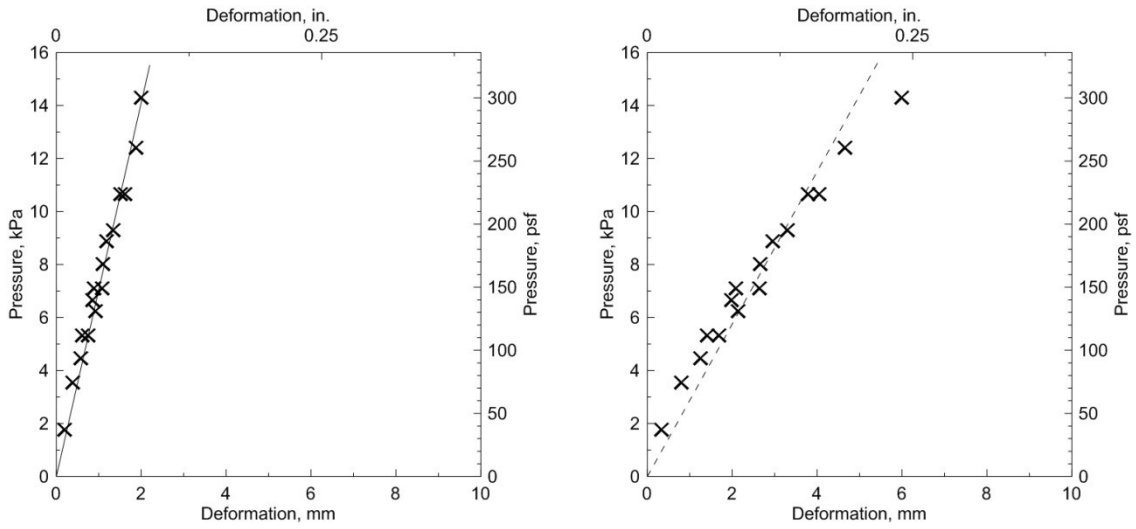

(a) x= 0 (b) x= L/2

Figure 6.9: Deformation of CCC coping under dynamic loading (enhanced experimental setup)

6.2.3 Performance Comparison

Table 6.1 summarizes the results achieved for both DCC and CCC edge systems in terms the existing experimental setup and the enhanced one. When tested by the existing setup, DCC failed by coping-cleat disengagement; however, it failed by both coping-cleat disengagement and cleat nail pull-out when tested by the enhanced setup. As for the CCC edge system, it did not fail when tested by the existing setup, but it failed by coping-cleat disengagement and cleat nail pull-out when tested by the enhanced setup. Thus, the enhanced experimental setup appeared to yield more realistic evaluation compared to the

existing setup. Overall, unlike the existing experimental setup, the enhanced setup is evidently capable of testing edge components more effectively by evaluating the resistance chain of the edge components, i.e. both Zone (1) and Zone (2) are evaluated; see Figure 6.1.

Table 6.1: Performance of DCC and CCC by using existing and enhanced experimental setup

Edge System	**Sustained**		**Failure Mode**	
	Existing Experimental Setup kPa (psf)	*Enhanced Experimental Setup kPa (psf)*	*Existing Experimental Setup*	*Enhanced Experimental Setup*
DCC	8.4 (175) Level (D)	6 (125) Level (B)	Coping-cleat disengagement	Coping-cleat disengagement and Cleat nail pull-out
CCC	14.35 (300) Level (E)	12.5 (263) Level (D)	N/A	Coping-cleat disengagement and Cleat nail pull-out

Table 6.2 below summarize the major differences between the pressure plane setup and the enhanced experimental setup:

Table 6.2: Advantages of the enhanced experimental setup over the existing setup

	Existing Experimental Setup	**Enhanced Experimental Setup**
Cleat Securement	The cleat is restricted from movement because of the pressure plane fasteners.	The cleat is normally secured since the pressure bags are independently installed.
Pressure Simulation	It uses pressure planes directly secured to the edge substrate. The edge substrate (pressure chamber) is pressurized which feeds the pressure plane.	It uses independently installed pressure bags connected to pressure pipe through hoses running inside the pressure chamber. The edge substrate is not pressurized but contains the pressure pipe.
Gust Simulation	The gust simulator controls the air flowing into the pressurized substrate and therefore the pressure plane.	The gust simulator controls the air flowing into the pressure bags through the pressure pipe and hoses.
Efficiency	Only coping-cleat integration can be tested (Zone 1).	Both coping-cleat integration (Zone 1) and cleat nails (Zone 2) can be tested.
Failure Mode	Edge systems tested by this setup are expected to have only coping-cleat disengagement failure mode.	Edge systems tested by this setup are expected to have both cleat nail pull-out failure mode in addition to coping – cleat disengagement.
Installation	Relatively complex, where the pressure plane should be carefully installed with batten bars so that it is air tight.	Less complicated installation where it uses pre-manufactured pressure bags that are connected by hoses to the pressure pipe and independent of the substrate.
Usability	The shape of the edge system may limit the use of pressure plane.	Independently installed pressure bags can be adjusted based on the shape of the components and their geometry.

6.3 Conclusion

The enhanced experimental setup proved its simplicity and reliability compared to the existing one. The use of pressure bags instead of pressure planes showed significant reduction in installation time and easier installation process. In terms of performance, the enhanced experimental setup transcended the technical limitation represented by cleat over-securement in the existing setup. By using the enhanced experimental setup, all edge components were involved and tested more realistically. Besides, the performance comparison showed a solid support of the efficiency of the enhanced experimental setup, where multiple failure modes and more realistic ratings were observed in comparison with those yielded by using the existing setup. The experimental results showed that the performance of DCC was better than that of the CCC. This conclusion was also made in Chapter 5.

Chapter 7. Conclusions and Recommendations for Future Research

7.1 Conclusions

The present thesis documented the process of establishing a new experimental method for testing roof edge systems. The developed experimental method was applied on a number of widely used roof edge systems. The study presented a comprehensive comparison for the performance of the tested edge systems. Enhancement was also suggested for the developed experimental method. Furthermore, the thesis included a detailed review of the mostly used wind load provisions. The following summarizes the contributions of the current thesis:

1. A clear understanding of both the NBCC and ASCE procedures for calculating design wind loads on roof claddings was demonstrated by taking side-by-side cities along Canada-USA border. These efforts clearly shared the differences and similarities between the NBCC and ASCE. Even though both the NBCC and ASCE provide the essential tools for calculating design wind loads, they differ from each other in many aspects, such as the specification of design parameters. Consequently, attempts to compare the design parameters in each code appear to be complex.
2. Wind-RCI Calculator is an online tool for calculating design wind loads on roof claddings. As a part of the current contribution, the existing version of the calculator was updated from NBCC2005 to NBCC2010 provisions.
3. The current study presented a new experimental method for testing and evaluating wind uplift resistance of roof edge systems by simulating wind pressure in a lab envi-

ronment on full-scale mock-ups. The test apparatus had a gust simulator device to mimic wind gusting.

4. Three widely used edge systems were investigated in this research: Continuous Cleat Configuration (CCC), Discontinuous Cleat Configuration (DCC) and Anchor Clip Configuration (ACC). The investigations demonstrated the procedures of the developed method. Data showed that CCC edge system resulted in higher resistance in comparison to DCC and ACC edge systems.
5. Presenting the lab data with industrial partners revealed that it is not sufficient for a roof edge system to only resist the design load, but it also needs to maintain a minimum level of weather protection. A roof edge system can achieve such a protection only with minimal deformations in order to avoid water intrusion. Based on the foregoing discussion, the CCC edge system adequately satisfied both wind loads and water protection requirements.
6. The enhanced experimental setup proved its simplicity and reliability compared to the existing one. The use of pressure bags instead of pressure planes showed significant reduction in installation time. In terms of performance, the enhanced experimental setup solved the technical limitation represented by cleat over-securement in the experimental setup.
7. By using the enhanced experimental setup, multiple failure modes and more realistic system ratings were observed. The experimental results further showed that the performance of CCC edge system was better than that of the DCC and ACC edge systems, which is consistent with Conclusion (6).

7.2 Recommendations for Future Research

Based on the lessons learnt from the present thesis, this section suggests some possibilities to expand the research contribution in both the wind load calculation part and further enhancement for the developed experimental method:

1. In Chapter 3, a detailed review of the NBCC and ASCE provisions were presented. It is suggested to extend the review to include international wind load provisions. This would enhance the designer's understanding and strengthen his/her skills by learning how different wind load provisions deal with wind load calculations.
2. In Chapter 3, a review of the online NBCC-based tool, the Wind-RCI Calculator, was presented. As a suggested future work, it is helpful to extend the current version to include the ASCE provision such that the calculator would be applicable in both Canada and the United States.
3. In Chapter 4 and 5, only three types of roof edges were investigated. It is highly recommended to employ a wider range of roof edge types, such as flashings, fasciae and gravel stops. Doing so would validate the applicability of the developed method such that any edge configuration can be evaluated.
4. In Chapter 4 and 5, only Set "A" and Set "B" of each roof edge system were included, but Chapter 2 concluded that the geometry of a roof edge would affect the wind pressure distribution over its surface. Thus, it is recommended to include varying roof edge geometries to be evaluated by the developed method. Furthermore, different edge lengths also shall be considered.

5. In Chapter 4, only substrates made of wood were discussed. It is valuable to test roof edge systems installed on different substrates, such as dense deck or steel to evaluate different installation conditions.
6. In Chapter 4, 5 and 6, the roof edge systems were tested under static and dynamic protocols. It is highly recommended to test the systems by using ES-1 test method in order to prove the advantage of the developed method.
7. The developed experimental method simulates wind loads on one face of the roof edge. Since all three sides of a roof edge are subjected to wind pressure in the field, it is appropriate to simulate wind pressure on all three edge sides, which would allow for evaluating different load combinations.

References

ASCE7-10. (2010). "Minimum Design Loads for Buildings and Other Structures." *American Society of Civil Engineers (ASCE),* Reston, VA.

ASCE7-05. (2005). "Minimum Design Loads for Buildings and Other Structures." *American Society of Civil Engineers (ASCE),* Reston, VA.

Baskaran, A., and Smith, T. L. (2005). "A guide for the wind design of mechanically attached flexible membrane roofs." *Institute for Research in Construction*, NRCC, Ottawa, ON.

Baskaran, A. (2005). "Top 10 Questions and Answers on Static vs. Dynamic Wind testing for Commercial Roofs." *RCI Inc. Interface Journal*, 24 (8).

Baskaran, A., Molleti, S. and Roodvoets, D. (2007) "Understanding low-slope roofs under hurricane Charley from field to practice." *Journal of ASTM International*, 4, (10).

Baskaran, A., Molleti, S., and Yew, H. (2008). "Wind-Roof Calculator on Internet (Wind-RCI)- Feel the Wind on Your Laptop." *Institute for Research in Construction*, NRCC, Ottawa, ON.

Baskaran, A., Molleti, S., Ko, S. and Van Reenen, D. (2011). "Field monitoring the wind performance of commercial roofs." *NRC Institute for Research in Construction,* IRC-RR 905.

Borzoee, M. (2012). "A pilot study on the Wind Uplift Performance Evaluation of Roof Edge Systems." M.Eng. project, the University of Ottawa, Ottawa, ON, Canada.

Chen, X., and Zhou, N. (2007). "Equivalent Static Wind Loads on Low-rise Buildings Based on Full-scale Pressure Measurements." *Journal of Engineering Structures* 29.10: 2563-575.

CSA A123.21-10 (2010) "Standard Test Method for the Dynamic Wind Uplift Resistance of Mechanically Attached Membrane Roofing System." (www.csashop.ca)

Dabbas, M. (2012). “Finite element analysis of wind-uplift resistance of roof edge components.” M.A.Sc. thesis, the University of Ottawa, Ottawa, ON, Canada.

FM Global (2005) “Approval Standard: Class I Roof Covers (FMG 4470).” Norwood, Massachusetts, USA.

Holmes, J. (2003) "Probability Distributions of Extreme Pressure Coefficients." *Journal of Wind Engineering and Industrial Aerodynamics* 91.7: 893-901.

Jiang, H. (1995). “Wind Effects on Metal Edge Flashings.” Master’s thesis, Texas Tech University, Lubbock, Texas, USA.

Kasperski, M. (1992). "Extreme Wind Load Distributions for Linear and Nonlinear Design." *Journal of Engineering Structures* 14.1: 27-34.

Kopp, G., D. Surry, and C. Mans (2005). "Wind Effects of Parapets on Low Buildings: Part 1. Basic Aerodynamics and Local Loads." *Journal of Wind Engineering and Industrial Aerodynamics* 93.11: 817-41.

Krishna, P. (1995). "Wind Loads on Low Rise Buildings — A Review." *Journal of Wind Engineering and Industrial Aerodynamics* 54-55: 383-96.

Lechner, J.A., E. Simiu, and N.A. Heckert (1993). "Assessment of ‘peaks over Threshold’ Methods for Estimating Extreme Value Distribution Tails." *Journal of Structural Safety* 12.4: 305-14.

LeClare, B. (2010). "Metal Edge Systems for Low Slope Roofs’ Design, testing and performance of edge investigated by RICOWI after Hurricane Ike" *ROICOWI Fall Seminar.*

Mcdonald, J., P. Sarkar, and H. Gupta (1997). "Wind-induced Loads on Metal Edge Flashings." *Journal of Wind Engineering and Industrial Aerodynamics* 72: 367-77.

National Research Council of Canada (2005) “National Building Code of Canada” NRCC, Ottawa, Canada.

National Research Council of Canada (2010) “National Building Code of Canada” NRCC, Ottawa, Canada.

Richards, P., and R. Hoxey (2008). "Wind Loads on the Roof of a 6m Cube." *Journal of Wind Engineering and Industrial Aerodynamics* 96.6-7: 984-93.

Simiu, E., and N. A. Heckert (1996). "Extreme Wind Distribution Tails: A “Peaks over Threshold” Approach." *Journal of Structural Engineering* 122.5: 539.

Simiu, E. (2007). "“Generalized Pareto Methods for Wind Extremes. Useful Tool or Mathematical Mirage?” by Ian Harris." *Journal of Wind Engineering and Industrial Aerodynamics* 95.2: 133-36.

Simiu, E. (1981). "Wind Direction Effects on Cladding and Structural Loads." *Journal of Engineering Structures* 3.3: 181-86.

Tieleman, H., Z. Ge, and M. Hajj (2007). "Theoretically Estimated Peak Wind Loads." *Journal of Wind Engineering and Industrial Aerodynamics* 95.2: 113-32.

User's Guide--NBC 2006 Structural Commentaries (Part 4). Ottawa: National Research Council of Canada, 2002.

User's Guide--NBC 2011 Structural Commentaries (Part 4). Ottawa: National Research Council of Canada, 2011.

SPRI. (2011). “*Wind Design Standard for Edge Systems Used with Low Slope Roofing Systems.”* Waltham, MA, USA.

Appendix A

A.1 Processing and Calculating Wind Speed

A.1.1 Classical Approach

In brief, this method involves the maximum wind speed in each year (epoch). Concerning the present example, fifteen (15) data points are considered based on the epochal approach. Then, a probability distribution curve is fitted into these points to estimate the design wind speed. This approach is criticized for the lack of representing less heavy storms since only the heaviest ones are considered (Simiu and Heckert, 1996).

A.1.2 Peak-over-Threshold Approach (POV)

To address the drawback of the epochal approach, peak-over-threshold approach makes use of data exceeding a certain threshold. In other words, a speed threshold is set, such that it divides the data points into two groups: data points above threshold and others below threshold. Only data points above threshold are considered for analysis, whereas the ones below the threshold are discarded. Therefore, less heavy storms are included in the process. Weaker storms tend to play a complementary role with the heavier storms to represent the wind behaviour more realistically. As for the determination of speed threshold, it should be sufficiently high, where a relatively low threshold might involve very weak storms, resulting in biased data. On the other hand, an excessively high threshold can neglect extreme winds, leading to an inadequate representation of the actual wind. Furthermore, the application of this method requires the data points to be separated by sufficiently long intervals such that each data point belongs to an independent storm. Optimum re-

sults can be achieved if the threshold is selected such that the exceedance rate λ (number of points above the threshold) is 10 to 15 data points per year (Simiu and Heckert, 1996)

As shown in Figure A.1, for the present example, only POV approach is considered. The record was divided into 548 intervals, each is 10 days long to avoid correlation of data. A threshold (u) of 15.75 m/s (33.2 mph) was selected such that 216 data points exceeded the threshold, and the exceedance rate λ is therefore:

$$\lambda = \frac{k}{n_{yr}} = \frac{216}{15} \approx 15/year$$

where k = the number of data points exceeding the threshold (u).

n_{yr}= length of the record in years.

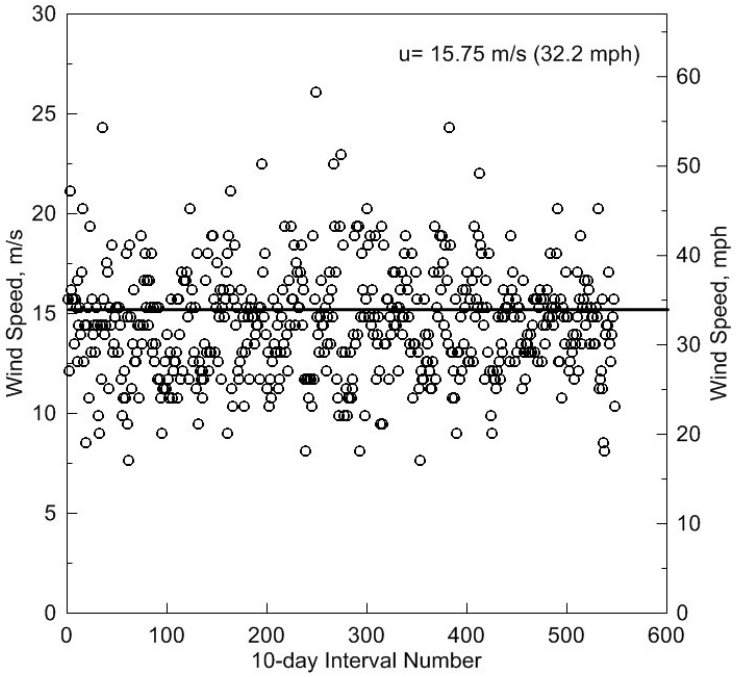

Figure A.1: Wind speed peaks for 10-day intervals (548 points)

A.1.3 Probability Distribution Model with POV Approach

Since exceedances of a sufficiently high threshold are rare events, they tend to follow the General Pareto Distribution (GPD) (Lecher, Simiu and Heckert, 1993).

Let Xdenote the wind speed and Y denote the excess of Xover the threshold (u). Thus, the random variable of the excess Y is distributed with GPD that is given by:

$$F(y) = prob[Y \leq y] = 1 - \left\{\left[1 + \frac{c}{a}.y\right]^{-1/c}\right\}$$

where a and c are the distribution parameters

$Y = X - u$

Three cases can be identified here:

1. $c = 0$: Gumbel Distribution (Type I extreme value)
2. $c > 0$: Fréchet Distribution (Type II extreme value)
3. $c < 0$: Reverse Weibull Distribution (Type III extreme value)

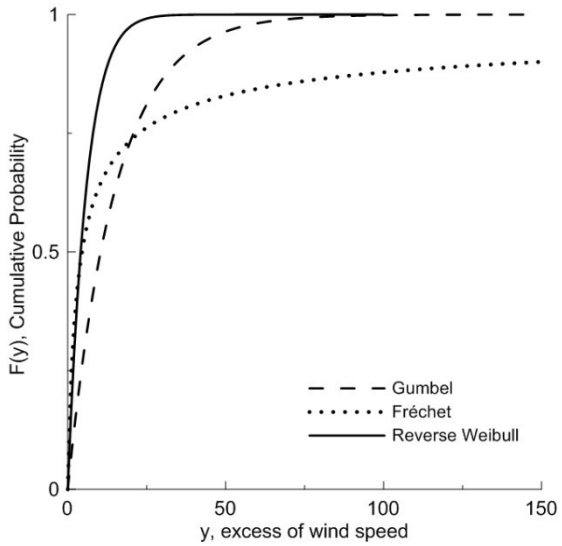

Figure A.2: Gumbel, Fréchet and reverse Weibull distribution

Figure A.2 illustrates the probability distribution curves. In fact, Gumbel and Fréchet distributions are unbounded, i.e. they have infinite upper tail, whereas reverse Weibull distribution has a limited upper tail. Given that extreme winds are bounded events, using the reverse Weibull distribution would be an adequate option.

As for the distribution parameters, Dekkers and de Haan (1989) presented a method for estimating these parameters. In addition, other methods are also available in the literature, such as Conditional Mean Exceedance method (CME) and Pickands method. However, it was proved that Dekkers-de Haan method performs the best among other methods (Lecher, Simiu, Lecher, and Heckert, 1993). The present example will be solely limited to Dekkers-de Haan method.

Dekkers-de Haan Method

Let $X_n, X_{n-1}, X_{n-2}, \ldots., X_{n-(k-1)}, X_{n-k}$ denote the highest wind speeds including the threshold (X_{n-k}), where (k) is the number of exceedances and (n) is the total number of the data points. The parameters estimators were calculated by the method of moments as follows:

$$\hat{c} = M_n^{(1)} + 1 - 0.5 \times \left[1 - \frac{M_n^{(1)}}{M_n^{(2)}}\right]^{-1}$$

$$\hat{a} = \frac{u}{\rho_1} \times M_n^{(1)}$$

where $M_n^{(r)} = \frac{1}{k} \times \sum_{i=1}^{k} [ln(X_{n-i+1}) - ln(X_{n-k})]^r$

$$c > 0 \rightarrow \rho_1 = 1$$

$$c < 0 \rightarrow \rho_1 = \frac{1}{1-c}$$

For the present example, these parameters are calculated as follows:

$$\sum_{i=1}^{k}\left[\ln\left(X_{n-i+1}\right)-\ln\left(X_{n-k}\right)\right]=1.796885175$$

$$\sum_{i=1}^{k}\left[\ln\left(X_{n-i+1}\right)-\ln\left(X_{n-k}\right)\right]^2=0.372504060$$

$$M_n^{(1)}=\frac{1}{15}\times 1.796885175=0.119792345$$

$$M_n^{(2)}=\frac{1}{15}\times 0.372504060=0.024833604$$

$$\hat{c}=0.119792345+1-0.5\times\left[1-\frac{\left(0.119792345\right)^2}{\left(0.024833604\right)}\right]^{-1}=-0.06463$$

As $c=-0.06463\prec 0\Rightarrow \rho_1=\frac{1}{1-\left(-0.06463\right)}=0.939291$

Hence

$$\hat{a}=\frac{15.75}{0.939291}\times 0.119792345=1.913023$$

A.1.4 Calculation of Design Wind Speed

The design wind speed is a function of the return period (R), also called mean recurrence interval (MRI). A return period of R years means that the chance of the design speed being exceeded is 1/R in any one year. For instance, if the design speed is $V = 20m/s(45\ mph)$, corresponding to a return period of $R = 100$ year, it means that the probability of exceeding this design speed is 1/100=0.01 in any year. As indicated in Section 3.4.2, the design wind speed is calculated in terms of the excess speed:

$$F(y) = prob[Y \le y] = 1 - \left[1 + \frac{c}{a}.y\right]^{-1/c} = 1 - \frac{1}{\lambda.R}$$

$$y = -\frac{a}{c} \times \left[1 - (\lambda.R)^c\right]$$

$$V_R = y + u$$

For the present example, by using the parameters calculated in Section 3.4.2, the design wind speed, based on a return period of 50 years, can be calculated as follows:

$$y = -\frac{1.913023}{(-0.06463)} \times \left[1 - (15 \times 50)^{-0.06463}\right] = 10.3$$

$$V_R = 10.3 + 15.75 = 26.05 \text{ m/s (56 mph)}$$

Selecting the return period should be associated with the importance level and the life span of the building. For a return period R, the probability of non-exceedance of the design wind speed in any one year is:

$$P_{non-exceedance} = 1 - \frac{1}{R}$$

Given that, the life span is L and the exceedance event is independent in each year, the probability of non-exceedance of the design wind speed during the structure's life is:

$$\left[1 - \left(\frac{1}{R}\right)\right] \times \left[1 - \left(\frac{1}{R}\right)\right] \times .... = \left[1 - \left(\frac{1}{R}\right)\right]^L$$

Therefore, the probability that the design wind speed will be exceeded during L years:

$$r = 1 - \left[1 - \left(\frac{1}{R}\right)\right]^L$$

It is clear that for a given life span, the higher the return period the lower the probability of exceedance. Thus, structures with long life span should be designed for longer return periods.